Earth-Science Reviews 112 (2012) 126–154

Contents lists available at SciVerse ScienceDirect

Earth-Science Reviews

journal homepage: www.elsevier.com/locate/earscirev

The Cambrian to Devonian odyssey of the Brabant Massif within Avalonia: A review with new zircon ages, geochemistry, Sm–Nd isotopes, stratigraphy and palaeogeography

Ulf Linnemann [a], Alain Herbosch [b,*], Jean-Paul Liégeois [c], Christian Pin [d], Andreas Gärtner [a], Mandy Hofmann [a]

[a] Senckenberg Naturhistorische Sammlungen Dresden, Museum für Mineralogie und Geologie, Sektion Geochronologie, GeoPlasma Lab, D-01109 Dresden, Germany
[b] Département des Sciences de la Terre et de l'Environnement, Université Libre de Bruxelles, B-1050 Brussel, Belgium
[c] Isotope Geology, Royal Museum for Central Africa, B-3080 Tervuren, Belgium
[d] Laboratoire de Géologie, Université Blaise Pascal, CNRS UMR-6524, 63038 Clermont-Ferrand Cedex, France

ARTICLE INFO

Article history:
Received 21 December 2011
Accepted 16 February 2012
Available online 25 February 2012

Keywords:
Avalonia
Lower Palaeozoic
Gondwana
Zircon age
Meguma

ABSTRACT

This study provides an up-to-date and comprehensive review of the Early Palaeozoic evolution of the Brabant Massif belonging to the Anglo-Brabant Deformation Belt. Situated at the southeastern side of Avalonia microplate, it is the only well-known part of the northern passive margin of the Rheic Ocean. The Cambrian–Silurian sedimentary pile is >13 km thick, with >9 km for the Cambrian only. The unraveling of this continuous registration reflects the successive rifting and drifting of Avalonia from the Gondwana mainland, followed by soft-collisional processes with Baltica and finally the formation of Laurussia. Based on recently established detailed stratigraphy, sedimentology and basin development, on U–Pb LA-ICP-MS analyses of igneous and detrital zircon grains along with geochemical data including Sm–Nd isotopes, a new geodynamic and palaeogeographic evolution is proposed. Brabant Megasequence 1 (lower Cambrian to lowermost Ordovician, >9 km thick) represents an embayment of the peri-Gondwanan rift from which the Rheic Ocean has evolved. Detrital zircon ages demonstrate that the Brabant is a typical peri-Gondwanan terrane with a major Pan-African (Neoproterozoic age) and a mixed West African and Amazonian source (Palaeoproterozoic, Archaean and some Mesoproterozoic age). The transition towards the Avalonia drifting is marked by an unconformity and a short volcanic episode. The northward drift of Avalonia towards Baltica is recorded by the Megasequence 2 (Middle to Upper Ordovician, 1.3 km thick). The source for Mesoproterozoic zircons vanished, as the result of the Rheic Ocean opening and the isolation from Amazonian sources. The transition to Megasequence 3 is marked by a drastic change in palaeobathymetry and an important (sub)volcanic episode during a tectonic instability period (460–430 Ma), reflecting the Avalonia–Baltica soft docking as also shown by the reappearance of Mesoproterozoic detrital zircons, typical of Baltica. Unradiogenic Nd isotope signature (ε_{Nd} −4/−5) and T_{DM} model ages (1.3–1.7 Ga) for Brabant magmatic rocks indicate an old recycled component. Megasequence 3 (uppermost Ordovician to lowermost Devonian; >3.5 km thick) includes the onset of a Silurian foreland basin that reflects the tectonic inversion of the core of the massif (Brabantian orogeny) in response to the Baltica–Avalonia–Laurentia collision. Finally, the comparison with the strikingly similar Cambrian successions of the Harlech Dome (Wales, Avalonia) and the Meguma terrane (Nova Scotia, peri-Gondwana) allows the construction of a new Early Cambrian palaeogeographic model for the whole Avalonia microplate, in which the Meguma terrane is included.

Contents

* Corresponding author. Tel.: +32 2 650 2201.
E-mail addresses: ulf.linnemann@senckenberg.de (U. Linnemann), herbosch@ulb.ac.be (A. Herbosch), jean-paul.liegeois@africamuseum.be (J.-P. Liégeois), c.pin@opgc.univ-bpclermont.fr (C. Pin).

0012-8252/$ – see front matter © 2012 Elsevier B.V. All rights reserved.
doi:10.1016/j.earscirev.2012.02.007

1. Introduction

Although largely concealed, the Brabant Massif is now very well known for its overall geology, due to recent multidisciplinary research and detailed (1/25,000 scale) geological mapping. The Lower Palaeozoic of the Brabant Massif is of major interest because it offers a nearly continuous record of the sedimentation from the upper part of Cambrian Stage 2 (~525 Ma) to the lowermost Lochkovian (~415 Ma) within a strongly developed,>13 km thick, sedimentary sequence. This sedimentary succession constitutes the only well known witness of the southern side of the eastern part of Avalonia facing Gondwana during Cambrian and subsequently the Rheic Ocean until its closure. The palaeogeographic positions of the Brabant Massif are broadly inferred from its location within Avalonia but no direct, or detailed provenance constraints are available from this thick sequence. Also, the nature and the significance of the magmatism have not been reassessed recently since the pioneering works 30 years ago.

This study provides an up-to-date review of the recently established stratigraphy of the Lower Palaeozoic of the Brabant Massif together with new constraints on geodynamic setting and palaeogeographic positions based on LA-ICP-MS U–Pb ages on single grains of detrital and igneous zircons (over 1000 spot analyses on 8 sediments and on 4 (sub)volcanic rock samples), and major, trace element and Nd isotope whole-rock analyses (24 samples). For the first time, a comprehensive evolutionary model is proposed for the Avalonian Brabant Massif during the Early Palaeozoic. This includes Cambrian rifting from Gondwana, drifting during the opening of the Rheic Ocean, soft docking with Baltica, the far-field effects of the remote Caledonian collision with Laurentia, and finally its behavior as a passive margin to the north-west of the Rheic Ocean, as part of the southern Old Red Sandstone Continent (Laurussia). Later, the Brabant Massif played the role of an indenter during the Variscan orogeny, and was not significantly affected except along his southern edge corresponding to the Variscan Front (Fig. 1). These new tight palaeogeographic constraints allow to place the Brabant Palaeozoic odyssey within the evolution of the entire Avalonia terrane, including both its American and European counterparts.

Throughout this paper, we follow the conception of Cocks and Fortey (2009) who consider that: "Avalonia was internally unified throughout the Lower Palaeozoic and not two independent "East" and "West" Avalonian terranes of some authors". In consequence we use "East" (in North America) and "West" (in Europe) Avalonia only for descriptive purposes. The chronostratigraphy and time scale by Ogg et al. (2008) is followed throughout.

2. Brabant Massif: general features

The Brabant Massif (Figs. 1, 2) consists of a largely concealed WNW–ESE directed fold belt developed during Early Palaeozoic times, documented in the sub-surface of central and north Belgium (Fourmarier, 1920; Legrand, 1968; De Vos et al., 1993; Piessens et al., 2006). At first sight, it appears as a gently ESE plunging broad anticlinal structure, with a Cambrian core flanked on both sides by Ordovician to Silurian strata. To the S, SW and SE, it is unconformably overlain by the Devonian to Carboniferous deposits of the Brabant Parautochthon (Mansy et al., 1999). The southern border of the latter shows Upper Palaeozoic thrust sheets belonging to the Brabant Massif (Condroz inlier, a 70 km long to 1 to 3 km large strip, elongated W–E along the Sambre and Meuse rivers; Michot, 1980; Vanmeirhaeghe, 2006). The Brabant Parautochthon is tectonically overlain by the Ardenne Allochthon along the Midi Fault System (Variscan overthrust; Fig. 2A). To the NW, the massif continues beneath the North Sea and links up with the East-Anglia Basin (Lee et al., 1993). Both areas form part of the Anglo-Brabant Deformation Belt (ABDB; Pharaoh et al., 1993, 1995; Van Grootel et al., 1997), the eastern branch of a predominantly concealed slate belt molded around the Neoproterozoic Midlands Microcraton. The ABDB belongs to the Avalonia microplate (Figs. 1 and 2A).

The Brabant Massif is poorly exposed and is almost completely covered by Meso-Cenozoic deposits (Fourmarier, 1920; Legrand, 1968). Along its southeastern rim, incising rivers (Figs. 2 and 3) provide narrow outcrop areas that were recently mapped at the 1/25,000 scale (Herbosch and Lemonne, 2000; Delcambre et al., 2002; Hennebert and Eggermont, 2002; Delcambre and Pingot, 2008; Herbosch and Blockmans, in press; Herbosch et al., in press-a,b). A substantial part

Fig. 1. Geological map of the Central European Variscides with location of the Brabant Massif and Fig. 2. From Ballèvre et al., 2009.

of the data is based on boreholes (Legrand, 1968; Herbosch et al., 1991, 2008b) and the interpretation of gravimetric and aeromagnetic survey (BGS: Belgian Geological Survey, 1994; Mansy et al., 1999; Sintubin, 1999; Sintubin and Everaerts, 2002; Everaerts and De Vos, 2012).

The Brabant Massif displays a very thick siliciclastic, often turbiditic sequence ranging from the upper part of the lower Cambrian in the core to the upper Silurian and even to the lowermost Devonian along the rims (Figs. 2, 4). Twenty years of stratigraphic research (André et al., 1991; Vanguestaine, 1991, 1992; Maletz and Servais, 1996; Verniers et al., 2001, 2002; Herbosch and Verniers, 2002; Vanmeirhaeghe et al., 2005; Owen and Servais, 2007; Herbosch et al., 2008a, b; Debacker and Herbosch, 2011) and mapping data suggests that the sedimentary record is continuous, with the exception of an important hiatus in the Lower Ordovician (Fig. 4). The total thickness of this sedimentary pile exceeds 13 km, with over 9 km for the Cambrian only (Herbosch et al., 2008a).

The Brabant rocks show a low-grade metamorphic overprint, ranging from epizone in the core to anchizone and diagenesis in the rim (Van Grootel et al., 1997). The origin of this metamorphism is mainly of burial origin (pre-kinematic) but an additional syn-kinemtic origin is needed in order to account for the higher metamorphic degree observed in the Silurian rims (Debacker et al., 2005).

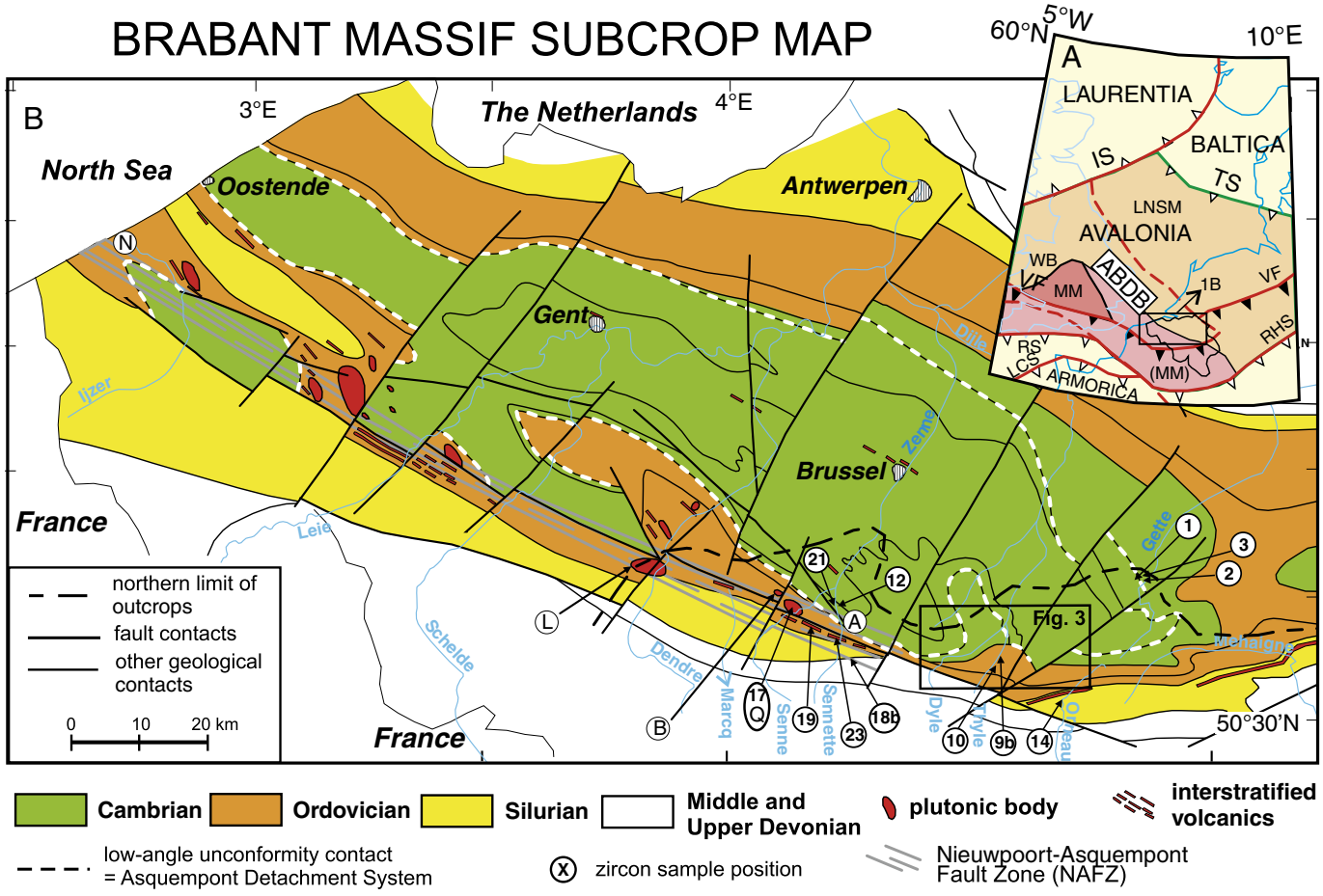

Fig. 2. (A) Position of the Brabant Massif within the Anglo-Brabant Deformation Belt (ABDB) along the NE-side of the Midland microcraton (MM) in the context of the terrane map of northwestern Europe (modified after Winchester and Network Team, 2002; Sintubin et al., 2009) Abbreviations: IS: Iapetus suture; LCS: Le Conquet suture; LNSM: Lüneburg-North Sea microcraton; (MM): extension of the Midland microcraton to the south-east under the Variscan front; TS: Tornquist suture; RHS: Rhenohercynian suture; RS: Rheic suture; VF: Variscan front; WB: Welsh basin. (B) Geological subcrop map of the Brabant Massif (after De Vos et al., 1993; Debacker et al., 2004a), with the position of the samples analyzed for zircon ages and the position of the detailed geological map of Fig. 3. Locality cited in the text: N: Nieuwpoort; L: Lessines B: Bierghes; Q: Quenast; A: Asquempont.

3. Brabant Massif: stratigraphy, sedimentology and basin evolution

The three sedimentary Megasequences bounded by basin-wide unconformities recognized in the Welsh basin by Woodcock (1990) have also been found in the Brabant Massif (Woodcock, 1991; Vanguestaine, 1992; Herbosch and Verniers, 2002; Verniers et al., 2002). The basement of the sedimentary sequence is not known at the surface or in boreholes. It has been speculated that the Brabant lies above a Neoproterozoic block (André, 1991) or alternatively on the boundary of two lithospheric blocks, namely the Midlands microcraton to the SW and the Lüneburg-North Sea microcraton to the NE (Sintubin and Everaerts, 2002; Sintubin et al., 2009; Fig. 2A). Throughout this paper, reported sedimentary formation thicknesses are best minimum or mean estimates based on recent detailed geological mapping taking into account the tectonic effects (Debacker, 2001; Debacker et al., 2011 and references therein).

3.1. Megasequence 1: a >9 km Cambrian rift sequence

The Megasequence 1 begins with the >1.5 km thick *Blanmont Formation* which consists of massive sandstone and quartzite with sparse slate intercalations. The lithology, the important thickness and the sedimentary structures (cross stratification, dewatering structure) indicate a high rate of sedimentation in a shallow and rapidly subsiding basin (Debacker and Herbosch, 2011) suggesting a rift environment. This is confirmed by the very thick remaining part of the Megasequence (>7.5 km) that was continuously deposited in a deep-sea marine environment. This deep-sea sequence comprises 5 formations spanning all the Cambrian from the base of Stage 3, the last one (Chevlipont Formation) being lowermost Ordovician in age (Fig. 4). Complete sections and contacts between these formations are nowhere observed, (micro-) fossils are scarce and their stratigraphical succession has been firmly established only recently (Herbosch et al., 2008a; NCS, 2009).

The >2 km thick *Tubize Formation* consists of green slate, siltstone, (arkosic) sandstone and greywacke interpreted as turbidites and hemi-pelagic to pelagic sediments. Magnetite is commonly observed in the siltstones inducing high relief in the aeromagnetic map (Chacksfield et al., 1993; Sintubin, 1999; Sintubin and Everaerts, 2002). This deep-seated sedimentation continued with the ~1.5 km thick, very fine and homogeneous slates, purple at the base and green at the top, of the Oisquercq Formation. The Blanmont, Tubize and Oisquercq formations are dated (*Oldhamia* or acritarchs) from the same age interval between Cambrian Stage 3 and three-quarter of Stage 5 (Vanguestaine, 1992; NCS, 2009; Herbosch and Verniers, 2011; Fig. 4). The *Jodoigne Formation*, >3 km thick, is made of slate, siltstone, sandstone and massive quartzite mostly of black color. It is interpreted as a sequence of turbidites and hemi-pelagic to pelagic sediments deposited in an anoxic, deep-sea environment. In the absence of any fossil, this formation is supposed to be middle Cambrian (Serie 3) in age (Herbosch et al., 2008a; NCS, 2009). The deep, anoxic

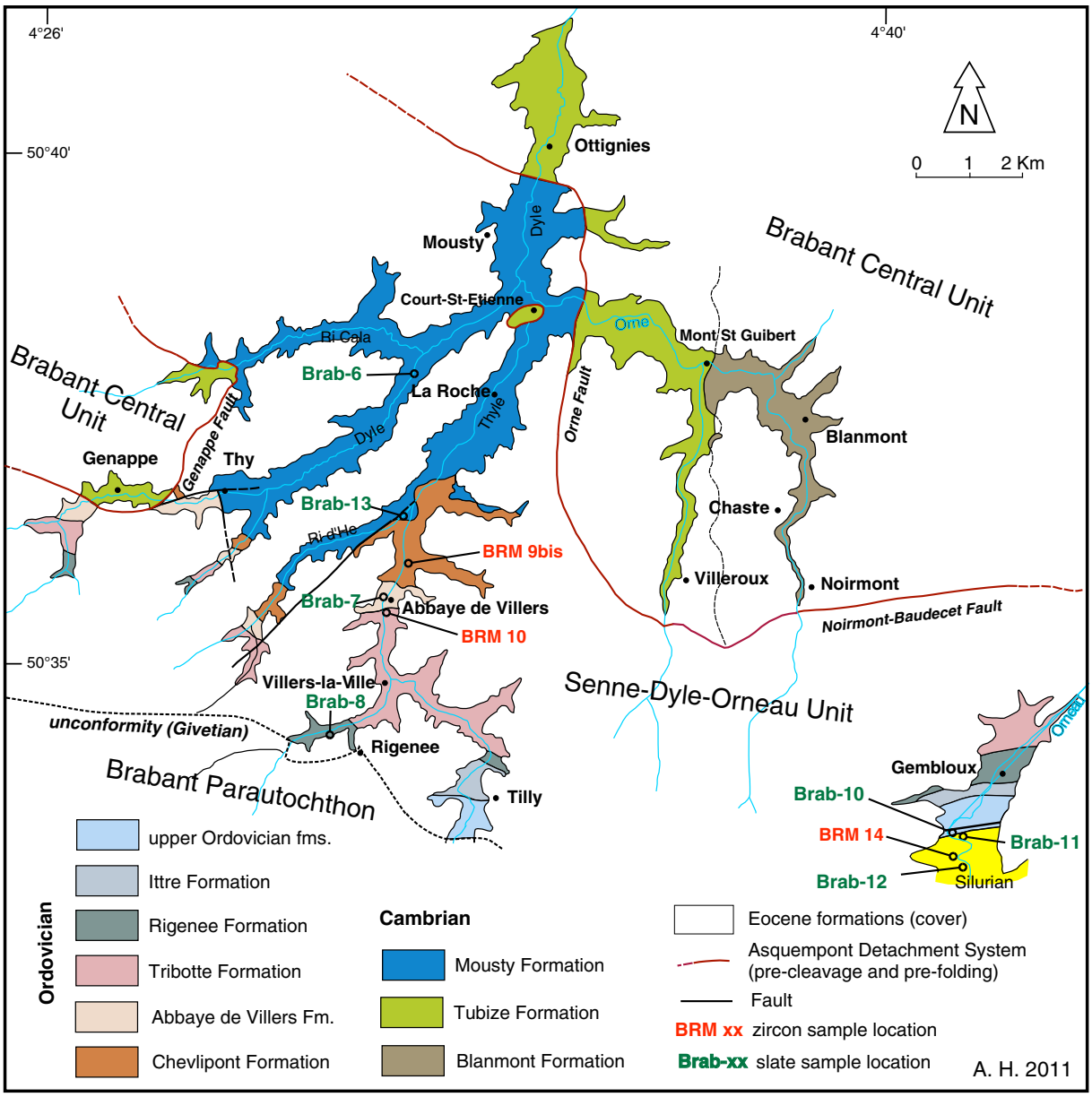

Fig. 3. Schematic geological map of the Lower Palaeozoic of the Dyle and Orneau (pro parte) basin outcrop area in the southern border of the Brabant Massif (see location in Fig. 2), with the position of sandstone samples analyzed for zircon and slate analyzed for Sm/Nd isotopes (modified from Herbosch and Lemonne, 2000; Delcambre et al., 2002; Debacker et al., 2004a; Herbosch and Blockmans, in press). Brabant Central Unit and Senne-Dyle-Orneau Unit are two sub-units of the Brabant Massif separated by the Asquempont Detachment System.

sedimentation continued during the *Mousty Formation*, with a minimum thickness estimate of 1 km. The Mousty sediments are mainly black graphitic and pyritic slates with episodic low-density turbidites. Frequent enrichments in Mn (up to 5% MnO, André et al., 1991; Table 3 sample Brab-6) are shown by black coatings in outcrops and by spessartite and Mn-ilmenite porphyroblasts in thin sections (de Magnée and Anciaux, 1945; André et al., 1991). The Mousty Formation ranges at least from the lower part of Furongian (Vanguestaine, 1992) to the lowest Tremadocian (graptolite *Rhabdinopora flabelliformis*; Lecompte, 1948). It passes gradually upward to the *Chevlipont Formation* formed by wavy bedded gray siltstone interpreted as silt turbidite. This formation, about 150 m thick, is dated from the Early Tremadocian by graptolites and acritarchs (Lecompte, 1949; André et al., 1991; Vanguestaine, 1992; NCS, 2011) and shows a shallowing trend.

To our best knowledge, the thickness of the Megasequence 1 is thus estimated at a minimum of 9 km, which is a huge value, only recently well established (Herbosch et al., 2008a; NCS, 2009). Such a thickness and the inferred deep-sea setting of the sediments that point to a rift environment, have also been recently depicted in the Cambrian of the Meguma terrane (Nova Scotia) and of the Harlech Dome (Wales, Avalonia) with similar thicknesses (Waldron et al., 2011; see discussion in Section 7.2). An earlier estimate already integrated in an extensional geodynamic setting was >3.7 km (Verniers et al., 2001, 2002; Debacker et al., 2005). Megasequence 1 is interrupted by a stratigraphic hiatus extending from the lower part of the Tremadocian (c. 485 Ma) to the upper part of the Floian or even the base of the Dapingian (c. 474 Ma) (Verniers et al., 2001, 2002; NCS, 2011). This unconformity is believed to reflect the drifting of the peri-Gondwana Avalonia microcontinent from Gondwana and the opening of the Rheic Ocean (Verniers et al., 2002; Herbosch and Verniers, 2002), usually dated from the end of the Tremadocian, around 480 Ma ago (Cocks and Torsvik, 2002, 2005; Linnemann et al., 2007; Cocks and Fortey, 2009).

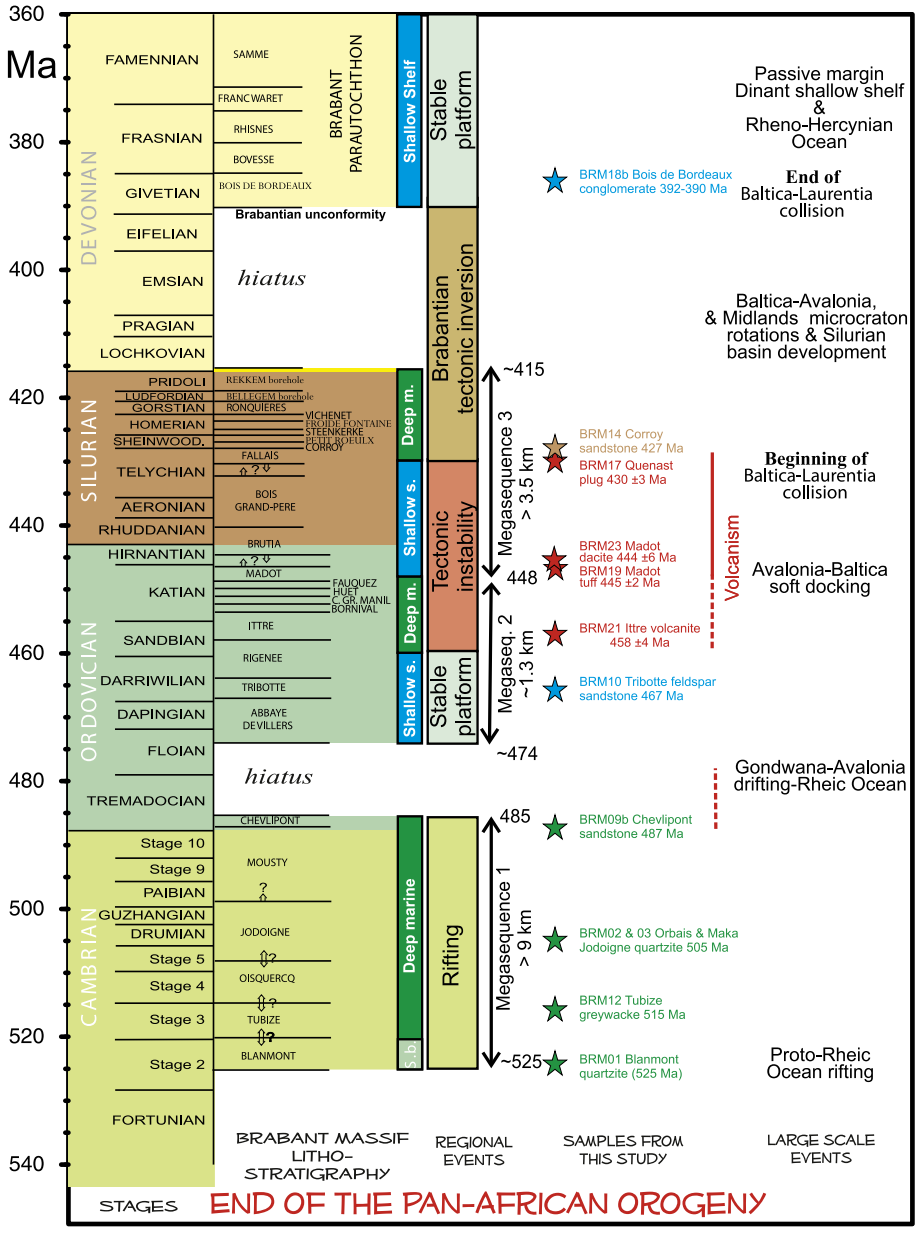

Fig. 4. Stratigraphical scale from Cambrian to Devonian for the Brabant Massif with (1) system and stage names and ages from the International Stratigraphic Chart (Ogg et al., 2008); (2) detailed lithostratigraphy of the Brabant Massif (see references in the text); (3) depth of deposition; (4) regional events; (5) Megasequence number and total thickness; (6) stratigraphic position of zircon-dated samples; (7) localization of large scale events. Abbreviation: s.: shelf; m.: marine; s.b.: shallow basin.

3.2. Megasequence 2: Avalonia as an island

The contact between Megasequences 1 and 2 has not been observed in the main outcropping part of the Brabant Massif but in the Wépion borehole within the Condroz Inlier, which palaeogeographically belongs to the southern continuation of the Brabant Massif. In this borehole the contact between the two Megasequences is marked by a slightly larger stratigraphic hiatus and a 5 cm thick basal microconglomerate that confirms an unconformity (Graulich, 1961; Vanmeirhaeghe, 2006 Fig. 31).

The sedimentary record begins with the *Abbaye de Villers* and *Tribotte Formations* made of outer to inner shelf clayey sandstone and silstone, the upper part of Tribotte evolving to an intertidal facies with abundant vertical bioturbation (Herbosch and Lemonne, 2000). An abrupt transition exists with the overlying *Rigenée Formation*, essentially dark siltstones to mudstones that record a regional transgression. The latter is well known in North Gondwana and Baltica as the "*Formosa* flooding Event" (Paris et al., 2007). The remaining part of Megasequence 2 corresponds to a deep marine environment (Fig. 4). These Upper Ordovician deposits consist of more or less distal dark turbiditic or hemi-pelagic sediments (*Ittre*, *Bornival* and *Fauquez formations*), very distal green turbiditic and pelagic slate (*Cimetière de Grand-Manil Formation*; Debacker et al., 2011; NCS, 2011), and gray muddy sandstone with some bioclastic levels (e.g.: corals, bryozoans, crinoids; *Huet Formation*) interpreted as tempestites (Verniers et al., 2002) or distal turbidites (Herbosch, 2005) (*Huet Formation*). The Huet and Madot formations, of mid to late Katian age (see below), both show shelly facies which have recorded the rapid shift of Avalonia to higher latitude as well as the pre-Hirnantian global "Boda Event" (Fortey and Cocks, 2005; Cherns and Wheeley, 2007).

The mean thickness of Megasequence 2 is estimated at about 1300 m (new estimation; NCS, 2011); this is considerably less than Megasequence 1. Megasequence 2 is believed to correspond to the behavior of Avalonia as an independent terrane, when this microplate

drifted very rapidly to higher latitudes from Gondwana to Baltica, with which it collided at c. 450 Ma (Cocks and Torsvik, 2005; Cocks and Fortey, 2009). These palaeogeographic deductions are confirmed by palaeontological investigations in the Brabant Massif and its southern prolongation, the Condroz Inlier (Brabant Parautochthon). In the latter, assemblages of trilobites show typical northwestern Gondwana (Avalonian) faunas up to the Sandbian (lower part of the Upper Ordovician); in the Katian, these faunal assemblages attest for the increasing proximity of Baltica (Verniers et al., 2002; Owen and Servais, 2007). Chitinozoan assemblages seem even more reactive: until the mid-Darriwilian, they have northwestern Gondwana affinities whereas a Baltoscandian signature exists from the lower Sandbian until the end of Ordovician (Samuelsson and Verniers, 2000; Verniers et al., 2005; Vanmeirhaeghe, 2006).

3.3. Megasequence 3: from Baltica to Laurentia docking

New stratigraphic investigations (Herbosch, 2005; Vanmeirhaeghe et al., 2005; Debacker et al., 2011) show the absence of any unconformity or hiatus in the Late Ordovician as it was still thought recently. Accordingly, we define the Megasequence 3 lower boundary at the base of the *Madot Formation* (~448 Ma, upper Katian), in a slightly higher stratigraphic position than Verniers et al. (2002) and Sintubin et al. (2009). Indeed, the transition documents a drastic change in palaeobathymetry, from deep-sea to shallow shelf (Fig. 4) accompanied by an important volcanic episode (see Section 5). The sedimentation changed abruptly from black pyritic slate (*Fauquez Formation*) interpreted as mud-turbidites deposited on the slope (Herbosch et al., 1991; NCS, 2011) to shelly facies and volcano-sedimentary cross-bedded tuff (*Madot Formation*, from 100 to >220 m according to the abundance of volcanic rocks) deposited on a very shallow shelf (NCS, 2011; Herbosch et al., in press-b). André (1991) and Verniers et al. (2005) gave a detailed description of these Madot volcanic and volcano-sedimentary rocks that are particularly abundant in the Sennette valley.

Megasequence 3 records shelf deposition from upper Katian to the upper Telychian (*Madot, Brutia* and *Bois Grand-Père formations*, about 500 m thick together) that evolved rapidly into deep-sea turbiditic deposits from the upper Telychian to the Gorstian (Fig. 4). Thick turbidite sequences are well developed from the upper Telychian (*Fallais Formation*, 500 to 600 m thick), continued during the Sheinwoodian and Homerian (*Corroy*, *Petit Roeulx*, *Steenkerque*, *Froide Fontaine* and *Vichenet formations*, together about 1200 m in c. 5 m.y.) and lasted until the Gorstian (*Ronquières Formation*, 540 to 600 m thick). These turbidites were distal at first, and more proximal from the end of Sheinwoodian onwards.

As a whole, the mean thickness of Megasequence 3 is estimated to be about 3400 m in the outcropping area (Verniers et al., 2001, 2002; Fig. 6). This important thickness, reflecting an acceleration of the subsidence from the upper Telychian (upper Llandovery), has been interpreted as heralding the onset of a Silurian foreland basin (Van Grootel et al., 1997; Debacker, 2001; Verniers et al., 2002). The upper part of Megasequence 3 is only known in boreholes (Verniers and Van Grootel, 1991; Fig. 4) and ended at c. 415 Ma (lowermost Lochkovian). No younger rocks are known in the Brabant Massif until the deposition of the Givetian conglomerates (*Bois de Bordeaux Formation*) belonging to the Brabant Parautochthon sedimentary cover. The latter deposited after the "Brabantian orogeny", responsible for the Early Devonian hiatus (tectonic inversion of the Brabant Massif; see Section 4 below), is located to the north and below the Variscan overthrust, which induced very limited movements in the northern part of this cover.

3.4. Subsidence analysis

The cumulative thickness curve for the whole Lower Palaeozoic sedimentary pile constructed by Debacker (2001) on the basis of the stratigraphical thicknesses of Verniers et al. (2001) has been repeatedly used (Verniers et al., 2002; Debacker et al., 2005; Sintubin et al., 2009) as an evidence for an extensional basin for Megasequence 1 (concave-up form), a non conclusive environment for Megasequence 2 (nearly straight curve) and the development of a foreland basin for Megasquence 3 (convex-up curve; see also Van Grootel et al., 1997).

New estimates of the sedimentary thicknesses, especially in Megasequences 1 and 2 (Herbosch et al., 2008a, in press-a,b; NCS, 2009, 2011) allow to us construct the cumulative thickness curve presented in Fig. 6. This curve is not a subsidence curve, because compaction and water column were not corrected for. Nevertheless, this curve reveals the major changes in rate of sedimentation. Megasequence 1 shows a very high sedimentation rate, especially from Blanmont to Jodoigne Formations (about 8 km deposited in 27 m.y.), only compatible with a rift environment. Megasequence 1 curve is concave-up, the Mousty and Chevlipont formations showing a slower sedimentation rate, announcing the Avalonia–Gondwana drifting marked by the Early Ordovician hiatus.

After this hiatus, Megasequence 2 began with a low sedimentation rate (from Abbaye de Villers to Rigenée formations; Fig. 6). This rate progressively increased from Ittre to Fauquez formations, which correspond to deep marine turbiditic sedimentation linked to incipient tectonic instability accompanied by volcanism.

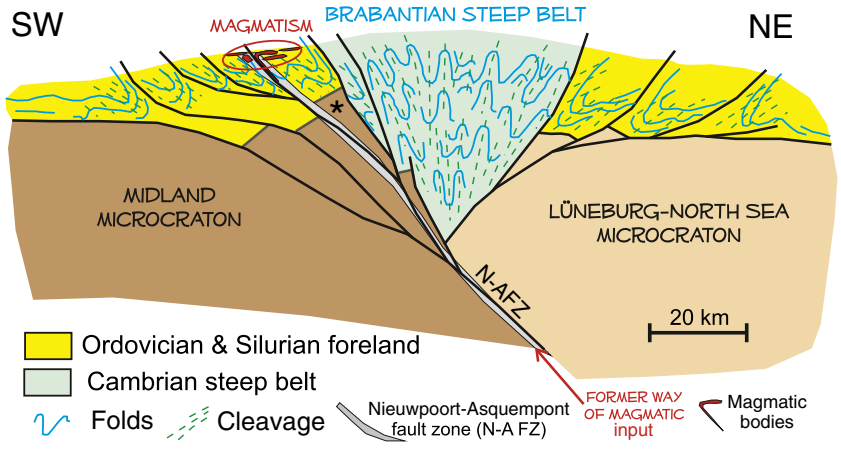

Fig. 5. Schematic (conceptual) SW–NE cross-section of the Brabantian belt along the Dendre River (see Fig. 2). Modified from Sintubin and Everaerts (2002) and Sintubin et al. (2009).

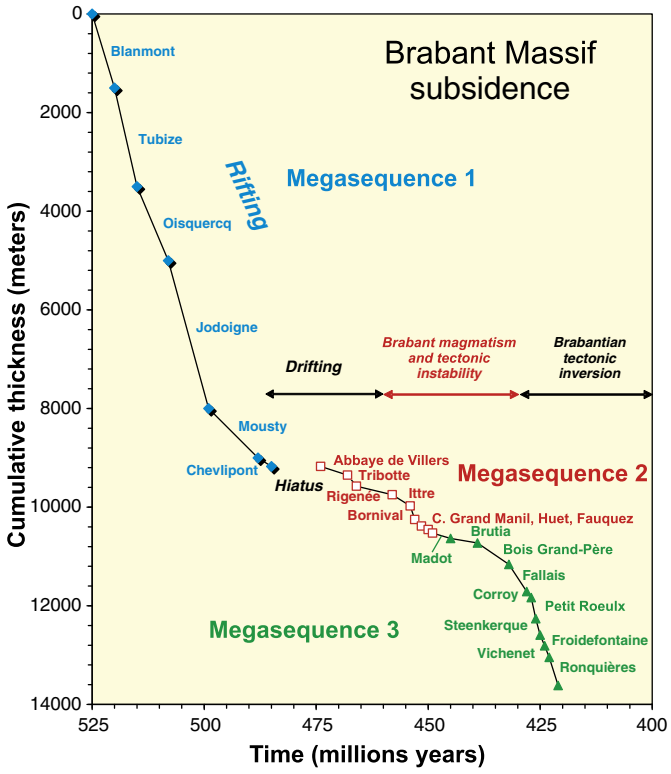

Fig. 6. Cumulative thickness curve of the Lower Palaeozoic sediments (by formation) of the Brabant Massif plotted against the stratigraphic age (time-scale from Ogg et al., 2008). For Megasequence 1 thicknesses are estimated minimum thicknesses (Herbosch et al., 2008a; NCS, 2009), for the Megasquence 2 it is mean thickness (Verniers et al., 2001, 2002; Herbosch, 2005; NCS, 2011) and for Megasequence 3 it is also mean thickness (Verniers et al., 2001, 2002).

Megasequence 3 marked a new slowdown of the sedimentation rate in its lower part (Madot and Brutia formations; Figs. 4 and 6), a progressive increase from Bois Grand-Père to Fallais formations and finally a very rapid rate of sedimentation from Corroy to Ronquières formations (about 1800 m in c. 7 m.y.; Fig. 6); corresponding to the development of the rim foreland basins, contemporaneous with the Brabantian tectonic inversion.

Subsidence curves for Cambrian–Ordovician sequences from Eastern Avalonia (Anglo-Welsh Basin; Prigmore et al., 1997) reveal four periods of regionally enhanced basement subsidence: the first, poorly dated, in the Early-Middle Cambrian, the second in the late Cambrian–Early Tremadocian, the third mid-Ordovician restricted to the southeast margin of the Welsh Basin and the fourth during the Caradocian. Grossly, this subsidence curve is similar to that of the Brabant Massif. A tight comparison is however not possible on the basis of the available documents because the local and international stratigraphy (Ogg et al., 2008; Gregory, 2011) has strongly changed since the pioneering work of Prigmore (1994).

4. The "Brabantian orogeny"

Since Fourmarier (1920), deformation within the Brabant Massif, or the "Brabantian orogeny", is unanimously considered to have taken place between the end of Gorstian (c. 422 Ma) and the Givetian (c. 390 Ma), leaving a time hiatus of about 32 Ma. These ages correspond respectively to the youngest deformed basement rocks in outcrop (*Ronquières Formation*) and the oldest cover rocks above the major Brabantian unconformity (*Bois de Bordeaux Formation*), at the base of the Brabant Parautochthon (Fig. 4). This hiatus was further narrowed by the discovery of Pridoli to lowermost Lochkovian (c. 415 Ma) deposits under the unconformity in borehole (Verniers and Van Grootel, 1991; Van Grootel et al., 1997). However, the nature, timing and geodynamic significance of the "Brabantian orogeny" have only been established recently (Sintubin et al., 2009 and references therein). By contrast to the old view of an anticlinal culmination, the architecture of the Brabant Massif is currently interpreted as a NW–SE trending compressional wedge consisting of a central steep belt composed of predominantly Cambrian metasediments, symmetrically bordered by less deformed Ordovician and Silurian metasediments (Fig. 5; Sintubin and Everaerts, 2002; Verniers et al., 2002; Debacker et al., 2005).

The sudden increase of subsidence and the installation of a deep marine turbiditic sedimentation in the late Telychian (c. 430 Ma; Fig. 4) mark the onset of a foreland-basin development in the Brabant rim domain. This suggests that a tectonic inversion began around 430 Ma in the Cambrian core of the massif. This inversion is called "Brabantian orogeny" (Debacker et al., 2005) by reference to the pioneering work of Michot (1980). The Early Devonian hiatus in the Brabant Parautochthon and the Silurian to lower Lochkovian reworked acritarchs (Steemans, 1989) found in the Lower Devonian just to the south in the Dinant Basin (belonging to the Ardenne Allochthon) suggest that the central part of the Brabant Massif emerged since the Lochkovian (Fig. 4). From the middle Silurian to Early Devonian, the progressive deformation results in a continued rising and steepening of the core and a gradual spreading of the deformation toward the rim of the massif. This Brabantian inversion cannot have lasted after c. 390 Ma, the age of the oldest undeformed rocks in the Brabant Parautochthon, the Bois de Bordeaux Formation (Fig. 4). Considering that the Burnot conglomerates (Late Emsian to Early Eifelian, 399–396 Ma) in the northern rim of the Dinant Basin resulted from the last increment of deformation of the Brabantian orogeny and using $^{40}Ar/^{39}Ar$ ages (426 to 393 Ma) on syn- to post-cleavage metamorphic muscovite/sericite grains, Debacker et al. (2005) placed the end of the Brabantian orogeny at c. 393 Ma, thus at the end of the Early-partly Middle Devonian hiatus (Fig. 4).

Detailed field studies have shown that throughout the outcropping areas, there is evidence for one single progressive deformation event only. The main features associated with this deformation are folds cogenetic with a well-developed axial plane cleavage: in the core, steeply plunging folds are associated with subvertical to steeply dipping cleavage while towards the south-eastern side, subhorizontal to gently plunging folds are associated with steep to moderately north dipping cleavage (Sintubin, 1999; Debacker, 2001, 2002; Verniers et al., 2002; Debacker et al., 2003, 2004b, 2005; Debacker, 2012; Fig. 5). The steepening of the central Brabant core could also explain the development of pre-cleavage and pre-folding low angle detachments at the edges of the steep core like the "Asquempont Detachment System" described by Debacker (2001) (Fig. 2B) and systematically observed during the geological mapping of the outcropping area (Fig. 3; Debacker et al., 2003, 2004a, 2004b, 2011; Debacker and Sintubin, 2008; Herbosch and Blockmans, in press; Herbosch et al., in press-a,b).

There is a main structure running NW–SE on the eastern flank of the Brabant Massif: the Nieuwpoort-Asquempont fault zone (Legrand, 1968; N-AFZ in Figs. 2B and 5), marked by a pronounced aeromagnetic and gravimetric lineament (Debacker et al., 2004b and references therein). Although initially considered as a strike-slip fault zone (André and Deutsch, 1985), recent observations indicate that this fault zone corresponds to subvertical movements along normal faults (Debacker et al., 2003; 2004b; 2011). These normal faults have been repeatedly reactivated, especially at c. 375 Ma (Frasnian–Famennian boundary; André and Deutsch, 1985), but also in historical times (1938 Grammont earthquake; Legrand, 1968).

The rapidly decreasing intensity of deformation to the SW of the N-AFZ (Fig. 5) and the inferred presence at depth of the Midlands microcraton to the SW and the Lüneburg-North Sea microcraton to the NE, led Sintubin and Everaerts (2002) to propose that the

Brabatian orogeny was the result of the convergence of these two microcratons (Figs. 2A, 5). This convergence would be the result of the anti-clockwise rotation of the former (Piper, 1997), during an intra-continental process within the Avalonia microcontinent (Sintubin and Everaerts, 2002; Sintubin et al., 2009).

5. Magmatism in the Brabant Massif

5.1. Description and literature data

The main igneous activity in the Brabant Massif extends from the Late Ordovician up to the mid-Silurian (Fig. 4) and is located in an arcuate belt along the south-western margin of the massif (Fig. 2B; André et al., 1986b, 1991; Verniers et al., 2002). It has been interpreted as related to a continental active margin (André et al., 1986b) or a volcanic arc (Van Grootel et al., 1997) and the presence of an important negative gravimetric anomaly suggested the presence of a granitic batholith, underlying the magmatic arc (Everaerts et al., 1996; Mansy et al., 1999). However, this low-density body is now interpreted as an elevated cratonic basement block in the framework of a compressional wedge model (Sintubin and Everaerts, 2002; Fig. 5). On the other hand, most original mineralogical features of the Brabant intrusive and extrusive rocks have been obliterated by late magmatic hydrothermal activity, greenschist facies recrystallization and penetrative deformation which also strongly modified the abundance of the most mobile elements (André and Deutsch, 1985, 1986b). This makes the geochemical characterization of these magmatic rocks and the determination of their palaeo-tectonic setting difficult (see below).

The interbedded volcanic rocks comprise a large proportion of pyroclastic rocks (ash fall and ignimbrite) of dacitic and rhyolitic composition. The earliest known volcanic activity started in the lower Tremadocian of the Chevlipont Formation where interstratified metarhyolite have been observed in boreholes and outcrops (Marcq area; Debacker, 1999; Verniers et al., 2002). Other volcanic rocks are observed in the Sandbian (e.g. Leffinge borehole, Verniers and Van Grootel, 1991; rhyolite at the base of Ittre Formation, Debacker et al., 2003) and also in the middle Katian with the eruptive center of Deerlijk. The activity reached a peak in the Late Katian during the deposition of the Madot Formation. Good outcrops of this Madot magmatic suite shows a volcanic complex made up of dacitic lavas, mud-flow breccias and coarse or fine graded-bedded tuffs interbedded with slates (André et al., 1991; Verniers et al., 2005). These slates are precisely dated by chitinozoan from the upper part of the Katian (Pusgillian–Cautleyan: 451–447 Ma; Vanmeirhaeghe et al., 2005). Volcanic activity continued towards the Silurian until the end of Telychian but with an intensity decreasing with time. Important volcanic levels are the 30 to 40 meter-thick rhyolite (ignimbrite?) interstratified at the very base of the Silurian (upper part of the Brutia Formation; Verniers et al., 2002) and the "Pitet rhyolite" observed at many places in the upper Telychian (*Fallais Formation*; Verniers and Van Grootel, 1991).

Several hypabyssal microdioritic bodies intrude the Ordovician sediments in the same arcuate belt along the south-western margin of the massif (Fig. 2B). Best known are the Quenast plug and the Lessines and Bierghes sills, which are exploited in large quarries. The Quenast quartz diorite forms a 2 km-wide elliptic and steeply plunging plug-like body intruding the Middle to Upper Ordovician slates (André, 1991; Debacker and Sintubin, 2008). The sill complex of Lessines forms a gently dipping 800 m thick body with a lateral extension of more than 10 km. This is actually a series of thinner sills interlayered with Upper Ordovician slates (André, 1991; Herbosch et al., 2008b). The emplacement of the Quenast plug has been dated at 433 ± 10 Ma by Isotope Dilution-Thermal Ionisation Mass Spectrometry (ID-TIMS) (3-zircon fractions lower intercept age with one nearly concordant fraction; André and Deutsch, 1984), and that of Lessines sill at 414 ± 16 Ma (whole-rock Rb–Sr age; André and Deutsch, 1984). Structural analysis of the Ordovician slates around the Quenast plug shows that it was emplaced prior to the Brabantian deformation event of Late Telychian to Early Eifelian age (see Section 4; Debacker and Sintubin, 2008).

5.2. New U–Pb LA-ICP-MS ages of igneous and volcaniclastic rocks

Locations of investigated samples are shown in Table 2 and Figs. 2B and 3. Analytical techniques of the analysis of U–Pb isotopes of magmatic and inherited zircon by Laser Ablation Inductively Coupled Plasma Mass Spectrometry (LA-ICP-MS) are described in Annex 1 while instruments settings are given in Table 5 (data repository). Concordia diagrams (with 2σ error ellipses) and Concordia ages (95% confidence level) were produced using Isoplot/Ex 2.49 (Ludwig, 2001), and frequency and relative probability plots using AgeDisplay (Sircombe, 2004) software. The $^{207}Pb/^{206}Pb$ age was taken for interpretation for all zircons >1.0 Ga, and the $^{206}Pb/^{238}U$ ages for younger grains, considering the higher error on ^{207}Pb in that age range. Analytical results are given in Tables 6 to 17 (data repository).

On the seven (sub) volcanic units that have been selected only four have given results (Fig. 4): the Ittre rhyolite interbedded close to the base of Ittre Formation (Burrellian = Late Sandbian; Vanmeirhaeghe et al., 2005; Vanmeirhaeghe, 2006), the Madot volcano-clastic tuff and the Madot dacite, interbedded in the upper part of Madot Formation (Late Katian), and the Quenast quartz diorite intrusive in the Middle to Upper Ordovician slates. The Bierghes sill (Brab-18), the Brutia rhyolite (Brab-16) and the "Pitet" tuff (Brab-19) have not given suitable zircons for dating.

Eleven spots from *BRM21 Ittre rhyolite* give a concordant age of 459 ± 5 Ma (Fig. 8B), in excellent agreement with the Late Sandbian chitinozoan biostratigraphic age (458–456 Ma; Ogg et al., 2008; Fig. 4), and are interpreted to date the volcanic emplacement. Ten other spots give a concordant age of 486 ± 5 Ma (Fig. 8A). This age, clearly in excess of the stratigraphic ages, might be interpreted either in terms of inheritance from an (igneous) source of the magma, or in terms of xenocrystic zircons, possibly reworked from country-rocks during ascent and/or explosive volcanism. Whatever its precise interpretation, this c. 486 Ma age corresponds to the age of the volcanic rocks known in the lower Tremadocian (486–488 Ma) at the end of the Megasequence 1. These c. 486 Ma zircons can then be ascribed to this episode but also to the beginning of the hiatus period suggesting that the latter corresponds to an emersion (already announced by the Chevlipont Formation characterized by a shallowing trend and a slower subsidence rate), accompanied by volcanism. A few much older zircon grains have also been found at (concordant age based on one crystal each time; Fig. 8A: 1076 ± 37 Ma, 1479 ± 42 Ma, 2298 ± 39 Ma).

Six spots on *BRM23 Madot dacite* give a concordant age of 444 ± 6 Ma (Fig. 9), in agreement within errors with the well constrained Late Katian stratigraphic age of these volcanic submarine flows (451–447 Ma; Pusgillian to Cautleyan in Vanmeirhaeghe et al., 2005). An additional crystal gives a concordant age of 587 ± 15 Ma with a very low Th/U ratio of 0.03 (Table 8), suggesting that this zircon might be metamorphic in origin and has crystallized during the Late Neoproterozoic. Seven spots on *BRM19 Madot tuff* give a concordant age of 445 ± 2 Ma (Fig. 10), also in good agreement with the upper Madot Formation stratigraphic ages.

The Quenast plug has been dated earlier by the zircon ID-TIMS U–Pb method but the age calculated (433 ± 10 Ma) relied on one subconcordant fraction only, the three analyzed fractions determining a poorly constrained lower intercept (André and Deutsch, 1984). For this reason, it was interesting to further study this intrusion. The *Quenast quartz diorite BRM17* has delivered a large range of ages, the lower group of 9 spots giving a concordant age of 430 ±

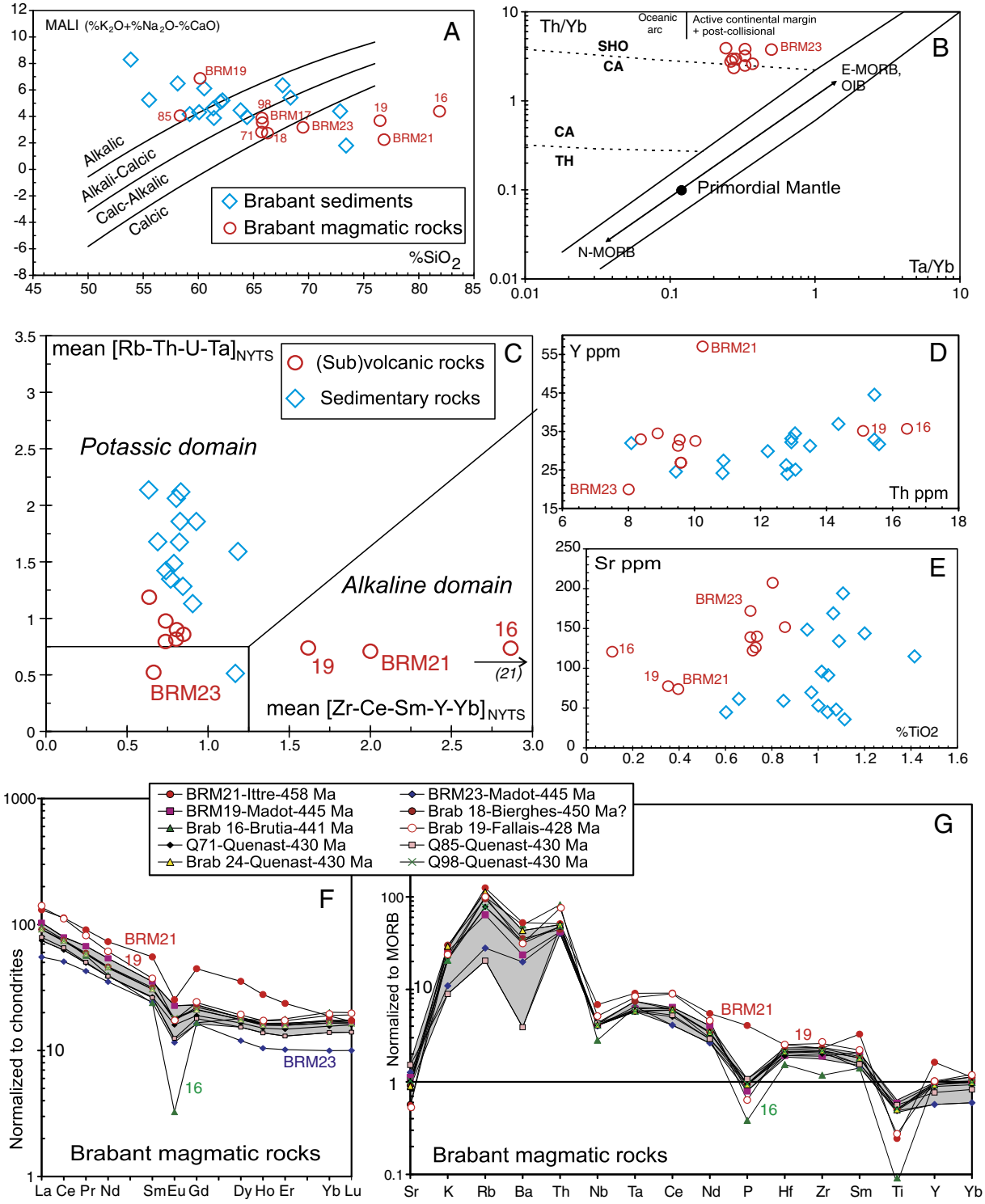

Fig. 7. Geochemistry of Brabant magmatic rocks (see text for explanation). (A) MALI diagram (Modified Alkali-Lime Index; Frost et al., 2001); (B) Th/Yb vs Ta/Yb diagram (Pearce, 1982a); (C) Sliding normalized values to the Yenchichi–Telabit reference series (Liégeois et al., 1998); (D) Y ppm vs Th ppm; (E) %TiO_2 vs Sr ppm; (F) Rare Earth Elements (REE) normalized to chondrites (Taylor and Mc Lennan, 1985); (G) Trace elements normalized to MORB (Sun, 1980; Pearce, 1982b). Gray areas in (F) and (G) enhanced the Brabant samples without outliers BRM21, BRM19, BRM23 and BRM16 whose respective positions in other diagrams are also shown when outside the main stream.

3 Ma (Fig. 11B), which, in the absence of any well-documented post-crystallization event likely to cause partial opening of the U–Pb radiometric system of zircons, is interpreted to date the intrusion of the Quenast plug. However, six other spots can be used to calculate a concordant age of 450 ± 4 Ma that could correspond, within error limits, to the Madot volcanism (Fig. 11A). A larger group of 25 spots give a concordant age of 479 ± 2 Ma, which might reflect an Early Ordovician zircon-forming event (Fig. 11 A) This age can be compared with the inherited age of 486 ± 5 Ma found in the Ittre rhyolite and can also be ascribed to the inferred volcanism of the hiatus period following Megasequence 1. Additional Neoproterozoic concordant ages based on a few crystals have been measured: 536 ± 10 Ma (1 spot), 565 ± 6 Ma (3 spots) and 620 ± 15 Ma (1 spot). High Th/U ratios suggest that these ages correspond to Pan-African magmatic events.

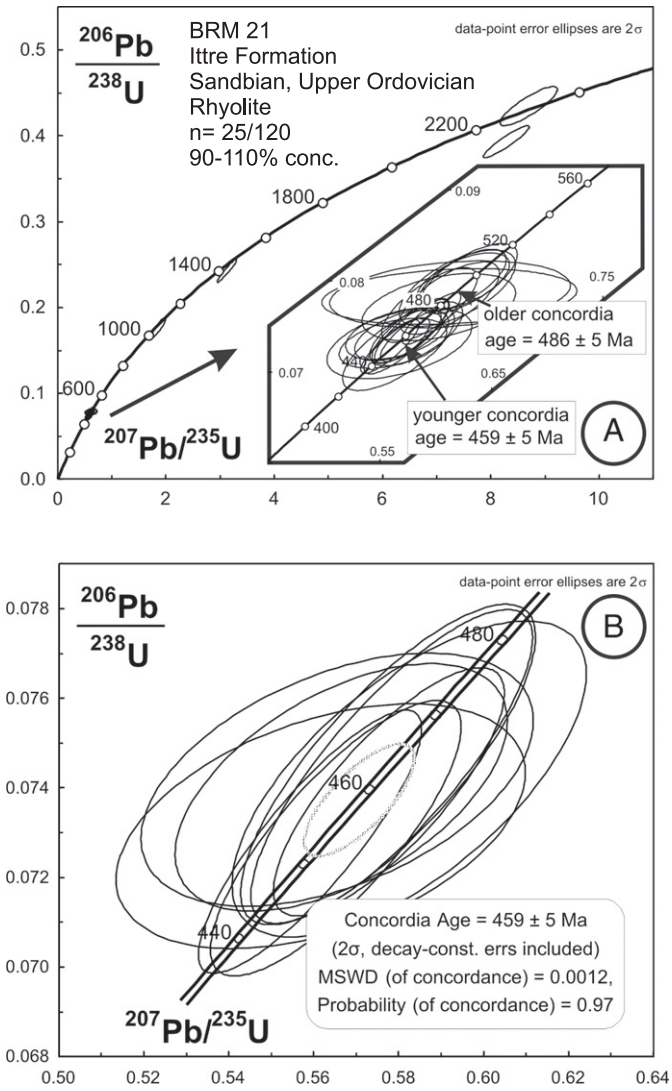

Fig. 8. Concordia plots of U–Pb zircon data of a rhyolite level at the base of the Ittre Formation (sample BRM 21, upper Sandbian, Upper Ordovician). (A) All zircon ages. (B) Concordia age of 459 ± 5 Ma from the youngest concordant grains, which is interpreted to as the age of extrusion.

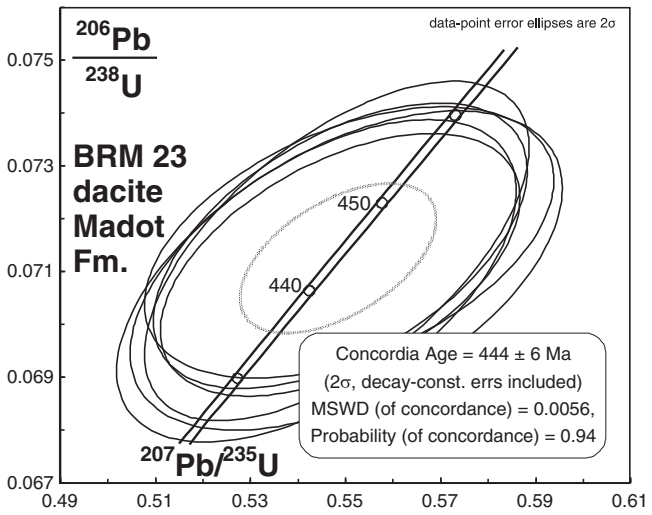

Fig. 9. Concordia plot of U–Pb zircon data of a dacitic submarine flow interbedded in the Madot Formation (sample BRM 23, upper Katian, Upper Ordovician). The Concordia age of 444 ± 6 Ma is interpreted to be the age of the extrusion.

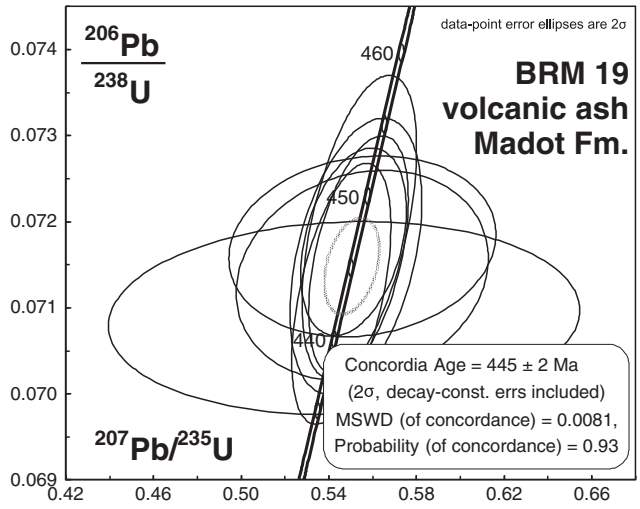

Fig. 10. Concordia plot of U–Pb zircon data of a volcano-sedimentary ash (cross stratification) thick level in the Madot Formation (sample BRM 19, upper Katian, Upper Ordovician). The Concordia age of 445 ± 2 Ma is interpreted to be the age of extrusion and reflect the age of sedimentation.

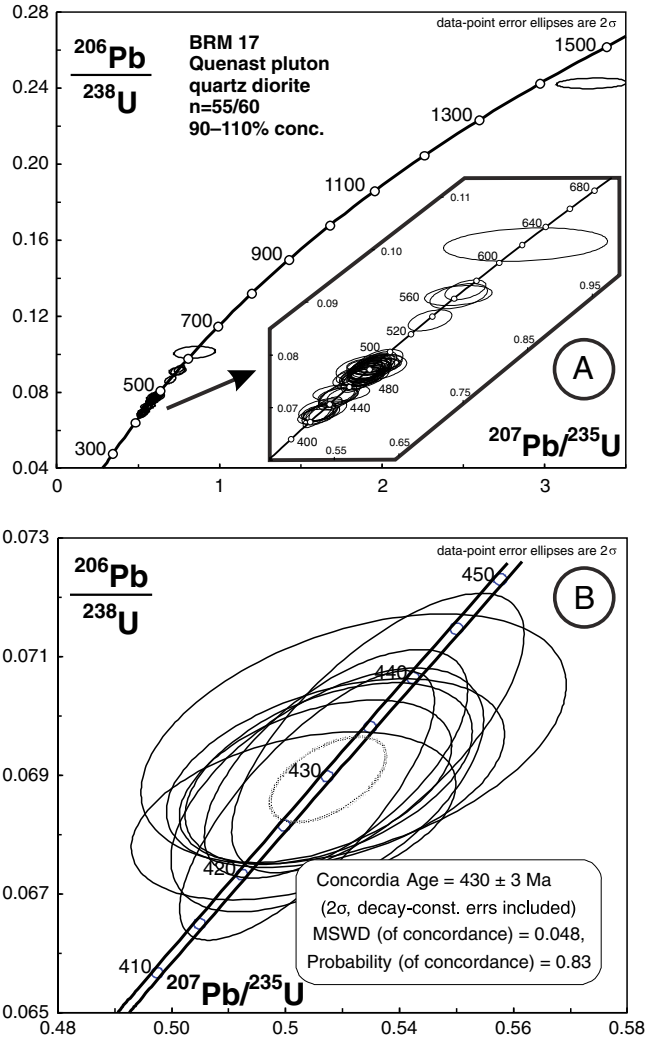

Fig. 11. Concordia plots of U–Pb zircon data of a quartz diorite from the Quenast pluton that intruded into Middle to Upper Ordovician sedimentary rocks (sample BRM 17). (A) All zircon ages. (B) Concordia age of 430 ± 3 Ma from the youngest concordant grains, which is interpreted as the age of extrusion.

A last grain gives discordant ages, but its $^{207}Pb/^{206}Pb$ age of 1595 ± 101 Ma provides a minimum estimate for its crystallization (Fig. 11 A).

These new LA-ICP-MS ages are all concordant within analytical uncertainties and provide geological constraints. They agree with the geological observation that showed that the Ittre and Madot volcanic units are interbedded flows or tuffs and extruded during the sedimentation of the Ittre and Madot formations. (Debacker et al., 2003, 2004b; NCS, 2011; Herbosch et al., in press-b). The Quenast plug is now more precisely dated at 430 ± 3 Ma. Older grains found in the Quenast plug and the Ittre volcanics reveal the existence of a well defined (35 zircon spots as a whole) igneous zircon forming event in the 490–480 Ma timespan, indicating that the Chevlipont Formation and the stratigraphical hiatus observed in the Lower Ordovician probably reflect an uplift process that was accompanied by a magmatic episode. In addition, the Brabant rocks contain Late Neoproterozoic zircons that suggest the presence at depth of a Pan-African segment, with some minor Palaeoproterozoic inheritance, except if all these zircons have been incorporated from the Brabant Cambrian sediments during ascent.

5.3. Geochemistry of the Brabant magmatic rocks

Sample location and description are shown in Table 1 and Figs. 2, 3 and 4. Major and trace element analyses can be found in Table 3. Geochemical analyses were done at Centre de Recherche Pétrographique et Géochimique at Nancy (France), following analytical techniques described in Annex 2. Major elements have been recalculated to 100% on an anhydrous basis, as recommended by IUGS (Le Maitre et al., 2002).

The Brabant magmatic rocks, now dated between 460 and 430 Ma have been affected by deformation and metamorphism, and altered by interactions with fluids giving rise to a secondary assemblage including chlorite, sericite, pyrite and carbonates. This was accompanied by significant disturbances of the most mobile elements such as K, Na, Rb, Sr, Ba, and U (André and Deutsch, 1985; Van Grootel et al., 1997). These most mobile elements, the large-ion lithophile elements (LILE) are actually the main constituents of plagioclase and K-feldspar that are, together with quartz, used for giving a name to the rocks (Le Maitre et al., 2002) and, in a more general way to attribute magmatic rocks to a series, especially for magmatic rocks of intermediate and acid compositions (e.g. Rickwood, 1989; Frost et al., 2001). This is well shown in the MALI diagram (Frost et al., 2001), a relooking of the initial classification of Peacock (1931) in alkalic, alkali-calcic, calc-alkalic and calcic series (Fig. 7A): the Brabant magmatic rocks display a trend strongly oblique to the igneous trajectories and one sample has a non-magmatic silica content >80% (Brab-16, Brutia rhyolite). This means that alkalies and LILE in general cannot be used for classifying the Brabant magmatic rocks, or with much care. Using only ratios of immobile elements (Fig. 7B), the Brabant magmatic rocks are tightly grouped in the high-K calc-alkaline ("shoshonitic") field. This signature can be present in active continental margins but is particularly abundant in post-collisional and in syn-orogenic intracontinental settings (Liégeois et al., 1998, 2003; Fezaa et al., 2010). The clustered position suggests that these elements indeed behaved as incompatible elements during a magmatic differentiation (liquid line of descent from basaltic andesites to dacites; André, 1991), implying that these ratios are close to that of the source. If considering the potential compatibility of these elements in these silicic rocks, the values of the Ta/Yb and Th/Yb should be considered as minimum, a correction implying even a more "shoshonitic" character. Taking into account the silica content of the rocks (varying from 57% to 75%, with one sample at 81%) using the sliding normalization (Fig. 7C; Liégeois et al., 1998), most of the Brabant magmatic rocks cluster in the potassic domain, with one sample in the normal calc-alkaline domain (BRM 23) and 3 samples in the alkaline domain (Brab-16, 19 and BRM 21), at odds with the sedimentary rock trend. This disposition is confirmed in the Y vs Th diagram (Fig. 7D), two immobile elements, where these four samples are either depleted or

Table 1
Description and location of sample used for geochemical and isotopic analysis (classified by stratigraphic age).

Sample	Lithology	Lithostratigraphy	Chronostratigraphy	Location	Coordinates
(Meta-)sedimentary rocks					
Brab-1	Biotite slate	Blanmont Formation	Lower Cambrian, Stage 2/3	Opprebais quarry, Opprebais	N 50°41′10.43″; E 4°48′15.60″
Brab-2	Green slate	Lower Tubize Formation	Lower Cambrian, Stage 3	Mont St Guibert, under church	N 50°38′00.11″; E 4°36′37.54″
Brab-3	Green slate	Middle Tubize Formation	Lower Cambrian, Stage 3	Rogissart, Tubize	N 50°40′46.73″; E 4°14′04.59″
Brab-9	Green slate	Upper Oisquercq Form.	Middle Cambrian, Stage 5	Hospice de Rebecq, Rebecq	N 50°39′45.06″; E 4°08′08.97″
Brab-22	Green slate	Upper Oisquercq Form.	Middle Cambrian, Stage 5	Km 40.95 canal trench, Asquempont	N 50°38′40.11″; E 4°14′22.44″
Brab-4	Black slate	Lower Jodoigne Formation	Middle Cambrian, Stage 5/Drumian	Temporary excavation, Orbais	N 50°41′49.85; E 4°50′26.10″
Brab-5	Black slate	Upper Jodoigne Formation	Middle Cambrian, Ghuzhangian	Old Grand Moulin, Jodoigne	N 50°43′38.26″; E 4°51′53.33″
Brab-6	Black slate	Middle Mousty Formation	Upper Cambrian, Stage 9	32.9 m Noirha borehole, Noirha	N 50°37′47.70″; E 4°32′10.89″
Brab-13	Black slate	Upper Mousty Formation	Upper Cambrian, Stage 10	15 m Tangissart borehole, La Roche	N 50°36′22.17″; E 4°32′14.93″
Brab-23	Gray slate	Chevlipont Formation	Lower Ordovician, Tremadoc	357 m Lessines borehole, Lessines	N 50°42′48″; E 3°51′46″
Brab-7	Argillaceous siltite	Abbaye de Villers Form.	Lower Ordovician, Floian/Dapingian	Abbaye de Villers, Villers-la-Ville	N 50°35′38″; E 4°31′47″
Brab-8	Gray slate	Rigenée Formation	Middle Ordovician, Darriwilian/Sandb.	Cocriamont Castle Park, Villers-Ville	N 50°34′07.00″; E 4°30′31.67″
Brab-20	Dark slate	Ittre Formation	Upper Ordovician, Sandbian/Katian	214 m Lessines borehole, Lessines	N 50°42′48″; E 3°51′46″
Brab-21	Black slate	Fauquez Formation	Upper Ordovician, Katian	149 m Lessines borehole, Lessines	N 50°42′48″; E 3°51′46″
Brab-10	dark gray slate	Middle Brûtia Formation	Base Silurian, Rhuddanian	Grand-Manil old quarry, Gembloux	N 50°33′08.92″; E 4°40′49.76″
Brab-11	Gray slate	Bois Grand-Père Form.	Silurian, Aeronian/Telychian	Grand-Manil, Gembloux	N 50°33′06″; E 4°41′09″
Brab-12	Green slate	upper Fallais Formation	Silurian, upper Telychian	Km 2.81 railway trench, Corroy	N 50°32′44.68″; E 4°41′19.05″
Intrusive and volcanic rocks					
BRM 21	Rhyolite	Base Ittre Formation	Upper Ordovician, mid Sandbian	Old railway trench, NW Asquempont	N 50°38′44.56″; E 4°13′41.50″
BRM 23	Dacite	Upper Madot Formation	Upper Ordovician, upper Katian	"Bois des Rocs", Fauquez	N 50°37′32.11″; E 4°13′09.71″
BRM 19	Tuff	Upper Madot Formation	Upper Ordovician, upper Katian	Km 24.4 railway trench, Hennuyères	N 50°38′40.43″; E 4°10′13.22″
Brab-16	Rhyolite	Upper Brûtia Formation	Lowest Silurian, Rhuddanian	Grand-Manil old quarry, Gembloux	N 50°33′07.80; E 4°40′49.93″
BRM 17	Microdiorite	Quenast pipe	Silurian, upper Telychian	Quenast quarry, Quenast	N 50°39′47.10″; E 4°09′24.44″
Q 71	Microdiorite	Quenast pipe	Silurian, upper Telychian	Quenast quarry, Quenast	N 50°39′47.10″; E 4°09′24.44″
Q 85	Microdiorite	Quenast pipe	Silurian, upper Telychian	Quenast quarry, Quenast	N 50°39′47.10″; E 4°09′24.44″
Q 98	Microdiorite	Quenast pipe	Silurian, upper Telychian	Quenast quarry, Quenast	N 50°39′47.10″; E 4°09′24.44″
Brab-18	Microdiorite	Bierghes sill	unknown, probably Silurian	Bierghes quarry, Bierghes	N 50°41′15.21″; E 4°06′00.14″
Brab-19	Tuff	Upper Fallais Formation	Silurian, upper Telychian	Km 2.8 railway trench, Grand-Manil	N 50°32′44.68″; E 4°41′19.05″

enriched relative to the main group. Samples Brab-16, Brab-19, BRM 21 are also depleted in Sr and TiO_2 relatively to the main group (Fig. 7E).

Rare earth elements (REE) of the main group are tightly grouped with enriched LREE (La_N: 75–104) and HREE (Yb_N: 14–17) with a moderate LREE/HREE fractionation (La_N/Lu_N: 4.7–6.2) and Eu negative anomalies (Eu/Eu*: 0.57–0.78) (Fig. 7F). These are typical values for high-K calc-alkaline and alkali-calcic granitoids (Liégeois et al., 1998). This is confirmed by other high-field strength elements (HFSE; Fig. 7G) where Nb–Ta anomaly relative to Ce is absent (Ta) or weak (Nb), a continuous decrease from Ta towards Yb, with the exception of Ti and P negative anomalies due to crystal fractionation (apatite, oxides, titanite). The gray area, which underlines the patterns of the main group, shows the much larger variation of LILE, especially K, Rb and Ba, constituent of the K-feldspar largely altered in Brabant rock specimens. Sample Brab-16 has a REE pattern within the main range but except a much more negative Eu anomaly (Eu/Eu* = 0.16; Fig. 7F); coupled with low concentrations in P, Zr, Hf and Ti (fractionation of apatite, oxides, titanite and zircon), this indicates that Brab16 was a highly differentiated rock, probably with a silica content around 76–78%. Samples BRM 21 and Brab-19 are enriched in most incompatible elements. This is particularly spectacular for REE pattern (Fig. 7F) but also for the other HFSE (Fig. 7G) for sample BRM 21. The SumREE is 236 ppm for sample 17 and 211 ppm for sample Brab-19 (compared to 104–167 ppm for other samples); LREE/HREE fractionation is higher ($La_N/Lu_N > 7$ for 4.7–6.2 for the main group). These characteristics can be partly related to their higher silica content (76% on an anhydrous basis compared to 58–66% for the main group) but probably also to a more enriched source.

Brab-17, 18, 19 and BRM 19 (58–74% silica), and the three Quenast samples (57–64% silica) have very similar patterns with high Th and LREE enrichment, strong fractionation of the LREE, almost not fractionated HREE at ca. 20 × chondritic abundances; small negative Eu anomaly; strong negative anomaly of Nb and Ti. Such profiles are fairly ubiquitous in igneous rocks of predominantly continental crustal origin. BRM 23 shows a broadly similar pattern, albeit with somewhat lower REE abundances. Brab-16 (81% silica) shows an extreme enrichment in Th (ca. 350 × chondrites); strong negative anomaly of Nb and Eu, and even more Ti; small negative anomaly of Zr; slight fractionation of the HREE with $(Gd/Lu)_N < 1$ (this cannot be ascribed to zircon fractionation which would produce the opposite trend). This rock probably reflects extreme igneous fractionation (with removal of plagioclase + Fe–Ti oxides, and some zircon) or hydrothermal alteration, or both. BRM 21 (74.5% silica) possesses a distinct fractionation of the HREE, with $(Gd/Lu)_N > 1$; this points to the fractionation of one or several phases enriched in HREE, possibly zircon pro parte (cf. the slight negative anomaly of Zr), and also garnet which might have been left in the solid residue following the partial melting and the extraction of a rhyolitic magma in the lower crust (in line with its fairly unradiogenic Nd isotope signature, $\varepsilon_{Nd} = -5$; see next section).

Put together and attempting to "see" through the strong alteration that affected these rocks, these geochemical analysis point to high-K calc-alkaline to alkali-calcic character, despite their relatively variable concentrations in K_2O and Na_2O that are attributed to a loss of alkalies during metamorphism.

5.4. Nd isotopic signature of the magmatic rocks

Analytical techniques are described in Annex 3. Locations of the same seven (sub)volcanic samples selected for dating are shown in Table 1. Nd isotope ratios have been corrected for in situ decay of ^{147}Sm and expressed by using the usual epsilon notation (Table 4).

For all but one sample, initial ε_{Nd} values show a restricted range from −3.7 to −4.9, while T_{DM} model ages are between 1.32 and 1.73 Ga. Considering a two-stage model, depleted mantle ages (taking a mean crustal Sm/Nd ratio for the pre-intrusion source evolution) are less scattered: 1.23–1.33 Ga. The distinctly unradiogenic Nd isotopes indicate that the volcanics were predominantly derived from a source reservoir with a low time-integrated Sm/Nd ratio (that is, that was enriched in LREE during a substantial timespan). The continental crust is the best candidate for such source reservoir. The Brutia rhyolite Brab-16 departs from the other samples with a distinctly more radiogenic Nd isotope signature ($\varepsilon_{Nd} = -0.8$) and a younger T_{DM} estimate at 1.03 Ga. Clearly, its parent magma was extracted from more juvenile sources, or incorporated a significant component derived from a time-integrated depleted reservoir (with positive ε_{Nd} values). In both cases, the Brabant Nd isotope signatures suggest that a source region with Proterozoic average crustal residence ages were involved (Table 4). This should not be identified with any specific geologically defined segment, but rather represents the geochemical result of the blending of ancient recycled sedimentary components with more juvenile Neoproterozoic igneous components. Except possibly in the Brutia rhyolite, the contribution of depleted mantle sources was limited to a fairly subordinate role, although a mantle heat source was clearly required to account for the partial melting of lower crustal sources and the production of hot, relatively dry magmas having the potential to reach the surface.

The rather important proportion of Palaeoproterozoic material needed compared to the measured high Neoproterozoic/Palaeoproterozoic inherited zircon ratio indicate that the Neoproterozoic Brabant segment was itself largely the result of the reworking of a Palaeoproterozoic crust, as it is often the case in West Africa (Liégeois et al., 2003; Errami et al., 2009; Fezaa et al., 2010; Linnemann et al., 2011). Indeed, the Nd isotopic on whole-rock signature integrates the whole story of the magmatic source region (mean crustal residence) and does not give the same information as the zircon crystals (Liégeois and Stern, 2010; Stern et al., 2010). In conclusion, the Brabant magmatic rocks, including dioritic rocks, have a mainly old lithospheric, probably crustal, source.

5.5. Geodynamic interpretation of the Brabant magmatic rocks

5.5.1. The Brabant magmatic rocks are not subduction-related

The Brabant magmatic rocks have always been interpreted within the framework of a SSE-dipping subduction zone beneath the Brabant Massif preceding the closure of a mid-European ocean separating Baltica and Armorica (including the Midlands–Brabant microcraton; André et al., 1986b) or between Baltica and Avalonia (André, 1991; Pharaoh et al., 1991; Van Grootel et al., 1997) or within Avalonia terrane itself (between East and Far-East Avalonia; Verniers et al., 2002).

However, the arguments used for such an origin by subduction are not tenable any longer. Indeed: (1) the existence of a magmatic polarity marked by calc-alkaline magmatism to the north (Brabant) and tholeiitic magmatism to the south (Ardenne Allochthon, southern Belgium), interpreted respectively as arc and back-arc setting (André et al, 1986b), is invalidated by the gross difference in age between the Brabant Massif magmatism (460–430 Ma) and that of the Ardenne Inliers (380–360 Ma, Late Devonian; Kramm and Bühl, 1985; Goffette et al., 1991). Even a more complex diachronous arc/back-arc setting (André, 1991) cannot be envisaged when considering the Brabant tectonic evolution described above in this paper (Section 4; Fig. 4). (2) The calc-alkaline composition was considered as typical for a subduction setting (André et al., 1986b; Verniers et al., 2002) even though qualified as "uncommon" by André (1991). However the Brabant magmatic rocks are actually high-K calc-alkaline to alkali-calcic in composition, and of predominantly crustal origin (Fig. 7), which is uncommon in subduction settings but very frequent in post-collisional periods (Liégeois et al., 1998 and references therein), including intracontinental reactivations at a distance from the suture in response to continental convergence (Liégeois et al., 2003; Fezaa et al., 2010). (3) The now much better knowledge of the stratigraphy and sedimentology of the Brabant

Massif (Section 3, Fig. 4) reflects a passive margin setting, not an active continental margin. This is in excellent agreement with palaeomagnetic data that indicate that Avalonia was facing to the south the Rheic Ocean, for more than 100 million years, between 480 and 350 Ma (e.g. Cocks and Fortey, 2009). (4) There is no trench available at a reasonable distance, the nearest being located at several hundred km to the north-east (Tornquist Ocean; Fig. 22B).

5.5.2. The Brabant magmatic rocks are related to the reactivation of an intracontinental boundary zone

The Brabant magmatic rocks intruded during the 460–430 time span, with most of the magmatic events between 450 and 430 Ma (Fig. 4). These magmatic bodies are aligned in a narrow band

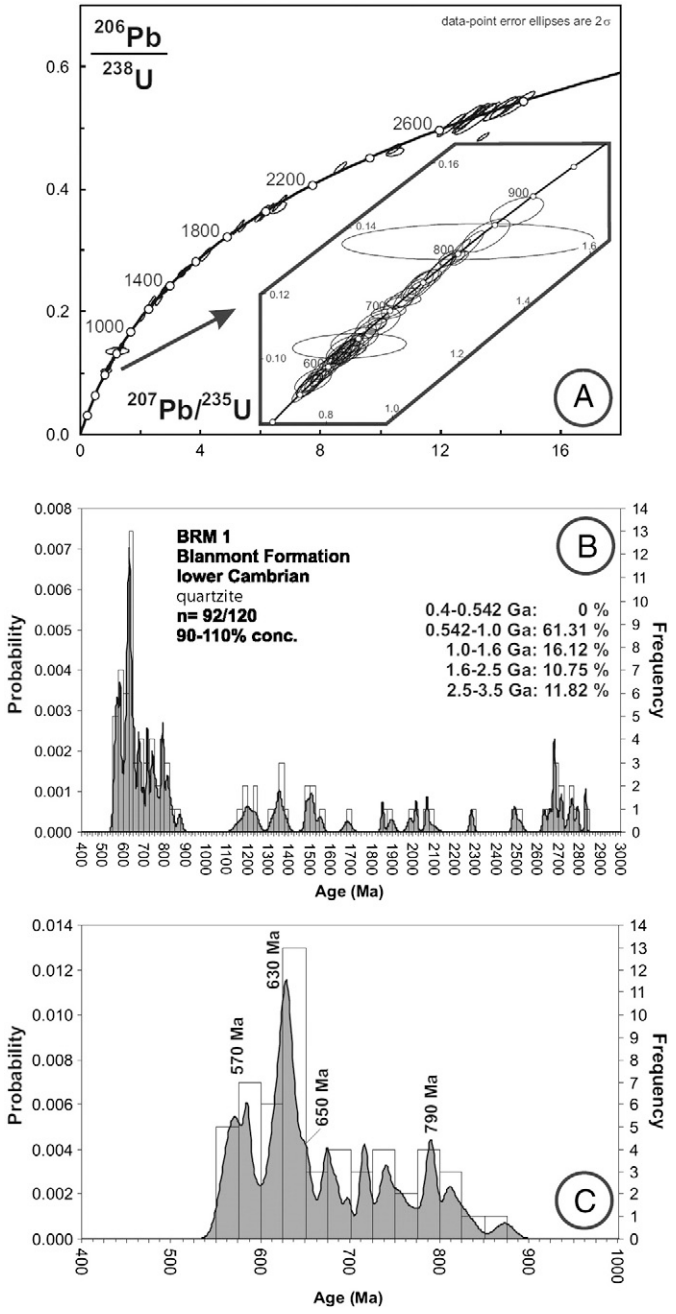

Fig. 12. U–Pb ages of detrital zircon grains from sample BRM 1 (quartzite, Blanmont Formation, lower Cambrian). Concordia diagram (A) and combined binned frequency and probability density distribution plots of detrital zircon grains in the range of 400 to 3000 Ma (B) and of 400 to 1000 Ma (C).

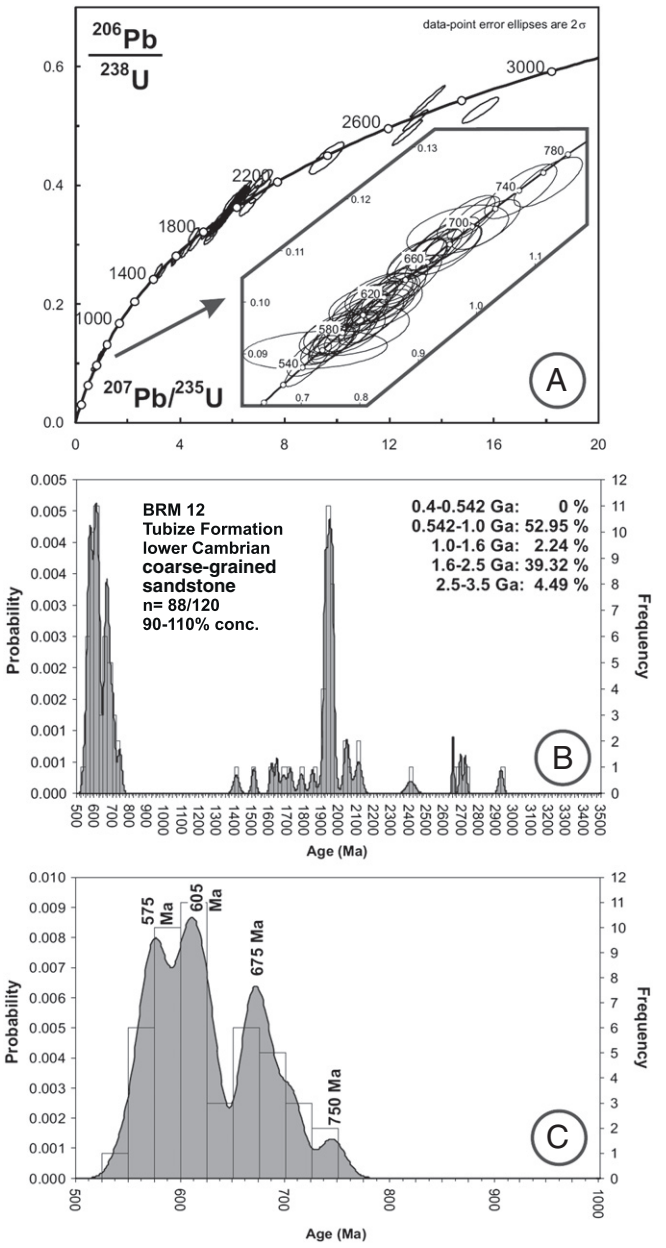

Fig. 13. U–Pb ages of detrital zircon grains from sample BRM 12 (coarse-grained sandstone, Tubize Formation, lower Cambrian). Concordia diagram (A) and combined binned frequency and probability density distribution plots of detrital zircon grains in the range of 400 to 3500 Ma (B) and of 400 to 1000 Ma (C).

following the NW–SE oriented Nieuwpoort-Asquempont fault zone (N-AFZ; Fig. 2B), corresponding to the south-western boundary of the Cambrian rift and which also allowed later the uplifting of a low-density rigid block (Sintubin and Everaerts, 2002; Debacker et al., 2005). The most prominent movements observed along the N-AFZ are subvertical (normal faults), post-cleavage and Late Devonian in age (Debacker et al., 2003, 2004b; Debacker and Sintubin, 2008) but reverse movements along this weakness zone during the Brabantian tectonic inversion are likely. Considering the tectonic instability that occurred during the emplacement of the Brabant magmatic rocks, we propose that extensional or transtensional movements occurred along the N-AFZ during that period, allowing magmas to be generated in the lower crust and to rise to the surface (Fig. 5). Indeed, 460 Ma corresponds to the sudden appearance of turbidites (onset of the deep marine sedimentation of upper Megasequence 2, Rigenée/Ittre formations; Fig. 4) and large-scale slumping processes

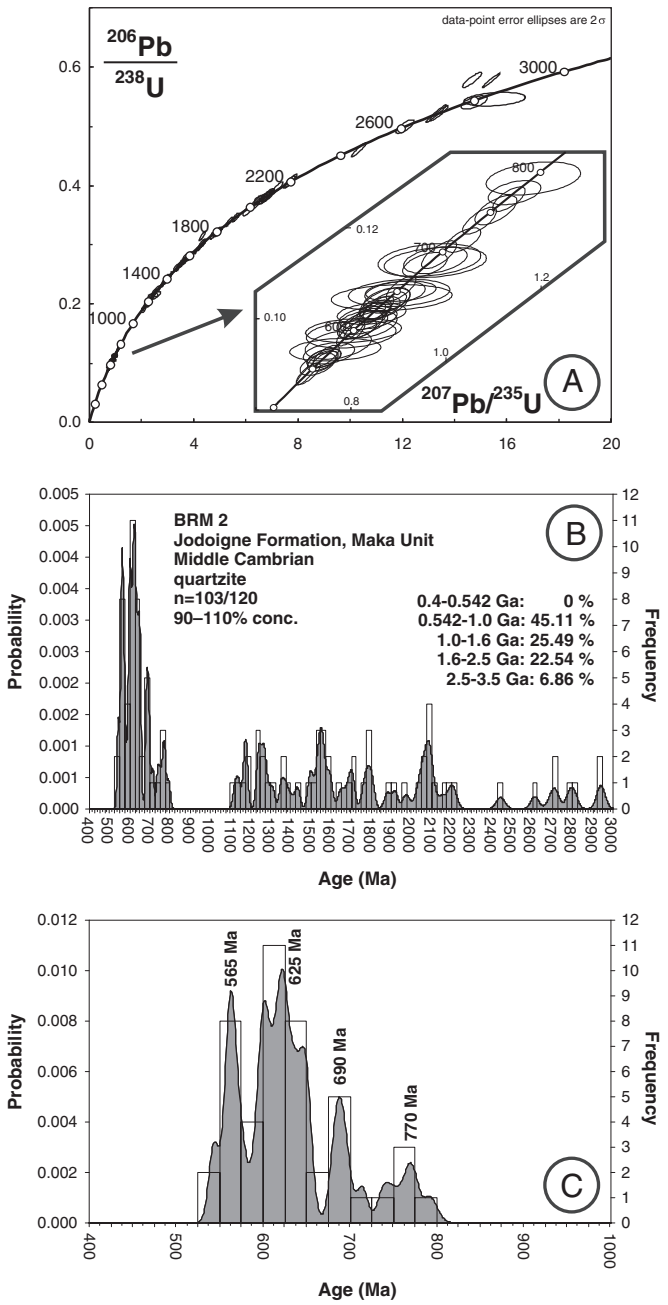

Fig. 14. U–Pb ages of detrital zircon grains from sample BRM 2 (quartzite, Jodoigne Formation, Maka Unit, middle Cambrian). Concordia diagram (A) and combined binned frequency and probability density distribution plots of detrital zircon grains in the range of 400 to 3000 Ma (B) and of 400 to 1000 Ma (C).

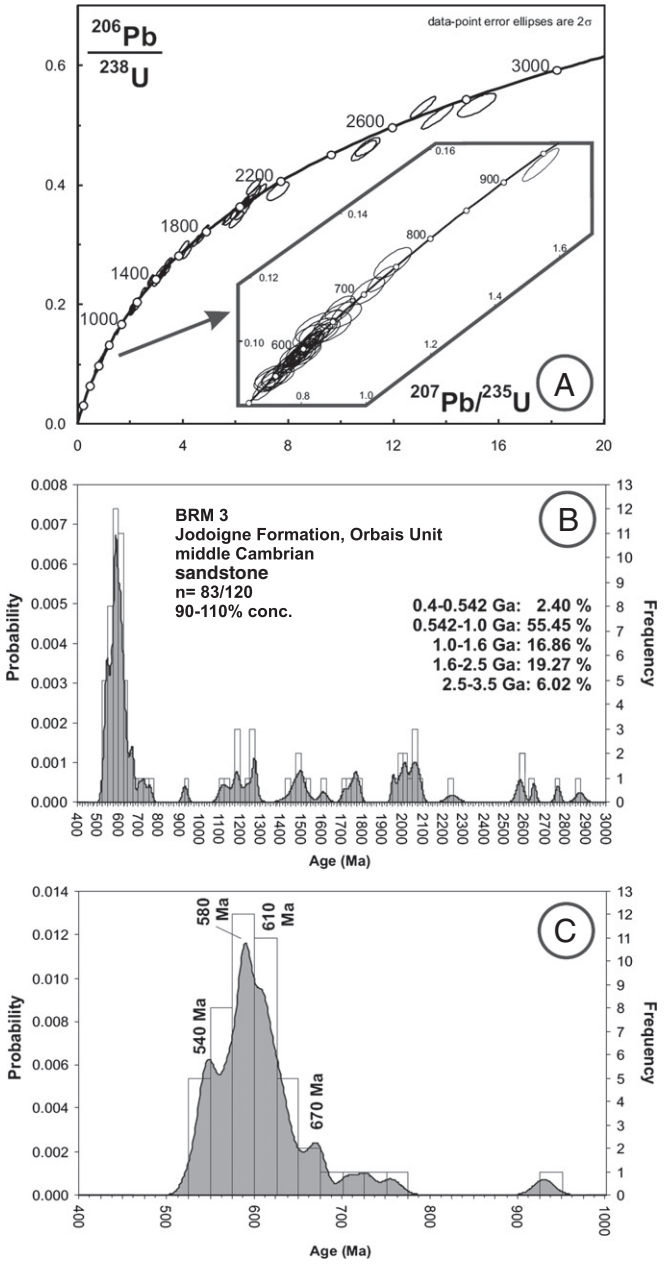

Fig. 15. U–Pb ages of detrital zircon grains from sample BRM 3 (turbidite sandstone, Jodoigne Formation, Orbais Unit, middle Cambrian). Concordia diagram (A) and combined binned frequency and probability density distribution plots of detrital zircon grains in the range of 400 to 3000 Ma (B) and of 400 to 1000 Ma (C).

(Bornival Formation; Debacker et al., 2001). It is also noticed that the N-AFZ is close to the southern boundary of the Brabant Cambrian thick rift (>9 km).

At a larger scale, the climax of the Brabant magmatic period (Madot Formation) can be correlated with the docking between Avalonia and Baltica at c. 445 Ma (Cocks and Torsvik, 2002, 2005; Torsvik and Rehnström, 2003). Its termination is coeval with the beginning of the Baltica–Laurentia collision at c. 435 Ma (Andréasson et al., 2003). Large stress applied to plate boundaries can induce intracontinental deformation at a distance larger than 1000 km, especially on preexisting lithospheric zones of weakness (e.g. Black and Liégeois, 1993; Liégeois et al., 2005; Fezaa et al., 2010). These far-field intracontinental deformations can be accompanied by magmatism, especially when they are associated to transtensive (Boullier et al., 1986; Hadj Kaddour et al., 1998) or transpressive movements (Liégeois et al., 2003; Fezaa et al., 2010). In addition to the source material involved, the nature of the magmatism depends on the deformation intensity and on the regional rheology (Black and Liégeois, 1993) and is either high-K calc-alkaline or alkaline (Liégeois et al., 1998 and references therein). Linear delamination along the lithospheric discontinuity can allow the uprise of the asthenosphere, its decompression melting and the melting of the lithosphere (Azzouni-Sekkal et al., 2003; Liégeois et al., 2003; 2005; Fezaa et al., 2010). The core of the Brabant Massif, a thick rift, is located above the boundary between the Midlands and Lüneburg-North Sea microcratons, within the Avalonia terrane (Sintubin et al., 2009; Fig. 5).

We propose that the Avalonia–Baltica docking induced, in the southern part of "East" Avalonia (Brabant; Fig. 22C), the reactivation of this lithospheric discontinuity, inducing movements of extension

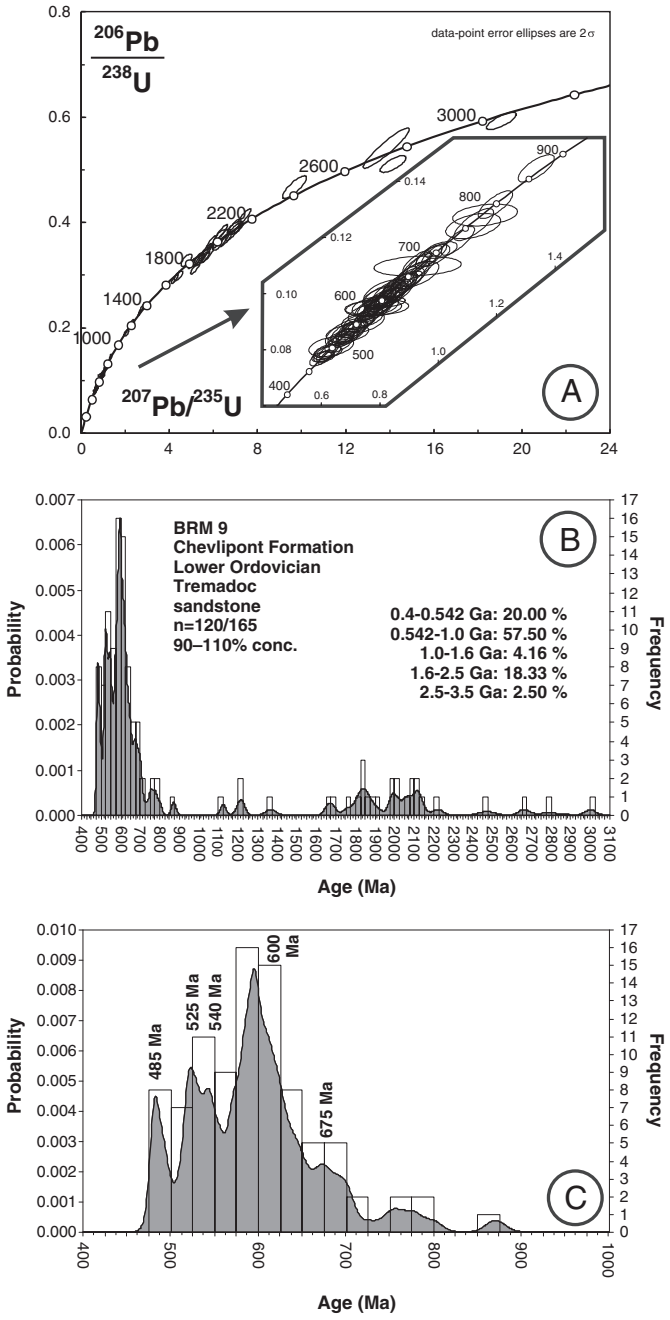

Fig. 16. U–Pb ages of detrital zircon grains from sample BRM 9 (sandstone, Chevlipont Formation, Lower Ordovician). Concordia diagram (A) and combined binned frequency and probability density distribution plots of detrital zircon grains in the range of 400 to 3100 Ma (B) and of 400 to 1000 Ma (C).

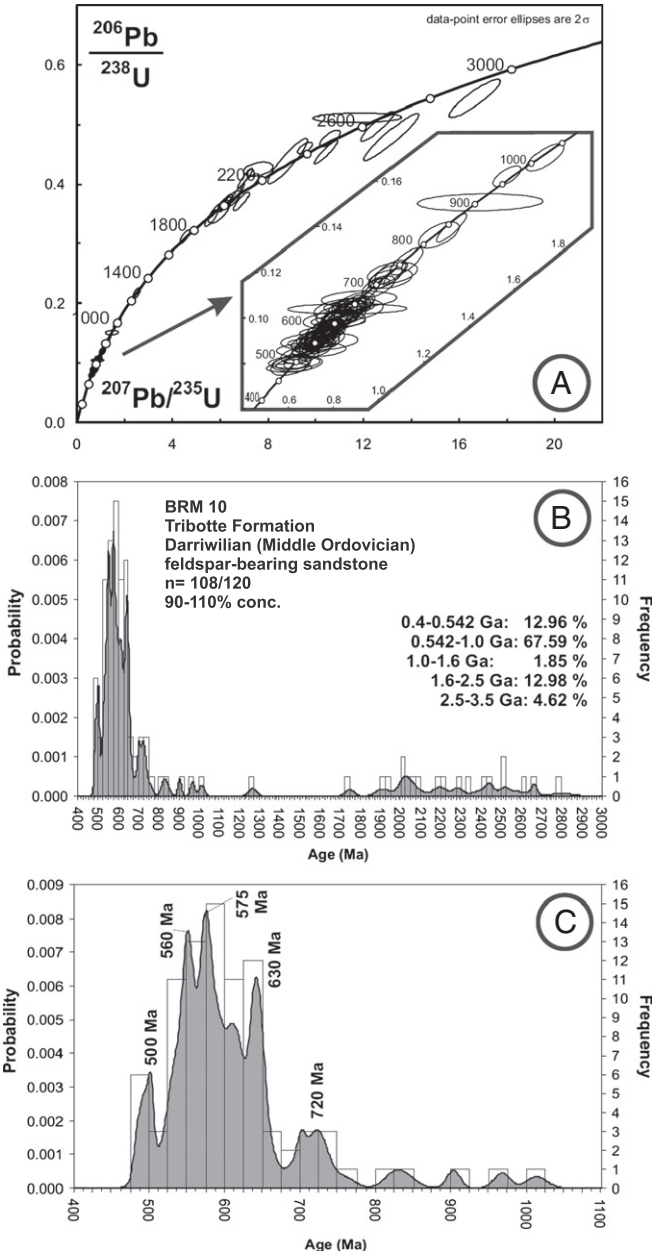

Fig. 17. U–Pb ages of detrital zircon grains from sample BRM 10 (feldspar-bearing sandstone, Tribotte Formation, Darriwilian, Middle Ordovician). Concordia diagram (A) and combined binned frequency and probability density distribution plots of detrital zircon grains in the range of 400 to 3000 Ma (B) and of 400 to 1100 Ma (C).

or transtension along a proto-Nieuwpoort-Asquempont Fault Zone, generating the partial melting of the lithosphere giving rise to the Brabant magmatism between 460 and 430 Ma (Figs. 5 and 22C). At c. 430 Ma, the Brabant magmatism ceased in response to the Brabant core inversion that was not favorable to magma generation and ascent. We propose that this inversion occurred in an intracontinental setting as a far-field effect of the collision Baltica–Laurentia. The relative rotation between the Midlands and North Sea-Lüneburg microcratons proposed by Sintubin et al. (2009) as the direct cause of the inversion would also be a consequence of this collision. The end of the Brabantian inversion (c. 390 Ma) corresponds to the end of the Caledonian orogeny in Baltica where the last eclogites-facies rocks are c. 400 Ma old (Glodny et al., 2008) and where the amphibolite-facies metamorphism ended at c. 380 Ma (Hacker et al., 2010). As a whole, the Brabant magmatism (460–430 Ma) and the Brabantian tectonic inversion (430–390 Ma) relate to the Caledonian orogeny (closure of the Iapetus Ocean; McKerrow et al., 2000). They should not be considered as related to Eovariscan events (Sintubin et al., 2009) which occurred, in the Variscides proper, at a significantly younger period (ca. 350–330 Ma), probably as a result of arc–continent collisional processes (Pin et al., 2002; 2006).

6. New U–Pb LA-ICP-MS ages on detrital zircons and Nd isotopes on sedimentary whole rocks from the Brabant Massif

6.1. U–Pb on detrital zircons results

Sample locations of rocks, from which zircon grains were analyzed by LA-ICP-MS, are shown in Table 2 and Figs. 2, 3 and 4. Seven

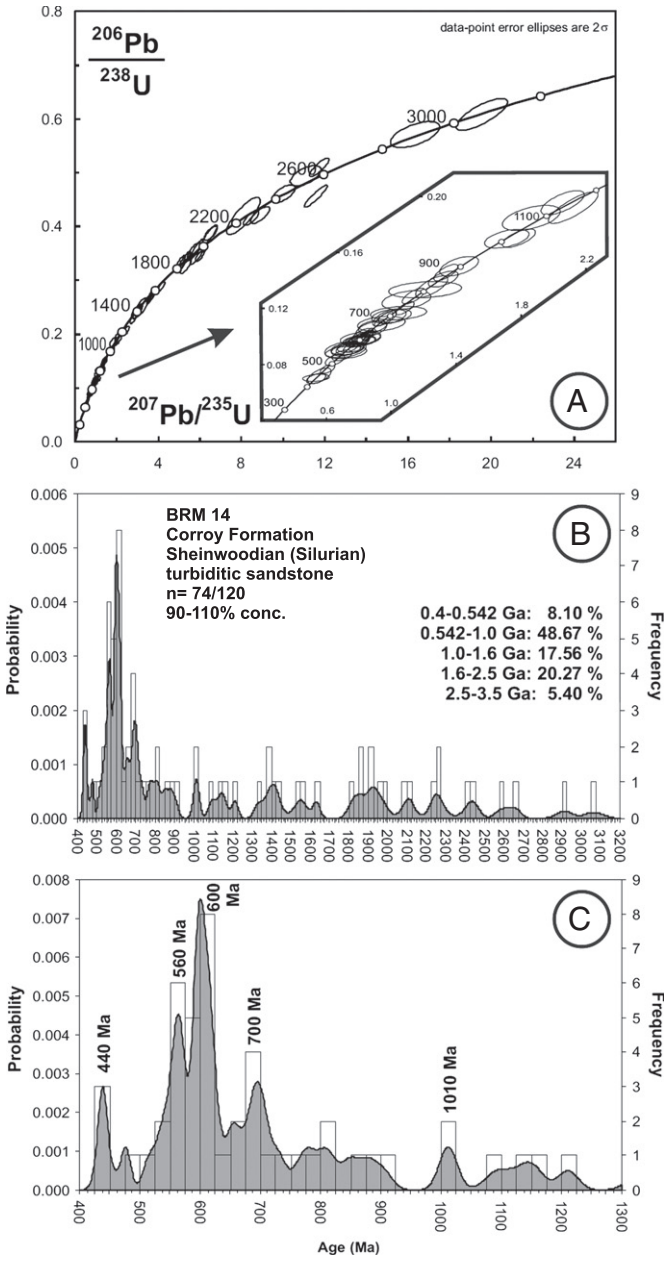

Fig. 18. U–Pb ages of detrital zircon grains from sample BRM 14 (sandstone, Corroy Formation, Sheinwoodian, Silurian). Concordia diagram (A) and combined binned frequency and probability density distribution plots of detrital zircon grains in the range of 400 to 3200 Ma (B) and of 400 to 1300 Ma (C).

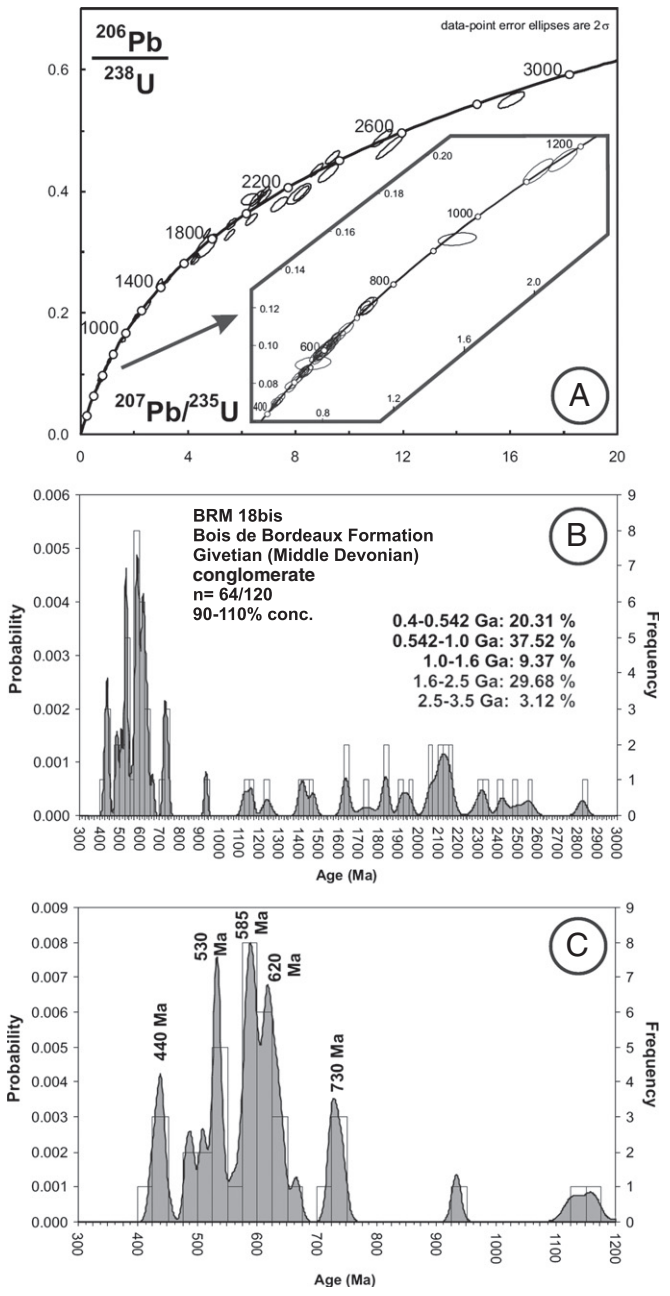

Fig. 19. U–Pb ages of detrital zircon grains from sample BRM 18bis (fine conglomerate, Bois de Bordeaux Formation, Givetian, Middle Devonian). Concordia diagram (A) and combined binned frequency and probability density distribution plots of detrital zircon grains in the range of 400 to 3000 Ma (B) and of 400 to 1200 Ma (C).

medium to coarse-grained sandstone that covered regularly the whole Brabant succession from the lower Cambrian to the middle part of the Silurian and one Givetian conglomerate from the base of the Devonian angular unconformity (Brabant Parautochthon) were sampled for zircon dating. The lithologies of the Upper Ordovician and most of the Silurian are too fine-grained (distal turbidites) for delivering zircons adequate for dating.

120 detrital zircon grains were analyzed in sample BRM 1 (Blanmont Formation, lower Cambrian, Table 10). Of these, only 92 grains provided U–Pb ages that can be considered as concordant (specifically in the 90–110% range of concordance; Fig. 12). The youngest concordant grain has a 555 ± 16 Ma $^{206}Pb/^{238}U$ age and the oldest zircon yields a $^{207}Pb/^{206}Pb$ age of 2791 ± 17 Ma. 61% of all concordant zircons in the sample are Neoproterozoic in age in the range of ~0.55–0.90 Ga (Fig. 12B). The probability plot shows two important distinct peaks at ~630 Ma and ~570 Ma (Fig. 12C). 16% of all grains are Mesoproterozoic and range from 1156 ± 42 to 1551 ± 23 Ma. Palaeoproterozoic zircons occupy 11% and Archaean zircon grains 12% with a distinct peak at ~2.7 Ga (Fig. 12B).

120 zircon grains of sample BRM 12 were analyzed (Tubize Formation, lower Cambrian, Table 11), from which 88 grains were concordant in the range of 90 to 110% (Fig. 13A). The youngest zircon grain has a 543 ± 21 Ma $^{206}Pb/^{238}U$ age. The oldest zircon is one of four Archaean grains, with a $^{207}Pb/^{206}Pb$ age of 2655 ± 10 Ma. 53% of concordant zircons in the sample are Neoproterozoic in age ranging from ~540 to 750 Ma (Fig. 13, Table 12). 39% of all grains are Palaeoproterozoic, in the range from 1724 ± 24 to 2413 ± 48 Ma. Major peaks in the probability plot occur at 575, 605, 675 and 1950 Ga (Fig. 13B). Mesoproterozoic zircons involve 2% of all grains

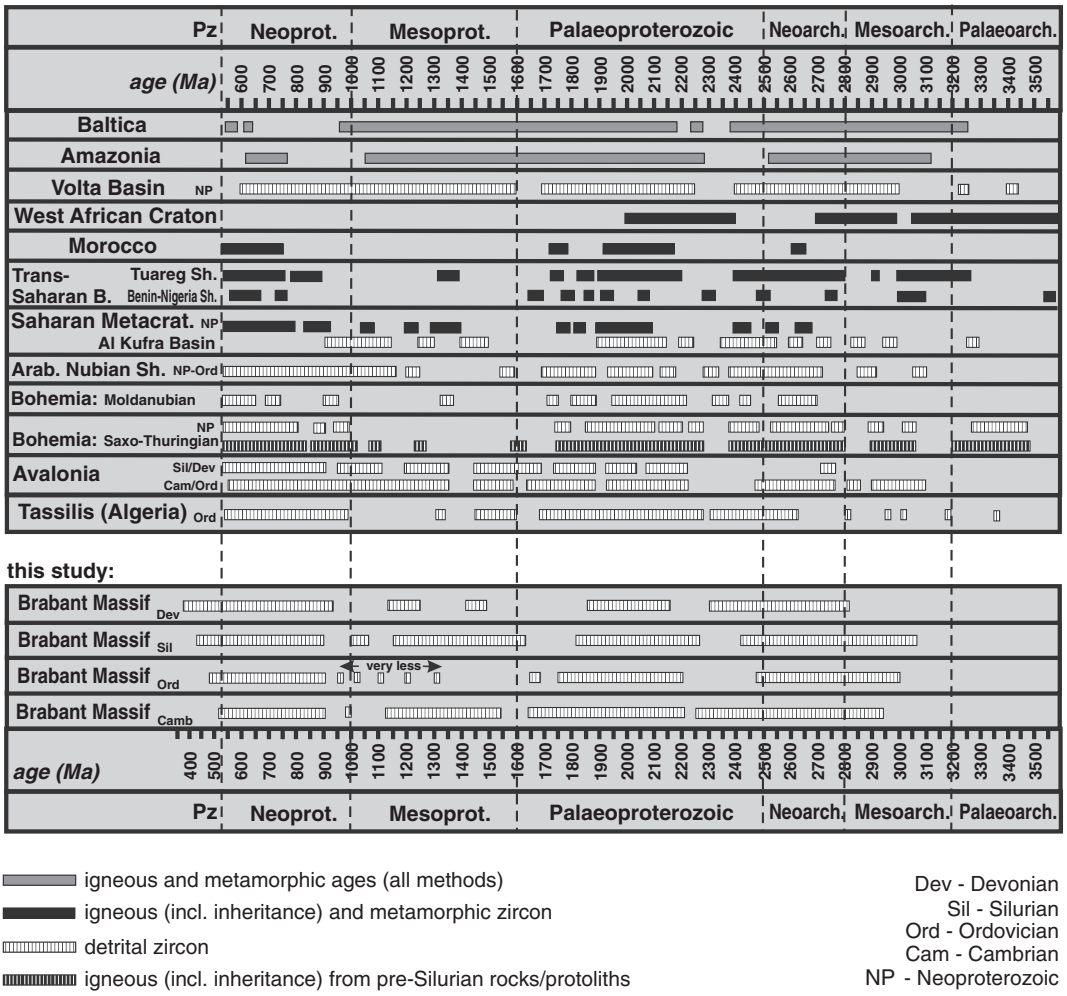

Fig. 20. Detrital zircon age distributions of the eight analyzed sandstone samples of the Brabant Massif compared with Tassili Ouan Ahaggar basin (Algeria), Amazonia, Cadomia, and other parts of Gondwana and potential source areas.
Data compilation from Drost et al., 2010; Linnemann et al., 2004, 2011.

and scatter between 1514 ± 23 and 1597 ± 26 Ma. Archaean zircon grains include 4% of all grains ranging from 2568 ± 77 to 2794 ± 90 Ma.

120 detrital zircon grains were analyzed in sample BRM 2 (Jodoigne Formation, Maka Unit, middle Cambrian, Table 12), from which 106 grains are 90 to 110% concordant (Fig. 14). The youngest grain has a 543 ± 12 Ma $^{206}Pb/^{238}U$ age. The oldest zircon yields a $^{207}Pb/^{206}Pb$ age of 2689 ± 16 Ma. 45% of all zircons in the sample are Neoproterozoic in age, in the range of ~543–792 Ma (Fig. 14, Table 12). The probability plot shows distinct peaks at 565, 625, 690, and 770 Ma (Fig. 14C). The second-strongest population of 25% is represented by Mesoproterozoic zircons in the range of ~1170 to 1600 Ma. Another strong population consists of Palaeoproterozoic zircons (23%) ranging from ~1670 to 2480 Ma. At last, 7% of all zircons provide Archaean ages (Fig. 14B).

120 zircon grains of BRM 3 (Jodoigne Formation, Orbais Unit, middle Cambrian) were analyzed, from which 83 grains were concordant in the range of 90 to 110% (Fig. 15; Table 13). The youngest zircon grain is Early Cambrian in age with a 526 ± 16 Ma $^{206}Pb/^{238}U$ age. The oldest zircon is one of five Archaean grains, with a $^{207}Pb/^{206}Pb$ age of 2874 ± 41 Ma. 55% of all zircons in the sample are Neoproterozoic in age ranging from ~525 to 930 Ma (Fig. 15, Table 13). The probability plot shows distinct peaks at 540, 580, 610, and 670 Ma (Fig. 15C). 19% of all grains are Palaeoproterozoic, in the range from 1718 ± 29 to 2158 ± 50 Ma. Particularly noteworthy is the content of Mesoproterozoic zircon grains (17%; Fig. 15B). Archaean grains are 6% of the whole population.

165 zircon grains of BRM 9 were analyzed (Chevlipont Formation, Tremadocian), from which 120 grains were concordant in the range of 90 to 110% (Fig. 16; Table 14). The youngest zircon grain has a $^{206}Pb/^{238}U$ age of 481 ± 9 Ma. The oldest zircon shows a $^{207}Pb/^{206}Pb$ age of 3075 ± 29 Ma. 57% of all zircons in the sample are Neoproterozoic, in the range of ~480–870 Ma (Fig. 16, Table 14). The probability plot shows dominant peaks at 540, 600 and 675 Ma (Fig. 16B and C). The second abundant population (20%) is represented by Cambro-Ordovician zircons with distinct peaks in the probability plots at 525 and 485 Ma. Another big portion (18%) of the whole population has Palaeoproterozoic ages. Only 4% of all grains are Mesoproterozoic and only three Archaean grains (2.5%) have been found (Fig. 16, Table 14).

120 zircon crystals from sample BRM 10 (Tribotte Formation, Lower Ordovician, Arenig, Table 15) were analyzed, of which 108 grains are classified as concordant (Fig. 17). The youngest grain yields a $^{206}Pb/^{238}U$ age of 484 ± 10 Ma, the oldest has a 2996 ± 37 Ma $^{207}Pb/^{206}Pb$ age. 68% of all zircons in the sample give Neoproterozoic ages, in the ~540–970 Ma range (Fig. 17, Table 15). The probability plot shows three major peaks at 560, 575, and 630 Ma (Fig. 17C). 13% of all grains analyzed are Cambro-Ordovician zircon grains ranging from 484 ± 10 to 541 ± 20 Ma. A larger peak in the probability plot is at ~500 Ma (Fig. 17). 13% of all zircon ages fall in the

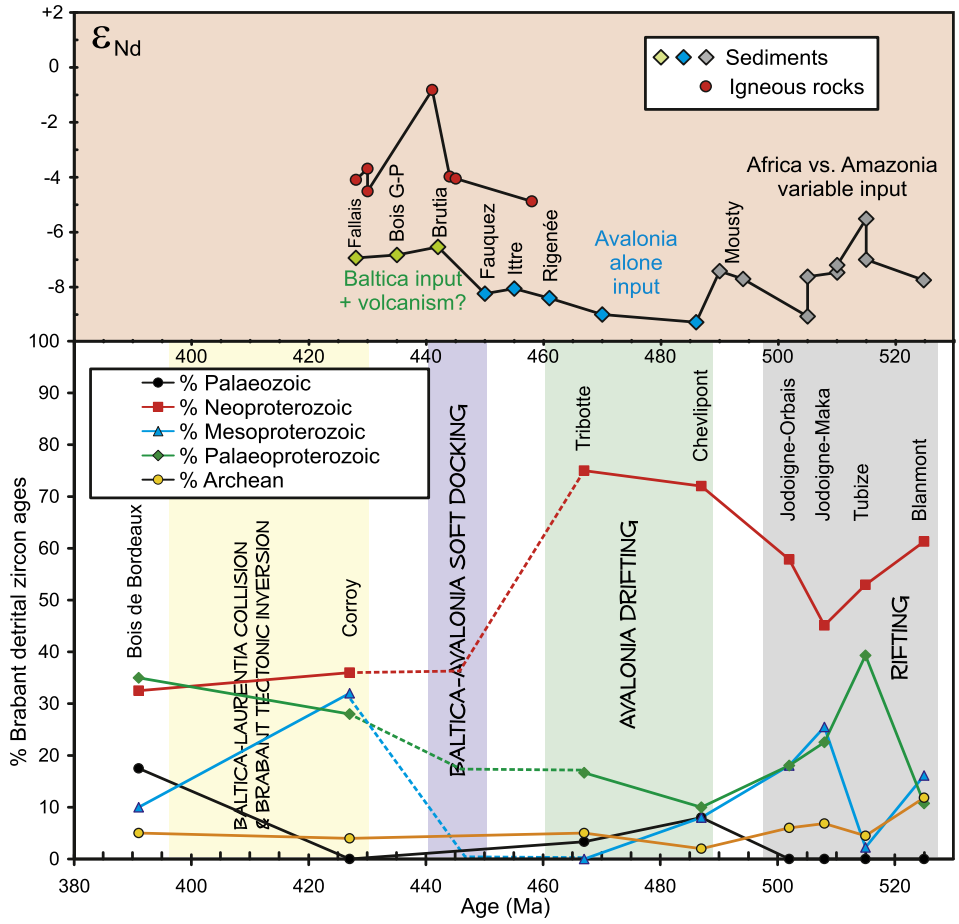

Fig. 21. Below: variation through time of the proportions of Brabant detrital zircon ages regrouped in five classes; for the time spans used for the main geodynamical events, see discussion in the text. Above: variation through time of the ε_{Nd} signatures of the Brabant sediments and magmatic rocks and the deduced signature of main concerned terranes. See text.

Palaeoproterozoic. Only less than 2% of the zircons are Mesoproterozoic, while 5% are Archaean (Fig. 17).

120 zircon grains were analyzed from sample BRM 14 (Corroy Formation, Silurian, Sheinwoodian, Table 16) of which of 74 grains are classified as concordant (Fig. 18). The youngest grain yields a 436 ± 18 Ma $^{206}Pb/^{238}U$ age. The oldest zircon has a Palaeoarchaean $^{207}Pb/^{206}Pb$ age (3073 ± 52 Ma). 49% of all zircons in the sample are Neoproterozoic, in the ~550–900 Ma range (Fig. 18C). The probability plot shows distinct peaks at 560, 600, and 700 Ma (Fig. 18). 20% of all grains yield Palaeoproterozoic ages. Mesoproterozoic grains are represented by 18% of all grains. 8% of the zircons are Cambro-Ordovician and Silurian in age with a distinct peak at 440 Ma (Fig. 18C). 5% of all zircons are Archaean.

120 zircon grains were analyzed from sample BRM 18bis (Bois de Bordeaux Formation, Middle Devonian, Givetian, Table 17) of which only 64 grains are classified as concordant (Fig. 19). The youngest grain has a 425 ± 13 Ma $^{206}Pb/^{238}U$ age. The oldest zircon is Neoarchaean, with a $^{207}Pb/^{206}Pb$ age of 2917 ± 26 Ma. 38% of all zircons in the sample are Neoproterozoic, with an age range of ~550–930 Ma (Fig. 19C). The probability plot shows large peaks at 585 Ma, 620 Ma, and 730 Ma (Fig. 19C). 30% of all grains are Palaeoproterozoic. Cambro-Silurian zircons in the ~425–535 Ma age range are represented by a strong population of 20% with distinct peaks at 530 and 440 Ma. Mesoproterozoic grains occur with a relative abundance of 9%. 3% of all zircons give Archaean ages.

To sum up, the detrital zircon of the Brabant Massif record shows following main results: (1) from the lower Cambrian until the mid Silurian strata, Neoproterozoic rocks were the most important zircon supplier although not always in majority (35–75%; Fig. 21). The Pan-African domain, from which these debris are derived, can be the main Gondwana land (West Africa) or the Avalonia basement itself (former magmatic arc at the peri-Gondwanan margin) or both. (2) The second dominant source is represented by an old continental basement, and/or sediments derived from, which is composed mainly by Palaeoproterozoic rocks. Such crustal units are documented in all major potential source domains (Amazonia, Baltica, West Africa). (3) Mesoproterozoic contribution exists in some Cambrian and Silurian sedimentary rocks (Fig. 21); such basement occurs in both Baltica and Amazonia. Interestingly, the Mesoproterozoic zircon supply vanished during the Ordovician rift-drift stage and reappeared during the Silurian compressive foreland basin stage (Fig. 21). (4) Cambro-Ordovician and Silurian igneous rocks contributed to the Palaeozoic debris and should thus have been exposed during the time of sedimentation.

6.2. Nd isotopes on sedimentary whole-rock results

Sample locations and description of sedimentary rocks analyzed for Nd isotopes are shown in Table 1 and the geochemical and isotopic results in Tables 3 and 4. These 17 fine-grained slates (claystone to mudstone and argillaceous siltstone) cover quite regularly all the stratigraphic range from the lower Cambrian to the middle of the Silurian. Most Brabant sedimentary rocks have usual Sm (5.8–12.5 ppm) and Nd (32–69 ppm) concentrations, giving rise to felsic continental crust $^{147}Sm/^{144}Nd$ ratios (0.098–0.125). The dark

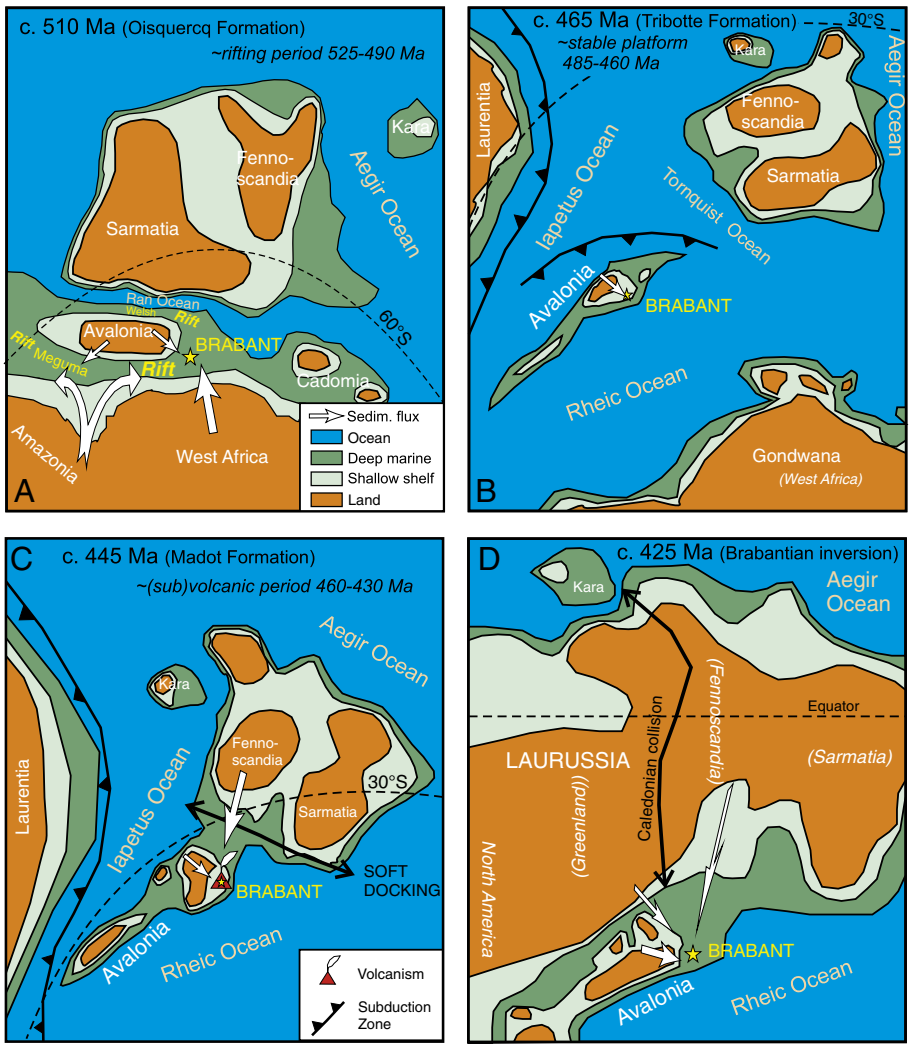

Fig. 22. Sketch of the palaeogeographic position, sedimentary input and volcanic activity of the Brabant Massif (yellow star) during its wandering history based on the new presented data from this paper.
Palaeogeography modified from Cocks and Torsvik, 2005.

Ordovician slate Brab-20 (Ittre Formation) is an outlier with 4.6 ppm Sm, 17.8 ppm Nd and a high $^{147}Sm/^{144}Nd$ ratio of 0.156.

Measured $^{143}Nd/^{144}Nd$ values are in the range 0.511885 and 0.512096, with Brab-20 at 0.512104. ε_{Nd} at the sedimentation age of the rock varies from −5.5 to −9.3, including Brab-20. Nd T_{DM} model ages (using depleted mantle curve after DePaolo, 1981; see Liégeois and Stern, 2010, for this choice and the use of T_{DM} model ages) vary from 1.44 and 1.70 Ga (with Brab-20 at 2.49 Ga) in a 1-stage model and from 1.43 to 1.70 Ga (including Brab-20) when using a 2-stage model (Table 4). These values are comparable with the few obtained earlier in Brabant (André et al., 1986a).

Negative ε_{Nd} and NdT_{DM} much older than the sedimentation ages indicate globally the presence of old components in the Brabant sedimentary rocks. Nd T_{DM} model ages, also known as crustal residence ages, actually correspond to the mean age of the initial sources, later reworked or not. A sedimentary rock whose source is a 2 Ga

Table 2
Description and location of sample used for zircon U–Pb dating (classified by stratigraphic age; see also Fig. 2 and 3).

Sample	Lithology	Lithostrati.	Chronostra.	Location	Basin/river
BRM1	Sandstone to quartzite	Blanmont Fm.	upper lower Cambrian	Dongelberg, N old quarry	Grande Gette Orbais valley
BRM12	Greywacke, turbidite	Tubize Fm., middle Mbr.	upper lower Cambrian	Tubize, Rogissart	Senne basin, Hain valley
BRM2	Quartzite, massive	Jodoigne Fm., Maka Unit	Middle Cambrian	Jauchelette, Rue de Maka	Grande Gette basin
BRM3	Lithic sandstone	Jodoigne Fm., Orbais Unit	middle Cambrian	Orbais	Grande Gette basin
BRM9bis	Sandstone, turbidite	Chevlipont Fm.	Tremadocian, lowest part	Chevlipont, railway cut	Dyle basin, Thyle valley
BRM10	Sandstone, arkosic	Tribotte Fm., lower part	Darriwilian, lower part	Abbaye de Villers	Dyle basin, Thyle valley
BRM21	Rhyolite, interstratified	Ittre Fm., basal part	Sandbian, upper part	Asquempont, old railway	Senne basin, Sennette val.
BRM19	Tuff, volcani-clastic	Madot Fm., upper part	Katian, upper part	Hennyères, railway cut	Senne basin, Coeurq val.
BRM23	Dacite, sub-marine flow	Madot Fm., upper part	Katian, upper part	Fauquez, Bois des Rocs	Senne basin, Sennette val.
BRM14	Sandstone, turbidite	Corroy Fm.	Sheinwoodian	Corroy, old quarry	Orneau basin
BRM17	Quartz diorite, quenast pipe	intrusive in Ordovician	Silurian, middle part	Quenast, quarry	Senne basin, Senne valley
BRM18bis	Conglomerate, unconformity	Bois de Bordeaux Fm.	Givetian	Monstreux	Senne basin, Thisnes val.

Table 3
Geochemical data (major and trace elements) on investigated magmatic and sedimentary rocks from the Brabant Massif. Abreviations: L.D.: lower limit of detection; PF: loss on ignition.

Sedimentary rocks

Sample		Brab-1	Brab-2	Brab-3	Brab-9	Brab-22	Brab-4	Brab-5	Brab-6	Brab-13	Brab-23	Brab-7	Brab-8	Brab-20
SiO_2	%	57.71	55.67	52.82	61.32	62.14	64.25	50.47	57.25	59.06	49.78	56.81	58.21	71.42
Al_2O_3	%	20.48	22.28	19.65	19.42	19.52	21.88	30.54	22.67	20.92	26.46	20.59	21.58	11.47
Fe_2O_3	%	7.34	7.45	10.88	7.59	7.54	1.07	2.57	4.57	6.87	7.00	9.29	7.66	7.83
MnO	%	0.09	0.08	0.09	0.15	0.13	0.00	0.02	0.13	0.38	0.11	0.14	0.08	0.24
MgO	%	2.28	2.49	3.49	2.06	2.02	0.55	0.73	1.67	1.97	1.86	1.87	1.73	1.70
CaO	%	0.22	0.22	1.06	0.09	0.10	0.04	0.10	0.16	0.07	0.17	0.28	<L.D.	0.92
Na_2O	%	0.90	0.78	1.55	0.72	0.45	0.24	0.99	0.62	0.15	0.63	0.67	0.76	1.32
K_2O	%	5.15	5.65	4.51	3.66	3.47	5.84	6.88	4.21	4.75	7.31	3.70	3.64	1.35
TiO_2	%	1.03	1.00	0.91	0.98	1.00	1.06	1.33	1.02	0.95	1.13	1.01	1.14	0.64
P_2O_5	%	0.12	0.15	0.17	0.08	0.10	<L.D.	0.07	0.11	0.08	0.22	0.23	0.10	0.40
PF	%	4.88	4.48	5.03	4.22	4.43	5.43	5.99	7.26	4.79	4.96	5.41	5.10	3.52
Total	%	100.20	100.25	100.14	100.29	100.90	100.36	99.67	99.67	100.00	99.63	99.99	99.97	100.83
As	ppm	<L.D.	2.54	4.62	39.36	53.41	<L.D.	6.20	<L.D.	36.84		20.40	29.10	63.35
Ba	ppm	964	865	1120	441	396	746	899	851	685	1398	913	755	226
Be	ppm	1.99	2.26	2.25	2.55	2.47	2.55	2.91	3.75	2.73	5.50	2.73	3.03	1.03
Bi	ppm	<L.D.	0.12	0.18	0.23	1.01	4.25	0.90	0.31	0.13		<L.D.	0.16	0.24
Cd	ppm	0.22	0.23	<L.D.	<L.D.	0.16	<L.D.	0.16	0.19	<L.D.		<L.D.	0.18	0.28
Ce	ppm	75.9	85.9	70.9	98.6	81.1	81.4	147.6	102.0	82.3		107.4	136.6	29.2
Co	ppm	13.9	15.1	24.6	6.8	3.5	1.6	2.3	8.2	13.0	35.0	15.9	4.9	25.7
Cr	ppm	108	111	118	96	95	109	173	117	99	168	114	122	48
Cs	ppm	1.9	4.8	7.2	6.5	4.7	4.7	11.8	12.4	8.7		6.7	5.0	1.9
Cu	ppm	14.2	23.0	37.4	13.9	10.2	<L.D.	16.1	19.2	12.9	42.0	17.4	10.0	19.9
Dy	ppm	6.00	6.41	4.65	4.41	4.28	4.74	6.53	5.70	4.85		6.01	5.86	5.52
Er	ppm	3.62	3.72	2.56	2.69	2.57	2.88	3.39	3.18	2.72		3.22	3.25	2.99
Eu	ppm	1.58	1.61	1.40	1.23	1.20	1.39	2.97	1.86	1.30		1.81	1.94	1.14
Ga	ppm	29	31	30	27	27	31	43	31	29	39	30	31	15
Gd	ppm	5.82	6.86	5.31	4.34	4.54	5.27	8.55	6.63	4.88		7.03	6.45	5.24
Ge	ppm	2.1	1.9	1.7	3.0	3.3	2.4	2.6	2.5	3.0		2.8	2.7	2.6
Hf	ppm	5.63	5.39	4.40	5.48	5.44	5.29	6.72	4.58	4.60		5.10	6.07	9.25
Ho	ppm	1.21	1.27	0.88	0.90	0.86	0.95	1.18	1.10	0.94		1.15	1.13	1.09
La	ppm	36.6	40.9	35.8	46.2	36.2	38.8	75.9	53.2	38.4		51.1	63.2	11.1
Lu	ppm	0.60	0.60	0.44	0.46	0.45	0.51	0.57	0.51	0.48		0.48	0.51	0.44
Mo	ppm	<L.D.	<L.D.	<L.D.	<L.D.	<L.D.	<L.D.	2.3	16.3	<L.D.		0.4	0.5	0.6
Nb	ppm	20.9	20.2	15.2	18.5	18.7	20.1	25.9	17.2	18.0	17.0	16.5	20.3	10.4
Nd	ppm	35.1	38.6	33.4	35.8	31.3	34.9	61.1	44.8	33.3		44.8	52.2	16.2
Ni	ppm	41.4	38.0	61.6	29.4	26.0	8.1	7.3	16.6	27.3	61.0	42.8	20.7	49.3
Pb	ppm	10.3	14.2	9.8	15.0	106.8	10.1	18.9	17.3	9.5		11.5	18.3	4.4
Pr	ppm	9.39	10.18	8.90	10.15	8.56	9.33	16.85	12.12	9.15		11.98	14.47	3.64
Rb	ppm	153	208	178	161	152	212	288	189	213	266	160	170	55
Sb	ppm	0.24	0.71	0.76	0.36	0.34	1.50	1.04	0.36	0.84		0.38	1.19	0.76
Sm	ppm	6.92	7.83	6.55	5.88	5.84	6.71	11.41	8.45	6.30		8.51	8.85	4.45
Sn	ppm	5.6	6.4	4.6	5.7	4.0	7.2	12.9	6.7	5.0		5.7	7.0	2.0
Sr	ppm	48	45	149	96	90	36	115	194	53	132	169	144	61
Ta	ppm	1.68	1.64	1.25	1.59	1.62	1.69	2.26	1.52	1.54		1.47	1.82	0.91
Tb	ppm	0.96	1.07	0.80	0.71	0.70	0.79	1.19	0.99	0.81		1.05	1.01	0.89
Th	ppm	13.1	14.4	9.4	13.0	10.9	12.8	15.6	13.5	12.9	13.0	13.0	15.5	8.1
Tm	ppm	0.56	0.57	0.40	0.43	0.41	0.47	0.52	0.50	0.42		0.48	0.49	0.43
U	ppm	2.3	1.8	1.8	2.1	3.7	2.6	4.0	5.6	2.5		2.1	3.0	2.2
V	ppm	116	135	173	118	115	136	199	172	141	166	116	175	66
W	ppm	3.2	2.5	2.0	4.3	3.0	3.0	2.8	2.7	4.1		3.2	3.1	5.8
Y	ppm	34	37	25	25	24	27	32	31	24	40	32	32	32
Yb	ppm	3.85	3.89	2.75	3.00	2.90	3.26	3.66	3.38	2.97		3.19	3.37	2.85
Zn	ppm	111	104	111	95	105	<L.D.	20	132	103	66	97	91	178
Zr	ppm	211	195	163	200	200	189	234	172	165	146	191	222	370

Magmatic rocks

Sample	Brab-21	Brab-10	Brab-11	Brab-12	BRM 21	BRM 23	BRM 19	Brab-16	Brab-19	Brab-18	BRM 17	Q 71	Q 85	Q 98
SiO_2	68.73	65.04	56.24	57.66	74.54	67.26	57.95	81.22	74.28	64.70	64.23	63.63	57.33	63.97
Al_2O_3	16.58	19.12	21.48	19.18	13.77	14.60	20.06	11.60	13.66	15.18	15.29	14.97	18.43	15.13
Fe_2O_3	2.19	3.75	9.81	9.45	3.45	3.76	7.32	1.23	3.78	5.21	5.68	5.68	6.93	5.51
MnO	0.03	0.02	0.38	0.17	0.09	0.01	0.05	0.00	0.04	0.03	0.10	0.10	0.11	0.11
MgO	1.20	1.38	1.93	2.25	0.63	1.22	2.96	0.59	0.97	3.69	2.41	2.37	3.46	2.86
CaO	0.25	0.03	<L.D.	0.26	0.69	3.03	0.22	<L.D.	0.18	2.66	2.81	3.25	3.53	2.54
Na_2O	0.33	0.09	0.50	0.35	0.11	5.01	4.26	2.31	1.47	2.33	3.34	3.77	6.63	4.23
K_2O	4.06	5.09	3.49	3.55	2.71	1.09	2.57	2.06	2.27	3.00	2.92	2.21	0.89	2.08
TiO_2	0.80	0.57	1.04	0.91	0.34	0.69	0.83	0.11	0.39	0.71	0.70	0.69	0.79	0.72
P_2O_5	0.16	0.07	0.09	0.11	0.53	0.12	0.10	<L.D.	0.08	0.12	0.12	0.12	0.14	0.12
PF	6.17	5.26	5.06	5.84	3.38	3.79	4.03	1.71	3.42	2.73	2.07	2.01	2.28	2.23
Total	100.51	100.41	100.01	99.72	100.23	100.57	100.34	100.82	100.53	100.36	99.66	98.79	100.51	99.50
As	<L.D.	<L.D.	24.61	22.93	6.22	<L.D.	12.40	<L.D.	4.42	1.86	<L.D.	<L.D.	<L.D.	<L.D.
Ba	802	972	518	551	630	238	283	594	378	425	519	376	47	401
Be	2.86	3.15	2.68	2.67	1.81	1.05	1.43	1.71	1.94	1.54	1.65	2.24	1.69	1.53

Table 3 (*continued*)

Magmatic rocks														
Sample	Brab-21	Brab-10	Brab-11	Brab-12	BRM 21	BRM 23	BRM 19	Brab-16	Brab-19	Brab-18	BRM 17	Q 71	Q 85	Q 98
Bi	0.14	0.43	0.17	0.95	0.30	0.10	<L.D.	0.11	0.21	<L.D.	<L.D.	<L.D.	<L.D.	<L.D.
Cd	<L.D.	0.19	0.20	<L.D.	<L.D.	<L.D.	<L.D.	<L.D.	<L.D.	0.15	0.18	0.25	0.22	0.21
Ce	70.2	111.0	114.0	100.2	91.3	41.0	63.9	61.4	89.9	60.6	60.0	50.7	52.9	59.5
Co	1.6	3.3	8.3	22.6	2.7	10.5	15.8	0.9	5.7	15.2	14.8	15.3	13.0	14.8
Cr	104	65	105	100	26	33	53	<L.D.	19	34	37	41	36	36
Cs	6.0	7.4	5.3	4.6	4.5	0.9	2.4	2.7	1.8	2.6	2.2	0.8	<L.D.	1.3
Cu	<L.D.	31.6	26.8	68.6	6.2	9.3	21.2	<L.D.	18.4	9.6	34.9	21.9	<L.D.	21.8
Dy	4.73	8.09	6.00	5.52	11.40	3.85	5.84	5.78	6.15	5.92	5.66	5.32	4.93	5.65
Er	2.68	4.66	3.31	3.14	4.97	2.13	3.39	3.75	3.62	3.47	3.32	3.10	2.73	3.34
Eu	1.14	1.74	1.91	1.59	1.86	0.85	1.66	0.24	1.28	1.27	1.31	1.18	0.92	1.34
Ga	24	29	30	27	21	15	24	14	19	20	19	18	23	19
Gd	4.92	8.60	6.89	6.13	11.54	4.22	5.99	4.30	6.21	5.72	5.45	4.91	4.64	5.50
Ge	2.5	2.3	3.2	2.6	2.1	1.0	1.8	1.7	2.0	1.6	1.7	1.9	2.6	1.6
Hf	4.24	5.66	4.50	4.79	6.27	5.12	4.82	3.85	6.32	5.56	5.31	4.80	5.19	5.24
Ho	0.93	1.62	1.15	1.08	2.00	0.75	1.16	1.24	1.24	1.18	1.15	1.08	0.99	1.14
La	34.3	51.6	57.3	49.5	40.5	17.1	32.0	29.7	42.4	28.3	28.4	23.1	24.6	28.3
Lu	0.43	0.72	0.51	0.50	0.55	0.32	0.54	0.64	0.62	0.56	0.54	0.51	0.45	0.52
Mo	26.4	4.4	<L.D.	<L.D.	0.6	<L.D.	<L.D.	<L.D.	<L.D.	0.4	0.8	<L.D.	<L.D.	<L.D.
Nb	14.2	14.9	19.1	16.1	17.1	10.0	10.3	7.1	12.9	10.6	10.3	10.2	10.8	10.2
Nd	29.0	47.3	51.5	41.3	43.8	21.1	32.3	23.8	36.7	27.8	27.5	23.2	23.3	27.1
Ni	11.2	18.0	44.4	62.2	14.2	14.7	26.3	<L.D.	13.1	19.6	19.5	21.3	23.8	19.8
Pb	5.9	47.6	5.5	28.1	25.9	6.1	13.7	8.5	6.7	14.6	14.4	11.7	11.7	9.1
Pr	7.74	12.59	13.69	11.28	11.08	5.21	8.22	6.91	9.99	7.27	7.14	6.03	6.13	7.09
Rb	182	244	160	160	125	28	64	100	100	95	113	78	20	78
Sb	0.38	0.46	0.35	0.46	<L.D.	0.23	0.85	0.86	0.24	0.39	0.44	0.28	1.72	0.24
Sm	5.81	10.07	9.30	7.68	10.80	4.71	6.87	4.66	7.28	6.16	5.98	5.20	5.13	5.98
Sn	4.2	7.3	5.8	5.1	5.8	1.8	3.0	3.8	4.9	2.7	7.1	1.8	2.3	1.8
Sr	59	44	134	70	77	172	152	121	74	124	122	139	207	140
Ta	1.43	1.59	1.64	1.38	1.45	1.04	0.98	1.02	1.31	1.19	0.94	0.92	0.95	0.92
Tb	0.78	1.37	1.03	0.95	1.98	0.66	0.97	0.83	1.02	0.95	0.91	0.85	0.79	0.91
Th	10.9	15.5	13.0	12.2	10.3	8.0	8.4	16.4	15.1	8.9	10.0	9.5	9.6	9.6
Tm	0.41	0.71	0.49	0.47	0.65	0.31	0.52	0.60	0.56	0.53	0.51	0.49	0.42	0.50
U	6.4	5.7	2.3	2.1	2.4	1.5	1.4	4.9	2.9	2.0	2.1	2.0	2.0	2.2
V	321	173	165	144	23	74	138	3	30	106	108	104	139	107
W	3.9	2.0	2.5	2.9	4.7	8.2	3.7	6.7	1.7	12.5	4.5	4.1	2.6	4.7
Y	27	45	33	30	57	20	33	36	35	34	33	31	27	33
Yb	2.80	4.83	3.34	3.24	3.93	2.09	3.57	4.21	3.97	3.57	3.47	3.26	2.90	3.45
Zn	30	79	127	145	46	58	106	29	72	73	69	57	51	58
Zr	159	183	169	179	204	186	167	104	229	203	192	178	191	190

Table 4
Sm–Nd isotope data of (meta-) sedimentary and igneous rocks of the Brabant Massif.

Sample	Age t (Ma)	Sm ($\mu g\ g^{-1}$)	Nd ($\mu g\ g^{-1}$)	$^{147}Sm/^{144}Nd$	$^{143}Nd/^{144}Nd$	2 std error	εNd(t)	TDM (Ga)	TDM (Ga) 2-stage	Lithology	Lithostratigraphy	System/stage
(Meta-)sedimentary rocks												
Brab-1	525	6.58	33.8	0.1177	0.511970	2	−7.8	1.70	1.61	Biotite slate	Blanmont Fm.	Lower Cambrian, Stage 2/3
Brab-2	515	7.77	39.3	0.1196	0.512020	2	−7.0	1.65	1.54	Green slate	Lower Tubize Fm.	Lower Cambrian, Stage 3/4
Brab-3	515	6.56	34.1	0.1163	0.512085	3	−5.5	1.50	1.43	Green slate	Middle Tubize Fm.	Lower Cambrian, Stage 3–4
Brab-9	510	6.37	39.5	0.0976	0.511938	3	−7.2	1.45	1.57	Green slate	Upper Oisquercq Fm.	Middle Cambrian, Stage 5
Brab-22	510	5.82	32.3	0.1090	0.511963	3	−7.5	1.57	1.58	Green slate	Upper Oisquercq Fm.	Middle Cambrian, Stage 5
Brab-4	505	6.68	35.6	0.1135	0.511973	3	−7.6	1.62	1.59	Black slate	Lower Jodoigne Fm.	Middle Cambrian, Serie 3
Brab-5	505	10.8	59.1	0.1108	0.511890	3	−9.1	1.70	1.70	Black slate	Upper Jodoigne Fm.	Middle Cambrian, Serie 3
Brab-6	494	8.49	46.4	0.1105	0.511965	4	−7.7	1.59	1.58	Black slate	Middle Mousty Fm.	Upper Cambrian, Furongian
Brab-13	490	6.41	35.3	0.1096	0.511979	2	−7.4	1.55	1.56	Black slate	Upper Mousty Fm.	Upper Cambrian, Furongian
Brab-23	486	12.5	69.3	0.1093	0.511885	3	−9.3	1.69	1.70	Gray slate	Chevlipont Fm.	Lower Ordovician, Tremadoc
Brab-7	470	8.80	48.1	0.1107	0.511913	2	−9.0	1.67	1.66	Argillaceous siltite	Abbaye de Villers Fm.	Lower Ordovician, Dapingian
Brab-8	461	6.61	40.6	0.0983	0.511911	2	−8.4	1.49	1.61	Gray slate	Rigenée Fm.	Middle Ordovician, Darriwilian
Brab-20	455	4.58	17.8	0.1558	0.512104	2	−8.1	2.49	1.57	Dark slate	Ittre Fm.	Upper Ordovician, Sandbian
Brab-21	450	6.38	35.3	0.1090	0.511958	2	−8.2	1.58	1.59	Black slate	Fauquez Fm.	Upper Ordovician, Katian
Brab-10	442	9.64	46.6	0.1250	0.512096	2	−6.5	1.62	1.45	Dark gray slate	Middle Brûtia Fm.	Base Silurian, Rhuddanian
Brab-11	435	8.59	47.9	0.1084	0.512037	4	−6.8	1.45	1.47	Gray slate	Bois Grand-Père Fm.	Silurian, Aeronian
Brab-12	428	8.07	45.9	0.1064	0.512030	2	−6.9	1.44	1.47	Green slate	Upper Fallais Fm.	Silurian, Telychian
Intrusive and volcanic rocks												
BRM 21	458	10.4	44.3	0.1415	0.512223	4	−4.9	1.73	1.34	Tuff	Base Ittre Fm.	Upper Ordovician, Sandbian
BRM 23	445	5.06	23.0	0.1329	0.512249	3	−4.0	1.49	1.26	Dacite	Upper Madot Fm.	Upper Ordovician, Katian
BRM 19	445	6.93	33.7	0.1243	0.512220	2	−4.1	1.40	1.27	Tuff	Upper Madot Fm.	Upper Ordovician, Katian
Brab-16	441	4.69	25.8	0.1097	0.512345	4	−0.8	1.03	1.03	Rhyolite	Upper Brûtia Fm.	Lowest Silurian, Rhuddanian
BRM 17	430	5.64	27.4	0.1245	0.512204	2	−4.5	1.43	1.29	Microdiorite	Quenast pipe	Silurian, upper Telychian
Brab-18	430	6.02	28.7	0.1270	0.512253	3	−3.7	1.39	1.23	Microdiorite	Bierghes sill	Unknown, probably Silurian
Brab-19	428	7.79	40.2	0.1172	0.512206	2	−4.1	1.32	1.26	Tuff	Upper Fallais Fm.	Silurian, upper Telychian

basement and a sedimentary rock whose source is a 0.6 Ga granite generated from the melting of a 2 Ga basement will have the same Nd T_{DM}. Brabant Nd T_{DM} model ages in the range 1.4–1.7 Ga indicate that the Brabant source results from the erosion either from a Mesoproterozoic segment or from the mixing of Neoproterozoic and Palaeoproterozoic basements, the two possibilities being not exclusive. The main point is that the Proterozoic inheritance shown by detrital zircons is also recorded by the whole-rock Nd isotope: this inheritance is not an artifact due to a high resistance of the mineral zircon and the zircon signature is not disconnected from the whole-rock signature as it is the case in the Neoproterozoic Arabian-Nubian shield (Stern et al., 2010).

ε_{Nd} values have been reported with the detrital zircon age information against stratigraphical ages in Fig. 21. During the Cambrian period, ε_{Nd} varies between −5.5 and −9, which is interpreted as a consequence of a variable input from Amazonia and NW Africa, also shown by the detrital zircons. The youngest Cambrian Mousty Formation shows values between −7.7 and −7.4. There is a significant decrease in ε_{Nd} in the Early Ordovician Chevlipont Formation (−9.3) that marks the beginning of the drifting of Avalonia. This ε_{Nd} value remains remarkably constant during the Ordovician (−9.3 to −8.1), when Avalonia was an isolated island during the Rheic Ocean opening. This ε_{Nd} value of -8.6 ± 0.5 can thus be considered as the signature of the Avalonia basement itself. Silurian rocks are significantly less negative, being at −6.9 to −6.5. This can be attributed to an additional input either from Baltica or from the Brabant igneous rocks, which have much less negative values, their ε_{Nd} varying between −4.9 and −0.8 (Fig. 21).

7. Palaeogeographical constraints for Avalonia from Brabant detrital zircon ages, Nd isotopes of sedimentary and magmatic whole-rocks and from the "Megumia" concept

7.1. The odyssey of the Brabant Massif

Several realms were potential suppliers of detrital zircons to the Brabant basin during the Early Palaeozoic (Figs. 21 and 22). Based on their different zircon age spectra, they may allow putting additional constraints on the palaeoposition of Avalonia with a much better time resolution than allowed by palaeomagnetism, by virtue of the detailed and precise stratigraphic control available for the Brabant sedimentary record. Admittedly, the spatial resolution inherent to this method is poor, but the detrital zircon approach nevertheless offers an excellent complement to palaeomagnetic studies. We consider here only the primary origin of the zircon, diagnostic of its initial origin. Because (1) the probability of cannibalism, considering the Ordovician sediments for example as resulting from the erosion of the Cambrian is unlikely as the Cambrian to Silurian period in the Brabant Massif is a subsident period, except during the 485–474 Ma period when no sediment was deposited (hiatus) as a result of a basement uplift (Fig. 4); (2) If there is an intermediate sedimentary reservoir, whose existence would be not recorded by zircons, this implies far-distant sediments, i.e. sediments associated with old basement itself and the conclusions will be similar. The same reasoning can be applied to the Nd isotope information.

The different continental zircon sources for the Brabant basin in Early Palaeozoic times are West Africa, Amazonia (both being part of Gondwana), Baltica, Laurentia, and Avalonia itself. Indeed, at the end of the Neoproterozoic, Avalonia was one of the Peri-Gondwanan terranes. During the Cambrian, it was located off Mauritania and left Gondwana in the Early Ordovician (e.g. Cocks and Torsvik, 2002, 2005; Linnemann et al., 2010), drifting towards Baltica with which it docked at c. 445 Ma (Cocks and Torsvik, 2002; Torsvik and Rehnström, 2003; Cocks and Fortey, 2009). Later, Baltica–Avalonia having collided with Laurentia between 435 and 385 Ma (Andréasson et al., 2003; Glodny et al., 2008; Hacker et al., 2010).

West Africa is characterized by the absence of Mesoproterozoic geological record: during the Cambrian, the reworked margins of the West African craton were available to deliver detrital zircons mainly of Palaeoproterozoic and Neoproterozoic ages with a minor component of Archaean age (Ennih and Liégeois, 2008 and references therein; Fig. 20). Amazonia can also deliver similar zircon populations but also Mesoproterozoic crystals (e.g., Linnemann et al., 2011; Fig. 20). Baltica is characterized by abundant Mesoproterozoic segments (e.g. Bingen et al., 2005). The part of Laurentia which was the closest to Brabant in the period 435–385 Ma is Greenland and especially its southern part, characterized by Palaeoproterozoic ages (Ketilidian; Kalsbeek and Taylor, 1985). All the above regional sources can also deliver zircons of Archaean age, but in limited amounts. In consequence, it appears that the best age groups to be used for constraining the palaeogeography of the Brabant Massif corresponds to the Precambrian Eons, Archaean, Palaeo-, Meso- and Neoproterozoic, in addition to Palaeozoic ages. This age division has been adopted and variations through time of the relative percentage of zircons are presented in Figs. 20 and 21.

During the Cambrian, the Neoproterozoic zircons constitute more than 50% of the stock (Fig. 21), in agreement with the well-documented Neoproterozoic evolution of Avalonia and its proximity to Gondwana, the latter delivering an additional Palaeoproterozoic signature (and a minor Archaean one, roughly constant). The Mesoproterozoic signature, believed to document an Amazonian supply, is variable: 16% in Blanmont Formation, 2% in Tubize Formation and 18–25% in Jodoigne Formation (Fig. 21). This can be interpreted as a combined supply from West Africa and Amazonia (Fig. 22A), the relative proportion varying following the fluviatile systems, itself being influenced by the rift tectonics at work during this period.

The very base of the Ordovician, corresponding to the top of Megasequence 1 (Chevlipont Formation) is characterized by a drop of Palaeoproterozoic, Mesoproterozoic and Archaean zircons and an increase of the Neoproterozoic zircon proportion. This is linked with more negative ε_{Nd} values, which can be explained by Neoproterozoic granitoids having an old source as it is the case in Hoggar (Liégeois et al., 2003; Fig. 21). The same signature is displayed by the Tribotte Formation (Middle Ordovician) in the lower part of Megasequence 2 (Fig. 4). The strong decrease of the sedimentation rate in the Chevlipont Formation can be considered as announcing the Abbaye de Villers and Tribotte shallow shelf environment (Fig. 6). We interpret the nearly similar Chevlipont and Tribotte age pattern as the Avalonia signature, alone for Tribotte (0% Mesoproterozoic zircons; Avalonia was an isolated island at that time; Fig. 22B) and with very little Gondwana input for Chevlipont (having still a small proportion of Mesoproterozoic zircons). We can in consequence consider that the signature combining more Neoproterozoic zircons associated with more negative ε_{Nd} is that of the Avalonia microcontinent itself. We can thus date precisely the beginning of the drifting of Avalonia in the Brabant at 485 Ma, a little earlier than previously thought in other place (c. 478 Ma; Cocks and Torsvik, 2005; Cocks and Fortey, 2009). Both Chevlipont and Tribotte formations contain an additional, minor proportion of Palaeozoic zircons (Fig. 21), which can be attributed to the Chevlipont volcanism and Lower Ordovician hiatus inferred volcanism, also recorded by the Quenast and Madot inherited zircons (see Section 5.2).

The sediments contemporaneous with the magmatic period (Ittre to Fallais formations) are all too fine-grained for delivering zircons adequate for dating purposes by LA-ICP-MS, but Nd isotopes are available for this period. The Rigenée, Ittre and Fauquez formations have similar Nd signature to Tribotte, although slightly less negative (Fig. 21). By contrast, the ε_{Nd} values for Brutia to Fallais formations are clearly less negative and can be attributed to the record of the Avalonia–Baltica docking. The latter can thus be interpreted to have triggered the Brabant magmatism (Fig. 22C). The first post-Tribotte zircon-bearing sample was collected from the mid-Silurian Corroy

Formation, just above the Fallais Formation (Fig. 4). Compared to the Tribotte Formation sample that shows a purely Avalonian detrital zircon signature, the Corroy Formation points to a greater contribution of Mesoproterozoic and Palaeoproterozoic zircons (Fig. 21), in keeping with the Nd isotopes signature. It is noticed that Avalonia became part of Laurussia at that time, following the collision of Baltica–Avalonia with Laurentia (Fig. 22D). The detrital zircon signature of the Corroy Formation can thus be attributed to Avalonia itself (Neoproterozoic zircons, the latter being uncommon in Baltica and Greenland-Laurentia), to Baltica (strong Mesoproterozoic zircons increase), but also possibly to Greenland (Laurentia).

Finally the Middle Devonian Bois de Bordeaux Formation (basal conglomerate above Brabantian angular unconformity; Fig. 4) contains the first important (17%) zircon population of Early Palaeozoic age probably supplied through the erosion of Brabant volcanic rocks. In this sample, the smaller proportion of the Mesoproterozoic contribution is interpreted to reflect the isolation of Baltica as a zircon source. However the still significant proportion of Palaeoproterozoic zircons, might suggest that Greenland formed reliefs within the Old Red Sandstone Continent, no mountain ranges separating Greenland and Brabant at this time (cf. Cocks and Torsvik, 2011).

7.2. Comparison of the Cambrian successions of the Brabant Massif with those of the Meguma Terrane (Nova Scotia) and the Harlech Dome (Wales); the "Megumia" concept

Recently Waldron et al. (2011) have shown that the Meguma Terrane of Nova Scotia (peri-Gondwana) and the Harlech Dome of North Wales ("East" Avalonia) present very similar Cambrian sedimentary successions. Both series comprise a very thick succession (Meguma > 11 km and Harlech Dome > 6 km) of lower Cambrian sandstone turbidites (with subordinate *Oldhamia* pelagic shales in Meguma) overlain by middle Cambrian alternating mud-rich and sand-rich units (turbidite) with many levels enriched in manganese. Above these, both successions comprise Furongian organic-rich mudstones and distal turbidites, shallowing upwards into paler, more bioturbated Tremadocian mudstone with *Rhabdinopora*. These two successions are unconformably overlain by Floian (Lower Ordovician) sediments in the Harlech Dome, and by lower Silurian rocks in the Meguma terrane. This close similarity strongly suggests proximity between the two terranes on the margin of Gondwana during the Cambrian. Waldron et al. (2011) suggested the term "Megumia" for the palaeogeographic domain that included the two successions. These two latter successions are amazingly similar to the Brabant succession described in this paper (see Section 3).

Without going into all stratigraphical, sedimentological and geochemical features out of the scope of this paper and which will which will be detailed in a further publication, we can emphasize the following similarities: (1) in the three regions, very thick Cambrian sequences were deposited in a basinal deep clastic sea, most probably a rift environment: Meguma > 11 km, Harlech Dome > 6 km and Brabant Massif > 9 km; (2) the three successions encompass the same stratigraphic interval, from lower Cambrian to Tremadocian–Floian (Dyfed sequence of Woodcock, 1990; Megasequence 1 of this paper), and their top is marked by an unconformity; (3) The base of the succession in the Brabant (Blanmont Formation, see Section 3.1) and in the Harlech Dome (Dolwen Formation, Rushton and Molyneux, 2011) are interpreted as shallow marine which is not the case for Meguma where the base is unknown. Otherwise, all the Cambrian sedimentary environments are basinal in the three regions, even though the Brabant Massif environments are generally more pelagic (distal) and those of Meguma and Harlech are more turbiditic (proximal); (4) numerous Mn-enriched levels are observed in thick successions of alternating black mudstone and sandstone of middle Cambrian age in Meguma and Harlech and in hemi-pelagic to pelagic black shale of Furongian age in Brabant; (5) in all three successions, the transition from oxic to anoxic conditions occurs synchronously, within biostratigraphic uncertainties, in the middle Cambrian; (6) volcanic components are absent in the Cambrian part of the three successions being only present at the top in the Tremadocian of the Brabant and Harlech Dome (7) detrital zircon ages (Krogh and Keppie, 1990; Waldron et al., 2009, 2011, this study) show a same age spectrum in the three regions: dominated by Neoproterozoic zircons, presence of Palaeoproterozoic zircons while Mesoproterozoic zircon are present but in smaller amounts. This strongly suggests that the three basins had a common source area in the West African Craton and/or Amazonia. (8) Similar ε_{Nd} negative values for sedimentary rocks in the Brabant (−5.5 to −9.3) and Meguma (−6.4 to −8.8; Waldron et al., 2009) are consistent with a similar ancient, evolved source. The few mildly positive ε_{Nd} values (0.8 to 0.9) indicative of a juvenile source in the lower part of Meguma are not observed in the Brabant.

Despite these similarities, differences are however present, as already emphasized by Waldron et al. (2011) between Meguma and Harlech Dome as well as with the Brabant Massif, but they are of minor importance. They can be explained by the large size of the inferred rift and thus the large distances that could have separated these three regions during the Cambrian. The Cambrian to lowest Ordovician histories of the three basins (and probably also of the Cambro-Ordovician Ardenne Inliers; Verniers et al., 2002; Herbosch et al., 2008a; Sintubin et al., 2009) record a distinctive peri-Gondwanan domain of rapid subsidence and deep-water sedimentation, oxic then anoxic, with Mn enrichment and with a distinct shallowing-up in the Tremadocian (announcing uplift and drifting from Gondwana). This sedimentary record contrasts strikingly with adjacent regions (British Caledonides and Canadian Appalachians) showing platformal successions (e.g. Landing, 1996; Hibbard et al., 2006, 2007; Rushton and Molyneux, 2011) regarded until now as typical of Avalonia. This also means that the Brabant Massif probably belonged to the "Megumia" palaeogeographic domain of Waldron et al. (2011). However, we do not follow these authors on the concept of a "Megumia" domain distinct from Avalonia in the Cambrian. Indeed, our detrital zircon and Nd isotopes data display a signature characteristic of the Avalonia basement when Avalonia was an island drifting in the Rheic Ocean towards Baltica. This extended domain that include Meguma–Harlech Dome–Brabant Massif (and Ardenne inliers) terranes, must be considered as a part of the proto-Avalonia microplate and the name "Megumia" is not necessary.

Indeed, the Avalonia microplate must be considered as being composed of (1) an emerged land, a mainly Neoproterozoic basement with an old ancestry (this paper chap. 6; Pe-Piper and Jansa, 1999; Hibbard et al., 2007; Cocks and Fortey, 2009; Waldron et al., 2009, 2011) represented, within "East" Avalonia, by the Midland microcraton to the West and the Lünebourg-North Sea microcraton to the East (Figs. 2A and 5); (2) a large marine platform corresponding to the classical shelf facies of the British Caledonides and Avalon terrane (e. g. Landing, 1996) and (3) a more distal rifted deep-sea zone represented by the Meguma terrane, the Brabant Massif (with the Ardennes Inliers) and the Harlech Dome.

Additional constraints can be used for proposing a new late Early Cambrian (c. 510 Ma) palaeogeographical reconstruction during the rifting period that preceded the Rheic Ocean opening (Fig. 23). They are: (1) during the Variscan collision between Avalonia and southern terranes (Fig. 1), Avalonia behaved as a rigid indenter: in Belgium, the Brabant Massif was not affected by the Variscan event, except on its southern side along the Midi Fault System (Variscan front in Fig. 2A). This means that the current geometry of the south-eastern boundary of the Avalonia microcontinent, corresponding to the Rheic suture (Figs. 1 and 23), can be considered as broadly unchanged since the formation of the Cambrian rift. (2) We consider, following Cocks and Fortey (2009) and Woodcock (2011) and by contrast with Waldron et al. (2011) that Avalonia was a single continuous

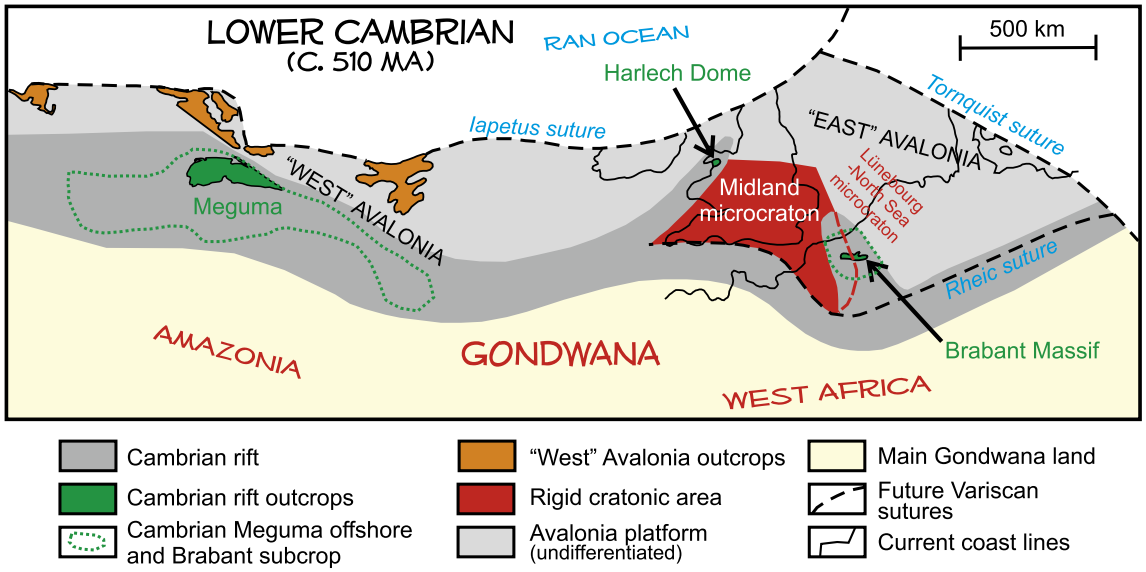

Fig. 23. Upper lower Cambrian palaeogeographic reconstruction of the large rift separating Gondwana from Avalonia that has led to the generation of the Rheic Ocean. Brabant Massif and Harlech Domes constitute embayments of this rift within "East" Avalonia along weakness zones formed by eastern (Harlech) and western (Brabant) boundaries of the Midland microcraton, the main branch being represented by the Meguma terrane. General palaeogeography after Cocks and Torsvik (2005). Contour of the Midland microcraton after Sintubin et al. (2009) for his SE prolongation under the Variscan front and Maguire et al. (2011) for his boundary in Wales and southern England. Offshore extension of Meguma terrane from Pe-Piper and Jansa (1999) and White (2010). Meguma position is drawn before Devonian-Carboniferous strike-slip (Hibbard and Waldron, 2009).

microcontinent. (3) This implies that the Brabant Massif was located to the north of the main Cambrian rift, elongated perpendicular to it (N–S elongation). We suggest accordingly that the Brabant basin constituted an embayment, which could be considered as an aulacogen (following the definition of Bates and Jackson, 1980), of the main E–W rift. (4) Using the same arguments, we can reach the same kind of conclusions for the Harlech Dome: it should also form a gulf elongated parallel to the Menai Strait Fault System that marks a major terrane boundary (Waldron et al., 2011; Woodcock, 2011).

The examination of this new palaeogeographical reconstruction (Fig. 23) shows that the Brabant Massif and the Harlech Dome are located aside the Midland microcraton, the former to the east and the latter to the west. We note also that the Rheic suture, and thus the Cambrian rift north-western boundary, are skirting around the Midland microcraton. We suggest that such a virgation has generated constraints at the origin of both Brabant and Harlech embayments. In that configuration (Fig. 23), the Meguma segment would be located in the western part of the main rift that led to the birth of the Rheic Ocean and the Appalachian Avalonia domain to the north of it, if we use the lower Cambrian (c. 510 Ma) palaeogeographic configuration of Cocks and Torsvik (2005). This means also that the Brabantian orogeny (Fig. 4) corresponds to the closure of the Brabant embayment and its inversion at c. 415 Ma.

8. Conclusions

Recent detailed field work including mapping, stratigraphical, sedimentological and tectonic studies, coupled with detrital zircon ages, geochemistry and Nd isotope data of sediments and magmatic rocks, allow to chronicle the odyssey of the Brabant Massif during the Early Palaeozoic, with implication to the entire Avalonia microplate.

The Brabant basin was born in Cambrian, upper Stage 2 (c. 525 Ma), as an embayment of a large rift that developed on the western Gondwana margin (Fig. 22A) just after the Pan-African orogeny. This rifting period lasted until the lowermost Ordovician (c. 485 Ma), generating the Megasequence 1 of >9 km thick (Fig. 4). These sediments are mainly slate, sandstone, quartzite and greywackes (Blanmont to Mousty formations; Fig. 4) and are interpreted as deep-water turbidites and hemi-pelagic to pelagic shales. Detrital zircon ages are late Neoproterozoic (Pan-African) in majority (45–65%), with additional Palaeoproterozoic and Archaean zircons and variable Mesoproterozoic input (0–20%), pointing to a West African source with variable additional contribution from Amazonia (Fig. 21). This is in agreement with the moderately negative Nd isotope signature ($\varepsilon_{Nd} = -5$ to -9). Megasequence 1 ended with a volcanic episode associated with a shallowing trend (Chevlipont Formation, lower Tremadocian) marking the drifting of Avalonia from Gondwana and the birth of the Rheic Ocean. This phase is also marked by an unconformity (hiatus 485–474 Ma) during which volcanism is inferred (abundant magmatic inherited zircon in subsequent igneous rocks).

Drifting of the Avalonia island between the Iapetus and Rheic oceans was a quiet period when located on the south passive margin, as it was the case for the Brabant Massif (Fig. 22B). The 1300 m thick Megasequence 2 began its deposition (474–460 Ma) within a stable platform with various shelf clayey sandstone and siltstone (Abbaye de Villers and Tribotte formations) and dark siltstone to mudstone (Rigenée Formation). While approaching the Baltica continent (460–448 Ma), tectonic instabilities occurred, documented by the deepening of the depositional environment (turbidites and pelagic shales: from Ittre to Huet formations; Fig. 4), increasing slumps and incipient volcanism (Ittre rhyolite, 458 ± 4 Ma, Fig. 8). During this drifting period, detrital zircons derived only from the Avalonia terrane, determining its signature. Detrital zircons (Fig. 21) are mostly Neoproterozoic (70–80%) with additional Palaeoproterozoic zircons (10–20%), other provenance being <10%, delineating a West African linkage of the Avalonia basement. Rather constant Nd isotopic signature ($\varepsilon_{Nd} = -9$ to -8, Fig. 21) suggests a rather limited outcropping surface, in agreement with an isolated island and the low thickness of the deposits.

Megasequence 3, >3.5 km thick, deposited between 448 Ma (Katian, Late Ordovician) and c. 415 Ma (lowermost Lochkovian, Early Devonian; Fig. 4), corresponds to an intracontinental tectonic active period accompanied by an important (sub)volcanic event (Madot tuff: 445 ± 2 Ma, Fig. 10; Madot dacite: 444 ± 6 Ma, Fig. 9; Quenast plug: 430 ± 3 Ma, Fig. 11). The transition is marked by a drastic change in palaeobathymetry from black pyritic slate (Fauquez Formation), interpreted as mud turbidites, to slate, shelly siltite, tuff and volcanic rocks (Madot Formation) deposited in a shallow shelf.

The Megasequence records shelf deposition from Katian to Late Telychian (Madot, Brutia, Bois Grand-Père formations) that evolved rapidly into thick deep-sea turbidity deposits from the Late Telychian to Late Gorstian (from Fallais to Ronquières formations; Fig. 4). Brabant Megasequence 3 recorded the Avalonia–Baltica soft docking (c. 445 Ma; Fig. 23C) marked by the (sub)volcanism peak and the appearance of Mesoproterozoic detrital zircons typical of Baltica (Fig. 21). Shortly after, Baltica–Laurentia Caledonian collision (from 430 Ma; Fig. 22D) points to the beginning of the tectonic inversion of the basin (Brabatian orogeny) that generated Silurian foreland-basins at the rims of the domain (Fig. 5) and finally the demise of sedimentation during the Earliest Lochkovian (c. 415 Ma). Intrusive bodies are high-K calc-alkaline to alkali-calcic in nature (Fig. 7), mostly of crustal derivation, and are aligned in a narrow band following the NW–SE oriented Nieuwpoort-Asquempont fault zone (N-AFZ, Fig. 2B and 5), corresponding to the southwestern boundary of the Cambrian rift. Brabant magmatism is interpreted as a far-distant result of the Avalonia–Baltica docking through the intracontinental reactivation of pre-existing lithospheric discontinuities and the Brabantian orogeny a far-distant result of the Caledonian Baltica–Laurentia collision through the inversion of the rift basin.

As a result of the Brabantian inversion, no sediment deposited during the Early–Middle Devonian (415–390 Ma). Sediment deposition restarted during Early Givetian with the conglomerate of the Bois de Bordeaux Formation (Fig. 4) that rests in angular unconformity on the southern side of the Brabant Massif (Figs. 2 and 3). Detrital zircons of this conglomerate (Figs. 19 and 21) are mostly Neoproterozoic and Palaeoproterozoic (35% each) but also Palaeozoic in age (20%) with the presence of 10% of Mesoproterozoic zircons. This suggests a largely internal Avalonia provenance but the overrepresentation of Palaeoproterozoic zircons suggests Laurentia (Greenland) as an additional source, no relief separating Brabant from Greenland at that time (Fig. 22D).

Finally, large stratigraphical and sedimentological similitudes between the Brabant Massif and the Harlech Dome in Wales ("East" Avalonia) on the one hand and with the Meguma Terrane in Nova Scotia (Canada, peri-Gondwana) on the other hand, allow the reconstruction of a lower Cambrian palaeogeographical map (Fig. 23). In the latter, Brabant and Harlech are embayments of the main rift, on each sides of the Midland microcraton, and Meguma is in the western continuation of the main rift, currently located in the American part of Avalonia. In consequence, the Meguma terrane, which is up to now of uncertain palaeogeographic provenance, should belong to the Avalonia microplate.

Supplementary materials related to this article can be found online at doi:10.1016/j.earscirev.2012.02.007.

Acknowledgments

U.L thanks Françoise and Alain Herbosch for their hospitality during the fieldwork. Further, U.L. thanks Ulrike Kloss (Dresden) for drawing some figures. AH thanks the Department of Earth and Environmental Sciences (DSTE) from the Université Libre de Bruxelles for the authorization to continue research activities during his retired period. C.P. gratefully acknowledges Prof. J. Lancelot and Dr P. Verdoux (GIS Lab, University of Nîmes) for generous access to the Triton mass spectrometer. We thank R.L.M. Cox and an anonymous reviewer for their constructive reviews as well as the Editor A.D. Miall for his helpful handling of the manuscript. UL, AG and MH did the zircon dating, CP the Sm–Nd isotopic measurements, AH the stratigraphy, AH and JPL interpreted the data and wrote the paper.

Annex 1. Analysis of U–Pb isotopes of zircon by LA-ICP-MS

Zircon concentrates were separated from 2 to 4 kg sample material at the *Senckenberg Naturhistorische Sammlungen Dresden* using standard methods. Final selection of the zircon grains for U–Pb dating was achieved by hand-picking under a binocular microscope. Zircon grains of all grain sizes and morphological types were selected, mounted in resin blocks and polished to half their thickness. Zircons were analyzed for U, Th, and Pb isotopes by LA-ICP-MS techniques at the Museum für Mineralogie und Geologie (GeoPlasma Lab, Senckenberg Naturhistorische Sammlungen Dresden), using a Thermo-Scientific Element 2 XR sector field ICP-MS coupled to a New Wave UP-193 Excimer Laser System. A teardrop-shaped, low volume laser cell constructed by Ben Jähne (Dresden) and Axel Gerdes (Frankfurt/M.) was used to enable sequential sampling of heterogeneous grains (e.g., core/rim) during time resolved data acquisition. Each analysis consisted of approximately 15 s of background acquisition followed by 30 s of data acquisition, using a laser spot-size of 25 and 35 μm, respectively. A common-Pb correction based on the interference- and background-corrected ^{204}Pb signal and a model Pb composition (Stacey and Kramers, 1975) was carried out if necessary. The necessity of the correction was judged on whether the corrected ^{207}Pb/^{206}Pb lies outside of the internal errors of the raw, measured ratios. Raw data were corrected for background signal, common Pb, laser induced elemental fractionation, instrumental mass discrimination, and time-dependent elemental fractionation of Pb/Th and Pb/U using an Excel® spreadsheet program developed by Axel Gerdes (Institute of Geosciences, Johann Wolfgang Goethe-University Frankfurt, Frankfurt am Main, Germany). Reported uncertainties were propagated by quadratic addition of the external reproducibility obtained from the standard zircon GJ-1 (~0.6% and 0.5–1% for the ^{207}Pb/^{206}Pb and ^{206}Pb/^{238}U, respectively) during individual analytical sessions and the within-run precision of each analysis. Concordia diagrams (with 2σ error ellipses) and Concordia ages (95% confidence level) were produced using Isoplot/Ex 2.49 (Ludwig, 2001), and frequency and relative probability plots using AgeDisplay (Sircombe, 2004) softwares. The ^{207}Pb/^{206}Pb age was taken for interpretation for all zircons >1.0 Ga, and the ^{206}Pb/^{238}U ages for younger grains, considering the higher error on ^{207}Pb in that age range. For further details on analytical protocol and data processing see Gerdes and Zeh (2006). Th/U ratios (Tables 6 to 17, data repository) are obtained from the LA-ICP-MS measurements of investigated zircon grains. U and Pb content and Th/U ratio were calculated relative to the GJ-1 zircon standard and are accurate to approximately 10%.

Annex 2. Whole-rock geochemistry

Analysis of sedimentary and magmatic rocks (Table 3) has been done at Nancy in Service d'Analyse des Roches et Minéraux (SARM-CRPG/CNRS). Whole-rock samples were decomposed by fusion with LiBO2 as a fluxing agent and then solubilized in acid. Major elements were analyzed by ICP-OES and trace elements by ICP-MS. Further details on precision and detection limit could be found at http://helium.crpg.cnrs-nancy.fr/SARM/

Annex 3. Analysis of Sm–Nd isotope on whole-rock

In preparation to Sm–Nd isotope measurements, whole-rock samples were decomposed by fusion in an induction furnace with $LiBO_2$ as a fluxing agent, as described by Le Fèvre and Pin (2005). Then, Sm and Nd were separated from matrix elements and from each other by a procedure adapted from Pin and Santos Zalduegui (1997) combining cation-exchange and extraction chromatography techniques. Sm concentrations were measured by isotope dilution with a ^{149}Sm-enriched tracer and an upgraded VG54E thermal ionization mass spectrometer (TIMS) in the single collector mode (Clermont-Ferrand), while Nd concentrations and ^{143}Nd/^{144}Nd isotope ratios were determined concomitantly with a ^{150}Nd-enriched tracer and a Triton TIMS machine operated in the static multicollection mode (GIS Laboratory, Nîmes). During the period of analyses, the Nd

isotope ratio standard of the Japan Geological Survey JNdi-1 gave an average value of 0.512101 (standard deviation = 7 10^{-6}, n = 5), corresponding to a value of 0.511844 for the La Jolla standard (Tanaka et al., 2000).

References

André, L., 1991. The concealed crystalline basement in Belgium and the "Brabantia" microplate concept: constraints from the Caledonian magmatic and sedimentary rocks. Annales de la Société Géologique de Belgique 114, 117–139.

André, L., Deutsch, S., 1984. Les porphyres de Quenast et de Lessines: géochronologie, géochimie isotopique et contribution au problème de l'âge du socle Precambrien du Massif du Brabant (Belgique). Bulletin de la Société belge de Géologie 93, 375–384.

André, L., Deutsch, S., 1985. Very low-grade metamorphic Sr isotopic resettings of magmatic rocks and minerals: evidence for a late Givetian strike-slip division of the Brabant Massif (Belgium). Journal of the Geological Society of London 142, 911–923.

André, L., Deutsch, S., Hertogen, J., 1986a. Trace-element and Nd isotopes in shales as indexes of provenance and crustal growth: the early Palaeozoic from the Brabant Massif (Belgium). Chemical Geology 57, 101–115.

André, L., Hertogen, J., Deutsch, S., 1986b. Ordovician–Silurian magmatic provinces in Belgium and the Caledonian orogeny in the middle Europe. Geology 14, 879–882.

André, L., Herbosch, A., Louwye, S., Servais, T., Van Grootel, G., Vanguestaine, M., Verniers, J., 1991. Guidebook to the excursion on the stratigraphy and magmatic rocks of the Brabant Massif, Belgium. Annales Société Géologique de Belgique 114, 283–323.

Andréasson, P.G., Gee, D.G., Whitehouse, M.J., Schöberg, H., 2003. Subduction-flip during Iapetus Ocean closure and Baltica–Laurentia collision, Scandinavian Caledonides. Terra Nova 15, 362–369.

Azzouni-Sekkal, A., Liégeois, J.P., Bechiri-Benmerzoug, F., Belaidi-Zinet, S., Bonin, B., 2003. The "Taourirt" magmatic province, a marker of the very end of the Pan-African orogeny in the Tuareg Shield: review of the available data and Sr–Nd isotope evidence. Journal of African Earth Sciences 37, 331–350.

Ballèvre, M., Bosse, V., Ducassou, C., Pitra, P., 2009. Palaeozoic history of the Armorican Massif: Models for the tectonic evolution of the suture zones. Comptes Rendus Geoscience 341, 174–201.

Bates, R.L., Jackson, J.A., 1980. Glossary of Geology. American Geological Institute, Virginia. 751 pp.

BGS: Belgian Geological Survey, 1994. Aeromagnetic map of the Brabant Massif: residual total field reduced to the pole. Scale 1/100000.

Bingen, B., Skår, Ø., Marker, M., Sigmond, E.M.O., Nordgulen, Ø., Ragnhildsveit, J., Mansfeld, J., Tucker, R.D., Liégeois, J.P., 2005. Timing of continental building in the Sveconorwegian orogen, SW Scandinavia. Norwegian Journal of Geology 85, 87–116.

Black, R., Liégeois, J.P., 1993. Cratons, mobile belts, alkaline rocks and continental lithospheric mantle: the Pan-African testimony. Journal of the Geological Society of London 150, 89–98.

Boullier, A.M., Liégeois, J.P., Black, R., Fabre, J., Sauvage, M., Bertrand, J.M., 1986. Late Pan-African tectonics marking the transition from subduction-related calc-alkaline magmatism to within-plate alkaline granitoids (Adrar des Iforas, Mali). Tectonophysics 132, 233–246.

Chacksfield, B., De Vos, W., D'hooge, L., Dusar, M., Lee, M., Poitevin, C., Royles, C., Verniers, J., 1993. A new look at Belgian aeromagnetic and gravity data through image-based display and integrated modelling techniques. Geological Magazine 130, 583–591.

Cherns, L., Wheeley, J.R., 2007. A pre-Hirnantian (Late Ordovician) interval of global cooling: the Boda event re-assessed. Palaeogeography, Palaeoclimatology, Palaeoecology 251, 449–460.

Cocks, L.R.M., Fortey, R.A., 2009. Avalonia: a long-lived terrane in the Lower Palaeozoic? In: Basset, M.G. (Ed.), Early Palaeozoic Peri-Gondwana Terranes: New Insights from Tectonics and Biogeography: Geological society, London, Special Publications, 325, pp. 141–155.

Cocks, L.R.M., Torsvik, T.H., 2002. Earth geography from 500 to 400 million years ago: a faunal and palaeomagnetic review. Journal of the Geological Society of London 159, 631–644.

Cocks, L.R.M., Torsvik, T.H., 2005. Baltica from the late Precambrian to mid-Palaeozoic times: the gain and loss of a terrane's identity. Earth-Science Reviews 72, 39–66.

Cocks, L.R.M., Torsvik, T.H., 2011. The Palaeozoic geography of Laurentia and western Laurussia: a stable craton with mobile margins. Earth-Science Reviews 106, 1–51.

de Magnée, I., Anciaux, P., 1945. Note préliminaire sur le métamorphisme à grenats du Brabant. Bulletin de la Société Belge de géologie 54, 77–85.

De Vos, W., Verniers, J., Herbosch, A., Vanguestaine, M., 1993. A new geological map of the Brabant Massif, Belgium. Special Issue on the Caledonides of the Anglo-Brabant Massif. Geological Magazine 130, 605–611.

Debacker, T.N., 1999. Fold trending at various angles to the transport direction in the Marcq area, Brabant Massif, Belgium. Geologica Belgica 2, 159–172.

Debacker, T.N., 2001. Palaeozoic deformation of the Brabant Massif within eastern Avalonia: how, when and why? Unpublished Ph. D. thesis, Lab. voor Palaeontologie, Universiteit Gent.

Debacker, T.N., 2002. Cleavage/fault relationship in the Silurian of the Mehaigne-Burdinale area, southeastern Brabant Massif, Belgium. Geologica Belgica 5, 3–15.

Debacker, T.N., 2012. Folds and cleavage/fold relationships in the Brabant Massif, southeastern Anglo-Brabant Deformation Belt. Geologica Belgica 15, 81–95.

Debacker, T.N., Herbosch, A., 2011. Field guide to the pre-cleavage deformation and stratigraphy of the Jodoigne area. Memoirs of the Geological Survey of Belgium 57, 1–27.

Debacker, T.N., Sintubin, M., 2008. The Quenast plug: a mega-porphyroclast during the Brabantian Orogeny (Senne Valley, Brabant Massif). Geologica Belgica 11, 199–216.

Debacker, T.N., Sintubin, M., Verniers, J., 2001. Large-scale slumping deduced from structural relations and sedimentary features: a study in the Lower Palaeozoic Anglo-Brabant fold belt, Belgium. Journal of the Geological Society of London 158, 341–352.

Debacker, T.N., Herbosch, A., Sintubin, M., Verniers, J., 2003. Palaeozoic deformation history of the Asquempont-Virginal area (Brabant Massif, Belgium): large-scale slumping, low-angle extensional detachment development (the Asquempont fault redefined) and normal faulting (the Nieuwpoort-Asquempont fault zone). Memoirs of the Geological Survey of Belgium 49, 1–30.

Debacker, T.N., Herbosch, A., Sintubin, M., 2004a. The supposed thrust fault in the Dyle-Thyle outcrop area (southern Brabant Massif, Belgium) re-interpreted as a folded low-angle extensional detachment. Geologica Belgica 8, 53–69.

Debacker, T.N., Herbosch, A., Verniers, J., Sintubin, M., 2004b. Faults in the Asquempont area, southern Brabant Massif, Belgium. Netherlands Journal of Geosciences/Geologie en Mijnbouw 83, 49–65.

Debacker, T.N., Dewaele, S., Sintubin, M., Verniers, J., Muchez, Ph., Boven, A., 2005. Timing and duration of the progressive deformation of the Brabant Massif, Belgium. Geologica Belgica 8, 20–34.

Debacker, T.N., Herbosch, A., Verniers, J., 2011. The presumed Upper Ordovician green rocks at Rebecq reinterpreted as a resurfacing of the Cambrian Oisquercq Formation (Senne Valley, Anglo-Brabant Deformation Belt, Belgium). Geologica Belgica 14, 249–264.

Delcambre, B., Pingot, J. L., 2008. Carte Perwez-Eghezée n°40/7-8, Carte Géologique de Wallonie, échelle 1/25000. Ministère de la Région Wallonne, DGRNE. Namur.

Delcambre, B., Pingot, J. L., Herbosch, A., 2002. Carte Chastre-Gembloux n°40/5-6, Carte Géologique de Wallonie, échelle 1/25000. Ministère de la Région Wallonne, DGRNE. Namur.

DePaolo, D.J., 1981. Neodymium isotopes in the Colorado Front Range and crust–mantle evolution in the Proterozoic. Nature 291, 193–197.

Drost, K., Gerdes, A., Jeffries, T., Linnemann, U., Storey, C., 2010. Provenance of Neoproterozoic and early siliciclastic rocks of the Teplá-Barrandian unit (Bohemian Massif): Evidence from U–Pb detrital zircon ages. Gondwana Research 19, 213–231.

Ennih, N., Liégeois, J.P., 2008. The boundaries of the West African craton, with a special reference to the basement of the Moroccan metacratonic Anti-Atlas belt. In: Ennih, N., Liégeois, J.-P. (Eds.), The Boundaries of the West African Craton. Geological Society, London, Special Publications, 297, pp. 1–17.

Errami, E., Bonin, B., Laduron, D., Lasri, L., 2009. Petrology and geodynamic significance of the post-collisional Pan-African magmatism in the Eastern Saghro area (Anti-Atlas, Morocco). Journal of African Earth Sciences 55, 105–124.

Everaerts, M., De Vos, W., 2012. Gravity acquisition in Belgium and the resulting Bouguer anomaly map. Memoirs of the Geological Survey of Belgium 58 64 p.

Everaerts, M., Poitevin, C., De Vos, W., Sterpin, M., 1996. Integrated geophysical/geological modelling of the western Brabant Massif and structural implications. Bulletin de la Société belge de Géologie 105, 41–59.

Fezaa, N., Liégeois, J.P., Abdallah, N., Cherfouh, E.H., De Waele, B., Bruguier, O., Ouabadi, A., 2010. Late Ediacaran geological evolution (575–555 Ma) of the Djanet Terrane, Eastern Hoggar, Algeria, evidence for a Murzukian intracontinental episode. Precambrian Research 180, 299–327.

Fortey, R.A., Cocks, L.R.M., 2005. Late Ordovician global warming: the Boda Event. Geology 33, 405–408.

Fourmarier, P., 1920. La tectonique du Brabant et des régions voisines. Mémoires de l'Académie Royale de Belgique, Classe des Sciences 4, 1–95.

Frost, B.R., Barnes, C.G., Collins, W.J., Arculus, R.J., Ellis, D.J., Frost, C.D., 2001. A geochemical classification for granitic rocks. Journal of Petrology 42, 2033–2048.

Gerdes, A., Zeh, A., 2006. Combined U–Pb and Hf isotope LA-(MC-) ICP-MS analysis of detrital zircons: comparison with SHRIMP and new constraints for the provenance and age of an Armorican metasediment in Central Germany. Earth and Planetary Science Letters 249, 47–61.

Glodny, J., Kühn, A., Austrheim, H., 2008. Diffusion versus recrystallization processes in Rb–Sr geochronology: isotopic relics in eclogite facies rocks, Western Gneiss Region, Norway. Geochimica et Cosmochimica Acta 72, 506–525.

Goffette, O., Liégeois, J.P., André, L., 1991. Age U–Pb sur zircon dévonien moyen à supérieur du magmatisme bimodal du Massif de Rocroi (Ardenne, France): implications géodynamiques. Comptes Rendus de l'Académie des Sciences de Paris, 312, pp. 1155–1161. Série II.

Graulich, J.M., 1961. Le sondage de Wépion. Mémoires explicatifs des Cartes Géologiques et Minières de Belgique 2, 1–102.

Gregory, R., 2011. A revised correlation of the Cambrian rocks in the British Isles. Geological Society Special Report, 25. 170 pp.

Hacker, B.R., Andersen, T.B., Johnston, S., Kylander-Clark, A.R.C., Peterman, E.M., Walsh, E.O., Young, D., 2010. High-temperature deformation during continental-margin subduction and exhumation: the ultrahigh-pressure Western Gneiss Region of Norway. Tectonophysics 480, 149–171.

Hadj Kaddour, Z., Liégeois, J.P., Demaiffe, D., Caby, R., 1998. The alkaline-peralkaline granitic post-collisional Tin Zebane dyke swarm (Pan-African Tuareg shield, Algeria): prevalent mantle signature and late agpaitic differentiation. Lithos 45, 223–243.

Hennebert, M., Eggermont, B., 2002. Carte Braine-le-Comte — Feluy n° 39/5-6, Carte géologique de Wallonie, échelle 1/25000. Ministère de la Région Wallonne, DGNRE. Namur.

Herbosch, A., 2005. Hospice de Rebecq: une nouvelle formation dans l'Ordovicien Supérieur du Massif du Brabant (Belgique). Geologica Belgica 8, 35–47.

Herbosch, A., Blockmans, S., in press. Carte Wavre — Chaumont-Gistoux n° 40/1-2, Carte géologique de Wallonie, échelle 1/25000. Ministère de la Région Wallonne, DGNRE. Namur.

Herbosch, A., Lemonne, E., 2000. Carte Nivelles-Genappe n°39/7-8, Carte Géologique de Wallonie, échelle 1/25000. Ministère de la Région Wallonne, DGRNE. Namur.
Herbosch, A., Verniers, J., 2002. The Lower Palaeozoic stratigraphy and sedimentology of the Brabant Massif in the Dyle and Orneau valleys and of the Condroz inlier at Fosses: an excursion guidebook. Geologica Belgica 5, 71–143.
Herbosch, A., Verniers, J., 2011. What is the biostratigraphic value of the ichnofossil *Oldhamia* for the Cambrian: a review. Geologica Belgica 14, 229–248.
Herbosch, A., Vanguestaine, M., Degardin, M., Dejonghe, L., Fagel, N., Servais, T., 1991. Etude lithostratigraphique, biostratigraphique et sédimentologique du sondage de Lessines (bord méridional du Massif du Brabant, Belgique). Annales de la Société Géologique de Belgique 114, 195–212.
Herbosch, A., Debacker, T.N., Piessens, K., 2008a. The stratigraphic position of the Cambrian Jodoigne Formation redefined (Brabant Massif, Belgium). Geologica Belgica 11, 133–150.
Herbosch, A., Debacker, T.N., Verniers, J., 2008b. Révision stratigraphique du sondage de Lessines (Massif du Brabant, Belgique). Geologica Belgica 11, 167–174.
Herbosch, A., Debacker, T., Dumoulin, V., Blockmans, S., in press-a. Carte Jodoigne-Jauche n° 40/3-4, Carte géologique de Wallonie, échelle 1/25000. Ministère de la Région Wallonne, DGNRE. Namur.
Herbosch, A., Dumoulin, V., Blockmans, S., Debacker, T., in press-b. Carte Rebecq-Ittre n° 39/1-2, Carte géologique de Wallonie, échelle 1/25000. Ministère de la Région Wallonne, DGNRE. Namur.
Hibbard, J., Waldron, J.W.F., 2009. Truncation and translation of Appalachian promontories: Mid-Palaeozoic strike-slip tectonics and basin initiation. Geology 37, 487–490.
Hibbard, J., van Staal, C.D.R., Williams, H., 2006. Lithotectonic Maps of the Appalachian Orogen (South), Canada-United States of America. Geological Survey of Canada, Map, p. 02096A.
Hibbard, J., van Staal, C.D.R., Rankin, D.W., 2007. A comparative analysis of pre-Silurian crustal building blocks of the northern and the southern Appalachian orogen. American Journal of Earth Science 307, 23–45.
Kalsbeek, F., Taylor, P.N., 1985. Isotopic and chemical variation in granites across a Proterozoic continental margin — the Ketilidian mobile belt of South Greenland. Earth and Planetary Science Letters 73, 65–80.
Kramm, U., Bühl, D., 1985. U–Pb zircon dating of the Hell tonalite, Venn-Stavelot Massif, Ardennes. Neues Jahrbuch für Geologie und Paläontologie, Abhandlungen 171, 329–337.
Krogh, T.E., Keppie, J.D., 1990. Age of detrital zircon and titanite in the Meguma Group, southern Nova Scotia, Canada: clue to the origin of the Meguma Terrane. Tectonophysics 177, 307–323.
Landing, E., 1996. Avalon: insular continent by the latest Precambrian. In: Nance, R.D., Thompson, M.D. (Eds.), Avalonian and Related Peri-Gonwanan Terranes of the Circum-North Atlantic: Geological Society of America, Special Paper, 304, pp. 29–63.
Le Fèvre, B., Pin, C., 2005. A straightforward separation scheme for concomitant Lu–Hf and Sm–Nd isotope ratio and isotope dilution analysis. Analytica Chimica Acta 543, 209–221.
Le Maitre, R.W., Streckeisen, A., Zanettin, B., Le Bas, M.J., Bonin, B., Bateman, P., Bellieni, G., Dudek, A., Efremova, S., Keller, J., Lameyre, J., Sabine, P.A., Scmid, R., Sorensen, H., Woolley, A.R., 2002. Igneous rocks: a classification and glossary of terms: recommendations of the International Union of Geological Sciences. Subcommission on the Systematics of Igneous Rocks. Cambridge University Press. 236 pp.
Lecompte, M., 1948. Existence du Trémadocien dans le Massif du Brabant. Bulletin de l'Académie Royale de Belgique 34, 677–687 Classe des Sciences, 5e série.
Lecompte, M., 1949. Découverte de nouveaux gîtes à *Dyctyonema* dans le Trémadocien du Massif du Brabant. Bulletin de l'Institut Royal des Sciences Naturelles de Belgique 25, 1–8.
Lee, M.K., Pharao, T.C., Williamson, J.P., Green, C.A., De Vos, W., 1993. Evidence of the deep structure of the Anglo-Brabant Massif from gravimetry and magnetic data. Special Issue on the Caledonides of the Anglo-Brabant Massif. Geological Magazine 130, 575–582.
Legrand, R., 1968. Le Massif du Brabant. Mémoires pour servir à l'Explication des cartes Géologiques et Minières de la Belgique, Mémoire 9, 1–148.
Liégeois, J.P., Stern, R.J., 2010. Sr–Nd isotopes and geochemistry of granite–gneiss complexes from the Meatiq and Hafafit domes, Eastern Desert, Egypt: No evidence for pre-Neoproterozoic crust. Journal of African Earth Sciences 57, 31–40.
Liégeois, J.P., Navez, J., Hertogen, J., Black, R., 1998. Contrasting origin of post-collisional high-K calc-alkaline and shoshonitic versus alkaline and peralkaline granitoids. Lithos 45, 1–28.
Liégeois, J.P., Latouche, L., Boughrara, M., Navez, J., Guiraud, M., 2003. The LATEA metacraton (Central Hoggar, Tuareg shield, Algeria): behaviour of an old passive margin during the Pan-African orogeny. Journal of African Earth Sciences 37, 161–190.
Liégeois, J.P., Benhallou, A., Azzouni-Sekkal, A., Yahiaoui, R., Bonin, B., 2005. The Hoggar swell and volcanism: reactivation of the Precambrian Tuareg shield during Alpine convergence and West African Cenozoic volcanism. In: Foulger, G.R., Natland, J.H., Presnall, D.C., Anderson, D.L. (Eds.), Plates, Plumes and Paradigms, Geological Society of America, Special Paper, 388, pp. 379–400.
Linnemann, U., McNaughton, N.J., Romer, R.L., Gehmlich, M., Drost, K., Tonk, C., 2004. West African provenance for Saxo-Thuringia (Bohemian Massif): did Armorica ever leave pre-Pangean Gondwana? — U–Pb–SHRIMP zircon evidence and the Nd-isotopic record. International Journal of Earth Sciences 93, 683–705.
Linnemann, U., Gerdes, A., Drost, K., Buschmann, B., 2007. The continuum between Cadomian orogenesis and opening of the Rheic Ocean: constraints from LA-ICP-MS U–Pb zircon dating and analysis of plate-tectonic setting (Saxo-Thuringian zone, north-eastern Bohemian Massif, Germany). In: Linnemann, U., Nance, D.R., Kraft, P., Zulauf, G. (Eds.), The evolution of the Rheic Ocean: from Avalonian-Cadomian Active margin to Alleghenian-Variscan Collision: Geological Society of America, Special paper, 423, pp. 61–96.
Linnemann, U., Hofmann, M., Romer, R.L., Gerdes, A., 2010. Transitional stages between the Cadomian and Variscan Orogenies: Basin development and tectonomagmatic evolution of the southern margin of the Rheic Ocean in the Saxo-Thuringian Zone (North Gondwana shelf). In: Linnemann, U., Romer, R.L. (Eds.), Pre-Mesozoic Geology of Saxo-Thuringia — From the Cadomian Active Margin to the Variscan Orogen. Schweizerbart Science Publishers, Stuttgart, pp. 59–98.
Linnemann, U., Ouzegane, K., Drareni, A., Hofmann, M., Becker, S., Gärtner, A., Sagawe, A., 2011. Sands of West Gondwana: an archive of secular magmatism and plate interactions — a case study from the Cambro-Ordovician section of the Tassili Ouan Ahaggar (Algerian Sahara) using U–Pb LA-ICP-MS detrital zircon ages. Lithos 123, 188–203.
Ludwig, K.R., 2001. Users Manual for Isoplot/Ex rev. 2.49: Berkeley Geochronology Center Special Publication No. 1a, pp. 1–56.
Maguire, P., England, R., Hardwig, A., 2011. LISPB DELTA, a lithospheric seismic profile in Britain: analysis and interpretation of the Wales and southern England section. Journal of the Geological Society of London 168, 61–82.
Maletz, J., Servais, T., 1996. Upper Ordovician graptolites from the Brabant Massif, Belgium. Geobios 31, 21–37.
Mansy, J.L., Everaerts, M., De Vos, W., 1999. Structural analysis of the adjacent Acadian and Variscan fold belts in Belgium and northern France from geophysical and geological evidence. Tectonophysics 309, 99–116.
McKerrow, W.S., Mac Niocaill, C., Dewey, J.F., 2000. The Caledonian orogeny redefined. Journal of the Geological Society of London 157, 1149–1154.
Michot, P., 1980. Le segment tectogénique calédonien belge. Mémoire de la classe des sciences 43, 1–61 2e série.
NCS, 2009. National Commission for Stratigraphy (Belgium), subcommission for Lower Palaeozoic, Revised Cambrian formations. http://www2.ulg.ac.be/geolsed/GB/SLP.htm.
NCS, 2011. National Commission for Stratigraphy, subcommission for Lower Palaeozoic, Revised Ordovician formations. http://www2.ulg.ac.be/geolsed/GB/SLP.htm.
Ogg, J.G., Ogg, G., Gradstein, F.M., 2008. The concise Geologic Time Scale. Cambridge University press, 177 p.
Owen, R.M., Servais, T., 2007. The Ordovician of the Condroz Ridge, Belgium. Palaeogeography, Palaeoclimatology, Palaeoecology 245, 272–294.
Paris, F., Boumendjel, A., Dabard, M.P., Ghienne, J.F., Loi, A., Tang, P., Videt, B., Achab, A., 2007. Chitinozoan-based calibration of Early–Mid Ordovician transgressive events on northern Gondwana. Acta Palaeontologica Sinica 46, 370–375.
Peacock, M.A., 1931. Classification of igneous rocks. Journal of Geology 39, 56–67.
Pearce, J.A., 1982a. Trace element characteristics of lavas from destructive plate boundaries. In: Thorpe, R.S. (Ed.), Andesites. John Wiley and Sons, Chichester, pp. 525–548.
Pearce, J.A., 1982b. Role of the sub-continental lithosphere in magma genesis at active continental margins. Continental Basalts and Mantle Xenoliths. Shiva Publication, Cheshire, U.K, pp. 230–249.
Pe-Piper, G., Jansa, L.F., 1999. Pre-Mesozoic basement rocks offshore Nova Scotia, Canada: new constraints on the accretion history of the Meguma terrane. Geological Society of America Bulletin 111, 1773–1791.
Pharaoh, T.C., Merriman, R.J., Evans, J.A., Brewer, T.S., Webb, P.C., Smith, N.J.P., 1991. Early Palaeozoic arc-related volcanism in the concealed Caledonides of southern Britain. Annales de la Société Géologique de Belgique 114, 63–92.
Pharaoh, T.C., Molyneux, T.C., Merriman, R.J., Lee, M.K., Verniers, J., 1993. The Caledonides of the Anglo-Brabant Massif reviewed. Geological Magazine 130, 330–346.
Pharaoh, T.C., England, R., Lee, M.K., 1995. The concealed Caledonides basement of eastern England and the southern North Sea — a review. In: Gee, D.G., Beckholmen, M. (Eds.), The Trans-European Suture Zone: Studia Geophysica et Geodaetica, 39, pp. 330–346.
Piessens, K., Vancampenhout, P., De Vos, W., 2006. Geologische Subcropkaart van het Massief van Brabant in Vlaanderen. Belgische Geologische Dienst, Brussels.
Pin, C., Santos Zalduegui, J.F., 1997. Sequential separation of light rare-earth elements, thorium and uranium by miniaturized extraction chromatography: application to isotopic analyses of silicate rocks. Analytica Chimica Acta 339, 79–89.
Pin, C., Paquette, J.L., Santos Zalduegui, J.F., Gil Ibarguchi, J.I., 2002. Early Devonian suprasubduction-zone ophiolite related to incipient collisional processes in the Western Variscan Belt: the Sierra de Careon unit, Ordenes Complex, Galicia. Geological Society of America, Special Paper, 364, pp. 57–71.
Pin, C., Paquette, J.L., Abalos, B., Santos, F.J., Gil Ibarguchi, J.I., 2006. Composite origin of an early-Variscan transported suture: the ophiolitic units of the Morais Nappe Complex (North Portugal). Tectonics 25, TC5001. doi:10.1029/2006TC001971.
Piper, J.D.A., 1997. Tectonic rotation within the British paratectonic Caledonides and Early Palaeozoic location of the orogen. Journal of the Geological Society of London 154, 9–13.
Prigmore, J.K., 1994. Sedimentology of Upper Cambrian and Lower Ordovician mudstones across Eastern Avalonia (Ph. D. thesis). Cambridge, University of Cambridge, 243 pp.
Prigmore, J.K., Butler, A.J., Woodcock, N.H., 1997. Rifting during separation of Eastern Avalonia from Gondwana: evidence from subsidence analysis. Geology 25, 203–206.
Rickwood, P.C., 1989. Boundary lines within petrologic diagram which use oxides of major and minor elements. Lithos 22, 247–263.
Rushton, A.W.A., Molyneux, S.G., 2011. Welsh basin. In: Gregory, R. (Ed.), A Revised Correlation of the Cambrian Rocks in the British Isles: Geological Society Special Report, 25, pp. 21–27.
Samuelsson, J., Verniers, J., 2000. Ordovician chitinozoan biozonation of the Brabant Massif, Belgium. Review of Palaeobotany and Palynology 113, 105–129.
Sintubin, M., 1999. Arcuate fold and cleavage patterns in the southeastern part of the Anglo-Brabant Fold Belt (Belgium): tectonic implications. Tectonophysics 309, 81–97.
Sintubin, M., Everaerts, M., 2002. A compressional wedge model for the Lower Palaeozoic Anglo-Brabant Belt (Belgium) based on potential field data. In: Winchester, J.A., Pharaoh, T.C., Verniers, J. (Eds.), Palaeozoic Amalgamation of Central Europe: Geological Society, London, Special Publ., 201, pp. 327–343.

Sintubin, M., Debacker, T.N., Van Baelen, H., 2009. Early Palaeozoic orogenic events north of the Rheic suture (Brabant, Ardenne): a review. Comtes Rendus Geoscience 341, 156–173.
Sircombe, K.N., 2004. AGE DISPLAY: an EXCEL workbook to evaluate and display univariate geochronological data using binned frequency histograms and probability density distributions. Computers and Geosciences 30, 21–31.
Stacey, J.S., Kramers, J.D., 1975. Approximation of terrestrial lead isotope evolution by a two-stage model. Earth and Planetary Science Letters 26, 207–221.
Steemans, P., 1989. Paléogéographie de l'Eodévonien ardennais et des regions limitrophes. Annales de la Société Géologique de Belgique 112, 103–119.
Stern, R.J., Ali, K.A., Liégeois, J.P., Johnson, P., Wiescek, F., Kattan, F., 2010. Distribution and significance of pre-Neoproterozoic zircons in juvenile Neoproterozoic igneous rocks of the Arabian-Nubian shield. American Journal of Science 310, 791–811.
Sun, S.S., 1980. Lead isotopic study of young volcanic rocks from mid-ocean ridges, ocean islands and islands arcs. Philosophical Transactions of the Royal Society of London A297, 409–445.
Tanaka, T., et al., 2000. JNdi-1: a neodymium isotopic reference in consistency with LaJolla neodymium. Chemical Geology 168, 279–281.
Taylor, S.R., Mc Lennan, S.M., 1985. The Continental Crust: Its Composition and Evolution. Blakwell, Oxford. 312 pp.
Torsvik, T.H., Rehnström, E.F., 2003. The Tornquist Sea and Baltica–Avalonia docking. Tectonophysics 362, 67–82.
Van Grootel, G., Verniers, J., Geerkens, B., Laduron, D., Verhaeren, M., Hertogen, J., De Vos, W., 1997. Timing of magmatism, foreland basin development, metamorphism and inversion in the Anglo-Brabant fold belt. Geological Magazine 134, 607–616.
Vanguestaine, M., 1991. Datation par acritarches des couches cambro-trémadociennes les plus profondes du sondage de Lessines. Annales de la Société Géologique de Belgique 114, 213–231.
Vanguestaine, M., 1992. Biostratigraphie par acritarches du Cambro-Ordovicien de Belgique et des régions limitrophes: synthèses et perspectives d'avenir. Annales Société Géologique de Belgique 115, 1–18.
Vanmeirhaeghe, J., 2006. The evolution of the Condroz-Brabant Basin from the Middle Ordovician to Llandovery: lithostratigraphical and chitinozoan biostratigraphical approach. Unpublished Ph.D., Dept. Geology and Soil Sciences, Ghent University, 261 p.
Vanmeirhaeghe, J., Storme, A., Van Noten, K., Van Grootel, G., Verniers, J., 2005. Chitinozoan biozonation and new lithostratigraphical data in the Upper Ordovician of the Fauquez and Asquempont areas (Brabant Massif, Belgium). Geologica Belgica 8, 145–159.
Verniers, J., Van Grootel, G., 1991. Review of the Silurian in the Brabant Massif, Belgium. Annales Société Géologique de Belgique 114, 163–193.
Verniers, J., Herbosch, A., Vanguestaine, M., Geukens, F., Delcambre, B., Pingot, J.L., Belanger, I., Hennebert, M., Debacker, T., Sintubin, M., De Vos, W., 2001. Cambrian–Ordovician–Silurian lithostratigraphical units (Belgium). Geologica Belgica 4, 5–38.
Verniers, J., Pharaoh, T., Andre, L., Debacker, T., De Vos, W., Everaerts, M., Herbosch, A., Samuelsson, J., Sintubin, M., Vecoli, M., 2002. The Cambrian to mid Devonian basin development and deformation history of Eastern Avalonia, east of the Midlands Microcraton: new data and a review. In: Winchester, J., Verniers, J., Pharaoh, T. (Eds.), Palaeozoic Amalgamation of Central Europe: Geological Society, London, Special Publications, 201, pp. 47–93.
Verniers, J., Van Grootel, G., Debacker, T.N., 2005. The Upper Ordovician lithostratigraphy and structure of the Fauquez area (Brabant Massif, Belgium). Geologica Belgica 8, 160–175.
Waldron, J.W.F., White, C.E., Barr, S.M., Simonetti, A., Heaman, L.M., 2009. Provenance of the Meguma terrane: rifted margin of Early Palaeozoic Gondwana. Canadian Journal of Earth Sciences 46, 1–8.
Waldron, J.W.F., Schofield, D.I., White, C.E., Barr, S.M., 2011. Cambrian successions of the Meguma Terrane, Nova Scotia and Harlech Dome, North Wales: dispersed fragment of a peri-Gondwanan basin? Journal of the Geological Society of London 168, 83–98.
White, C.E., 2010. Stratigraphy of the Lower Palaeozoic Goldenville and Halifax groups in southwestern Nova Scotia. Atlantic Geology 46, 136–154.
Winchester, J.A., Network Team, P.A.C.E., 2002. Palaeozoic amalgamation of central Europe: new results from recent geological and geophysical investigations. Tectonophysics 360, 5–21.
Woodcock, N.H., 1990. Sequence stratigraphy of the Palaeozoic Welsh basin. Journal of the Geological Society of London 147, 537–547.
Woodcock, N.H., 1991. The Welsh, Anglian and Belgian Caledonides compared. Annales de la Société Géologique de Belgique 114, 5–17.
Woodcock, N.H., 2011. Terranes in the British and Irish Cambrian. In: Gregory, R. (Ed.), A Revised Correlation of the Cambrian Rocks in the British Isles: Geological Society Special Report, 25, pp. 15–20.